



U.S. Department
of Transportation
**National Highway
Traffic Safety
Administration**



DOT HS 812 087

December 2014

Development of Integrated Vehicle-Occupant Model for Crashworthiness Safety Analysis

DISCLAIMER

This publication is distributed by the U.S. Department of Transportation, National Highway Traffic Safety Administration, in the interest of information exchange. The opinions, findings, and conclusions expressed in this publication are those of the authors and not necessarily those of the Department of Transportation or the National Highway Traffic Safety Administration. The United States Government assumes no liability for its contents or use thereof. If trade or manufacturers' names or products are mentioned, it is because they are considered essential to the object of the publication and should not be construed as an endorsement. The United States Government does not endorse products or manufacturers.

Suggested APA Format Citation:

Reichert, R., Park, C-K., & Morgan, R. M. (2014, December). *Development of integrated vehicle-occupant model for crashworthiness safety analysis*. (Report No. DOT HS 812 087). Washington, DC: National Highway Traffic Safety Administration.

Technical Report Documentation Page

1. Report No. DOT HS xxx xxx DOT HS 812 087	2. Government Accession No.	3. Recipient's Catalog No.	
4. Title and Subtitle Development of Integrated Vehicle-Occupant Model for Crashworthiness Safety Analysis		5. Report Date December 2014	
		6. Performing Organization Code	
7. Author(s) Rudolf Reichert, Chung-Kyu Park, and Richard M. Morgan		8. Performing Organization Report No.	
9. Performing Organization Name and Address National Crash Analysis Center 45085 University Blvd. Ashburn, VA 20147		10. Work Unit No. (TRAIS)n code	
		11. Contract or Grant No. FHWA Contract No. DTFH61-09-D-00001	
12. Sponsoring Agency Name and Address National Highway Traffic Safety Administration 1200 New Jersey Avenue SE. Washington, DC 20590		13. Type of Report and Period Covered Study Accomplishments in 2013	
		14. Sponsoring Agency Code	
15. Supplementary Notes			
16. Abstract <p>During 2013, the accomplishment of this research study was the development of an integrated occupant-vehicle model for the analysis of safety in crashes. The 2010 Toyota Yaris Finite Element Model (FEM) was used with full interior and occupant models. Three-point belt restraints with pre-tension and force limiter characteristics, folded driver air bag, collapsible steering column, and interior components were modeled. The integrated vehicle-occupant model was validated against laboratory crashes of (1) NCAP frontal test; (2) IIHS 40-percent offset test; and (3) NHTSA oblique frontal test, using either the Hybrid III or THOR FEM occupant models.</p> <p>The Toyota Yaris model was used for sensitivity analysis and for occupant studies with one of the Hybrid III, THOR, or THUMS. The sensitivity studies considered (1) impact parameters, such as vehicle speed and overlap percentage; (2) occupant seating positions; and (3) restraint system variations. Occupant results of the advanced THOR were compared to the Hybrid III. Injury risks have been evaluated using the detailed THUMS human model.</p> <p>In due course, the integrated occupant-vehicle model will serve as a platform for rapid modeling and future development of prototype occupant-protection designs for use in the full vehicle fleet.</p>			
17. Key Words Frontal crash simulations, sensitivity analysis, finite element vehicle model, finite element occupant model		18. Distribution Statement Document is available to the public through the National Technical Information Service www.ntis.gov	
19. Security Classif. (of this report) Unclassified	20. Security Classif. (of this page) Unclassified	21. No of Pages 106	22. Price

Table of Contents

1. Development of an integrated vehicle model for occupant safety analysis	5
1.1 Vehicle, occupant, and component models	5
1.1.1 Vehicle structure model.....	5
1.1.2 Occupant models	6
1.1.3 Generic driver air bag model	7
1.1.4 Generic seat belt model.....	8
1.1.5 Generic steering column model.....	9
1.2 Integrated vehicle-occupant model preparations	9
1.2.1 Occupant model tree file	10
1.2.2 Seat model mechanism.....	11
1.2.3 Seat squash	12
1.2.4 Belt fit.....	13
1.3 Complete and reduced model methodology.....	14
1.3.1 Modular input deck using include option	15
1.3.2 Reduced model technique	16
1.3.3 Positioning.....	17
1.4 Crash configurations	18
1.4.1 IIHS frontal offset.....	18
1.4.2 NCAP full overlap frontal impact	18
1.4.3 Oblique offset frontal impact.....	19
1.5 Evaluation procedure of test and simulation results.....	20
1.5.1 Overall comparison of test and simulation.....	20
1.5.2 Qualitative comparison.....	20
1.5.3 CORA	21
1.5.4 Quantitative comparison	23
1.6 IIHS frontal offset configuration results.....	25
1.6.1 IIHS overall comparison of test and simulation	25
1.6.2 IIHS qualitative comparison of test and simulation	26

1.6.3 IIHS quantitative comparison of test and simulation	27
1.7 NCAP frontal full overlap results.....	28
1.7.1 NCAP overall comparison of test and simulation	28
1.7.2 NCAP qualitative comparison of test and simulation	29
1.7.3 NCAP quantitative comparison of test and simulation.....	30
1.8 Oblique load case results	31
1.8.1 Oblique load case overall evaluation	32
1.8.2 Oblique load case qualitative comparison of test and simulation.....	33
1.8.3 Oblique load case quantitative comparison of test and simulation	33
1.9 Conclusion Subtask I	35
2. Sensitivity Analysis	36
2.1 Methodology.....	36
2.2 Sensitivity Analysis using NCAP load case.....	39
2.2.1 Variation of impact speed.....	40
2.2.2 Variation of x-seating position	41
2.2.3 Variation of seating height.....	43
2.2.4 Seat belt with and without pre-tensioner	44
2.2.5 Variation of air bag venting.....	46
2.2.6 Variation of steering column collapse	47
2.2.7 Variation of air bag time-to-fire	49
2.2.8 Variation of leg position.....	50
2.3 Sensitivity Analysis using IIHS load case	52
2.3.1 Variation of overlap percentage	53
2.3.2 Variation of impact speed.....	55
2.3.3 Variation of x-seating position	56
2.3.4 Variation of air bag venting.....	59
2.3.5 Variation of air bag time-to-fire	60
2.3.6 Variation of seat belt force limiter.....	62
2.3.7 Variation of torso angle	64
2.4 Sensitivity Analysis using oblique load case.....	66
2.4.1 Differences in vehicle structure	66
2.4.2 Overall evaluation	66

2.4.3 Qualitative evaluation	68
2.4.4 Quantitative evaluation	68
2.5 Conclusion Subtask II sensitivity analysis.....	70
3. Use and evaluation of different occupant models	71
3.1 THOR	71
3.1.1 Overall Evaluation	71
3.1.2 Femur loads.....	72
3.1.3 Chest loads.....	73
3.1.4 Neck loads.....	74
3.1.5 Head acceleration	76
3.1.6 THOR - Hybrid III comparison conclusion	76
3.2 THUMS human model.....	78
3.2.1 THUMS description	78
3.2.2 THUMS preparations.....	78
3.2.3 THUMS evaluation of loads.....	80
3.2.4 IIHS results using THUMS.....	82
3.2.5 THUMS torso posture evaluation	85
3.3 Conclusion Subtask III	89
4. Summary and acknowledgment	90
5. Appendix	92
5.1. FE model of 2010 Toyota Yaris.....	92
5.2. NHTSA frontal oblique test	93

I Background

Combined (integrated) occupant and vehicle finite element models have been used by car manufacturers and suppliers for many years to develop, evaluate, and optimize safety measures using vehicle structural, interior, and restraint system components. These integrated occupant-vehicle models are used to simulate and validate available laboratory test results. Calibrated models are used to design and optimize entire systems for a variety of crash configurations before full-scale crash tests are conducted with an actual vehicle. In addition to these detailed simulation tools, component and subsystem tests are performed to capture physical phenomenon such as failure that cannot be covered by simulation alone. Ideally the tests that are performed with prototypes in a vehicle development cycle confirm the simulation results. Further these test results are used to validate the simulation models for the specific new vehicle structural, interior, and restraint system characteristics in all relevant crash load cases. The final test results with a fully developed structural body-in-white, interior components, and restraint systems usually take place at a later point in time of the development process. At this time, it is too late to perform major changes to most of the components, and therefore the test and development results are used to confirm and certify the safety performance for the regulatory and consumer information requirements.

II. Objective

The objective of this research is to develop an integrated occupant-vehicle model for occupant safety analysis that is capable of evaluating various interior treatments and restraint systems, demonstrating the efficacy of the model in representing various crash scenarios, and allowing the applicability of a range of occupant models. The methodologies used for the developed integrated model shall have the potential to evaluate current as well as future vehicles (e.g., those developed in the light-weighting research).

Detailed finite-element models are developed to evaluate performance of different occupants in full frontal, frontal offset, and oblique frontal impact configurations.

Available finite element models of vehicle structure and occupants are used in combination with generic interior and restraint system component models that were developed during this project. The fully integrated vehicle-occupant models shall then be validated and evaluated with available full-scale crash test data for the different laboratory crash configurations.

The developed and validated integrated occupant-vehicle model shall then be used to perform several sensitivity analysis simulations, using the different load cases in order to evaluate the effect of various parameter variations, such as impact speed, air bag characteristics, seat belt characteristics, and seating position, on the occupant response. The objective of this subtask is to confirm that the developed model is robust and is able to predict realistic results for crash configurations other than the validated scenarios.

Furthermore, the developed integrated occupant-vehicle model is used to analyze more detailed occupant models, such as the THOR dummy and the THUMS human model.

III Outline

This study was performed under Task Order 25 of FHWA Contract No. DTFH61-09-D-00001. Task Order 25 is divided in the following four subtasks:

Subtask I: Integrated occupant-vehicle model creation and validation

In the first subtask, models for all relevant interior and restraint system components were developed and assimilated into available vehicle structure, barrier, and respective occupant models according to the chosen full-scale crash test configurations. The integrated simulation results were validated to test results for the following laboratory load cases:

- New Car Assessment Program (NCAP) full overlap frontal impact with a 50th percentile HIII dummy at 56km/h into a rigid barrier.
- Insurance Institute for Highway Safety (IIHS) 40-percent offset frontal impact with a 50th percentile HIII dummy at 64km/h into a deformable barrier.
- Oblique frontal impact with a 50th percentile THOR dummy impacted by a moving deformable barrier at 90km/h, at a 15 degree angle with a 35-percent overlap.

Subtask II: Perform Sensitivity Analysis

The developed and validated integrated occupant-vehicle models from Subtask 1 were used to evaluate the effect on occupant response with varying different parameters, such as

- Vehicle parameters (impact speed, different engine).
- Barrier parameters (offset percentage).
- Occupant parameters (seating position, torso angle).
- Air bag parameters (time-to-fire, air bag venting).
- Seat-belt parameters (use of pre-tensioner, level of belt force limiter).
- Steering column parameters (amount of steering column collapse).

Subtask III: Use and evaluation of different occupant models

The developed and validated integrated occupant-vehicle models from Subtask 1 were used to evaluate different occupant models in the various crash configurations. The following dummy and human models were used:

- 50th percentile Hybrid III dummy,
- 50th percentile THOR dummy, and
- 50th percentile THUMS (Total HUMAN Model for Safety) human body model.

Subtask IV: Preliminary report

Methodologies and findings from Subtask I, II and III were documented in monthly presentations, discussed during telephone conferences, and were documented in this report.

IV Subtask I

1. Development of an integrated vehicle model for occupant safety analysis

1.1 Vehicle, occupant, and component models

1.1.1 Vehicle structure model

The Toyota Yaris structural vehicle model was chosen to be used for creation of the integrated vehicle-occupant simulation model. It consists of 771 parts and about 1 million elements. Appropriate connections and materials derived from more than 150 tensile tests were used to create this model. Accelerometers at distinct locations and vehicle inertia values were used to compare and validate the structural Yaris model using full-scale crash test data from a frontal full overlap configuration at 40 and 56 km/h and an IIHS 40-percent offset frontal impact at 64km/h.

1.1.2 Occupant models

The Livermore Software Technology Corporation (LSTC) Hybrid III 50th Fast Dummy Version 2.0¹ was adapted and used for the NCAP frontal full overlap and for the IIHS 40-percent frontal offset load cases.

In the oblique frontal offset full-scale crash test which will be used to evaluate the simulation results later in this report, a 50-percent adult male THOR (Test Device for Human Occupant Restraint) MK (Mod Kit) anthropometric test device (ATD) as described in the NHTSA test report² was seated in the left front seat. The so-called "Mod Kits" were designed to make changes to the head/neck, thorax, abdomen, and knee/femur/pelvis of the dummy described in (Ridella et al., 2011, Modifications to Improve the Durability, Usability and Biofidelity of the THOR Dummy).³ For the oblique load case simulations, available FE model of the THOR which was previously developed by NHTSA and their collaborators (Untaroiu et al., 2009)⁴ was adapted and used. In order to implement the available THOR model, several preparations, such as unit conversion, renumbering, positioning, and some mesh modifications were conducted. The units used in the simulation model are tons, millimeter, Newton, and seconds. The mesh modifications consisted of elimination of initial penetrations that caused numerical instabilities.

¹ LSTC.H3_50TH_FAST.111130_V2.0_Documentation, www.lstc.com

² Report for Frontal Oblique offset program Testing on a 2011 Toyota Yaris NHTSA No. RB5136

³ Ridella, S. A., & Parent, D. P. Modifications to Improve the Durability, Usability and Biofidelity of the THOR Dummy. Paper Number 11-0312. Proceedings of the 22nd International Conference on the Enhanced Safety of Vehicles (ESV). 2011

⁴ Untaroiu, C., Lim, J. Y., Shin, J., Crandall, J., Malone, D. P., & Tannous, R. E., (2009) Evaluation of a finite element of the THOR dummy in frontal crash environment, Paper 2009-0272, 21st ESV Conference, Stuttgart, Germany.

1.1.3 Generic driver air bag model

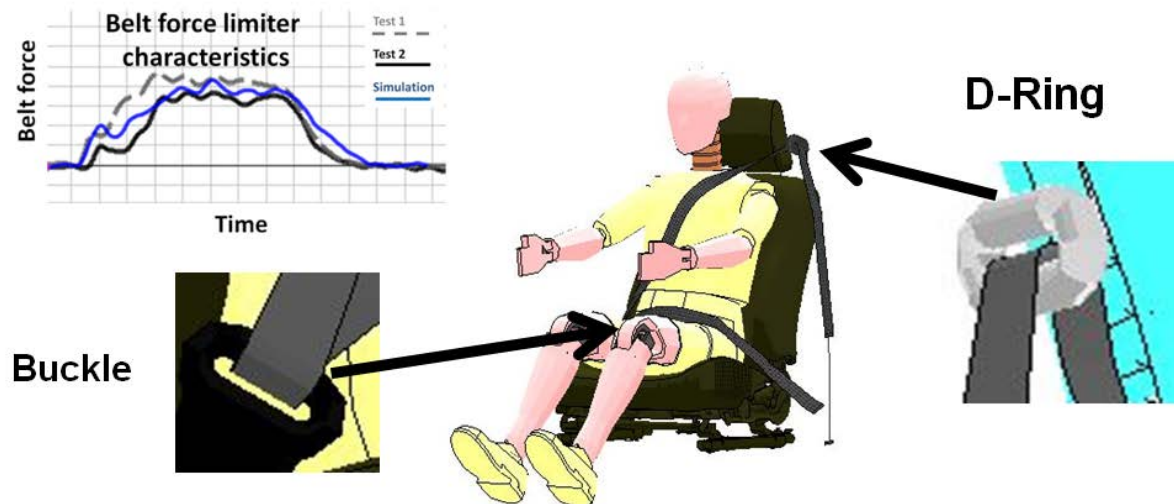
A generic driver air bag model was developed and validated. Model creation was achieved by using the software tool "Primer" as preprocessor. The procedure is shown in Figure 1.

Figure 1: Generic air bag model

First, a flat unfolded round air bag was created. The Primer integrated "star fold" tool was then used to fold the driver air bag. In order to fit the air bag into the available package in the steering wheel cover, an LS-Dyna3D pre-simulation was performed. Having reduced the package of the folded air bag, it was fitted into the available air bag cover and attached to the steering wheel. Inflator mass flow and air bag venting characteristics were defined (LS-Dyna keyword card *AIRBAG_HYBRID_ID) and validated using available full-scale crash test data.

1.1.4 Generic seat belt model

A generic seat belt model with pre-tensioner and belt force limiter was developed and validated. Figure 2 shows how the seat belt runs realistically through buckle and d-ring without the usage of simplified slip ring definition, which is a numerical homologous model that allows continuous sliding of seat belt elements through a sharp change of angle.



Belt runs realistically through D-Ring and Buckle Using Contact

Figure 2: Generic seat belt model

Pre-tensioner and retractor belt force limiter characteristics were developed and validated using results and information from available full-scale crash test data. A pyrotechnic pre-tensioner with a belt force limit of 4kN was used.

1.1.5 Generic steering column model

A generic steering column model with optional steering column collapse characteristics was created. A maximum possible steering column collapse of about 90 mm in the longitudinal direction was implemented. Force displacement characteristics as depicted in Figure 3 can be applied.

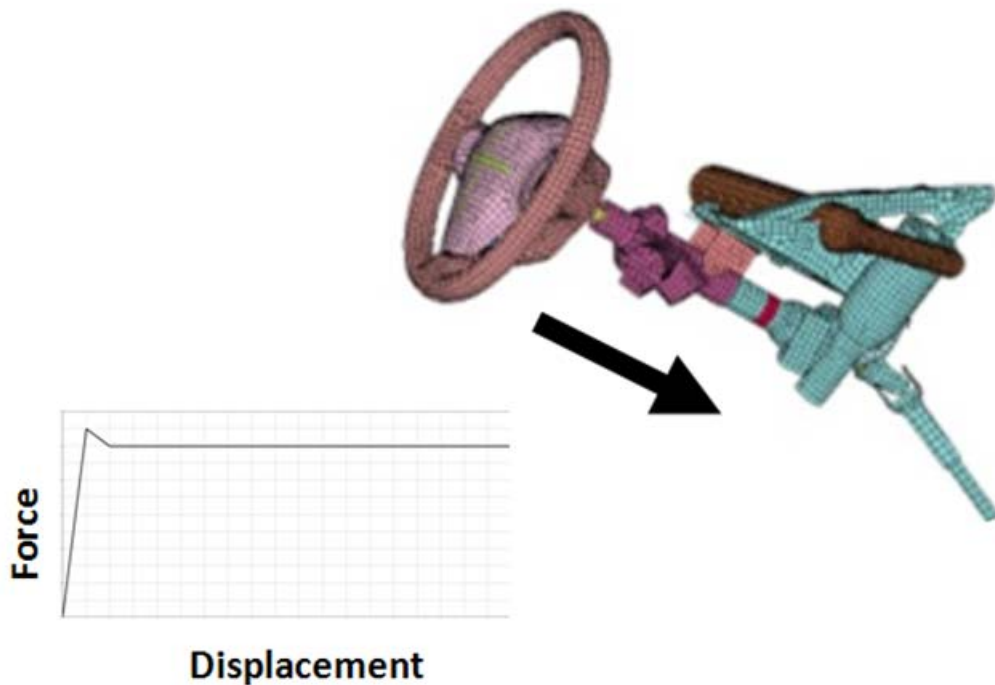


Figure 3: Generic collapsible steering column model

1.2 Integrated vehicle-occupant model preparations

"Mechanisms" for positioning dummy and seat, seat squash, and belt fit were used to prepare each load case. The different techniques are described in this chapter.

1.2.1 Occupant model tree file

A so-called “tree file” is the definition of how the different dummy parts are connected and how they can move relative to each other. For example, it is defined that the upper arm is connected to the torso at the shoulder joint, the lower arm is connected to the upper arm at the elbow joint, and the hands are connected to the lower arm at the wrist joint. In addition, it is defined how many degrees and which direction each limb (also called child-part) can move relative to its connected previous body part (also called parent part). This definition for the entire occupant model is called the tree file and allows an easy positioning of the dummy using adequate pre-processing software. Tree files for positioning the 50th percentile Hybrid III and THOR occupant models according to the seating position of the hardware dummies in the respective full-scale crash tests were used. An example with differently positioned occupant limb positions can be seen in Figure 4 to demonstrate possible tree file usage.

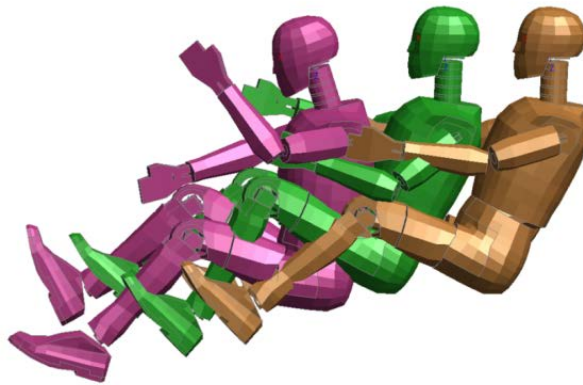
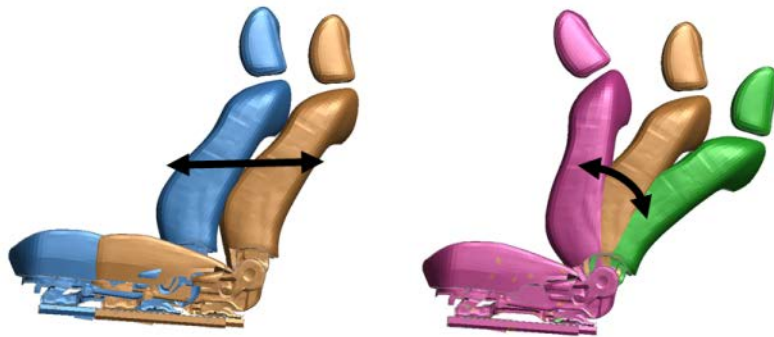


Figure 4: Tree file for occupant model positioning

1.2.2 Seat model mechanism

Similar to the tree file for a dummy, a definition was used to define how the different parts of the driver seat are connected and how they can move relative to each other. This definition is called the seat mechanism. For example, it is defined that the entire seat can move longitudinal from the most forward to the most rearward position along the seat rail. It also is defined, that the seat back can rotate around the longitudinal axis (y-axis) relative to the seat cushion. An example of a mechanism for easy positioning of the driver seat model into the respective seating position is illustrated in Figure 5.



**Seat Mechanism
created for easy positioning**

Figure 5: Mechanism for seat model positioning

1.2.3 Seat squash

After occupant and seat were positioned in the correct location according to the respective full-scale crash test configuration, a so-called seat squash simulation needs to be conducted. In reality a dummy or occupant deforms the seat foam during the process of sitting into the seat. In order to deform the seat model in the simulation accordingly, a quasi-static simulation is done. First, the occupant is moved out of the seat until no penetration is visible. Second, the occupant moves very slowly into its final sitting position, deforming the seat foam through the defined contact definition in LS-DYNA3D. This procedure requires the knowledge of the respective positions of both seat and occupant, which is usually the case for standard regulation and consumer information load cases. Alternatively, the occupant model can be seated into the seat using gravity. The simulation in this case has to be run until equilibrium between the occupant and the seat foam is reached. Having proper material characteristics and correct position information for seat and dummy, both methods can be used. The first method has been applied in this study. A deformed seat can be saved as a separate model, as illustrated in Figure 6, and integrated together with the occupant without penetrations into the occupant-vehicle simulations.

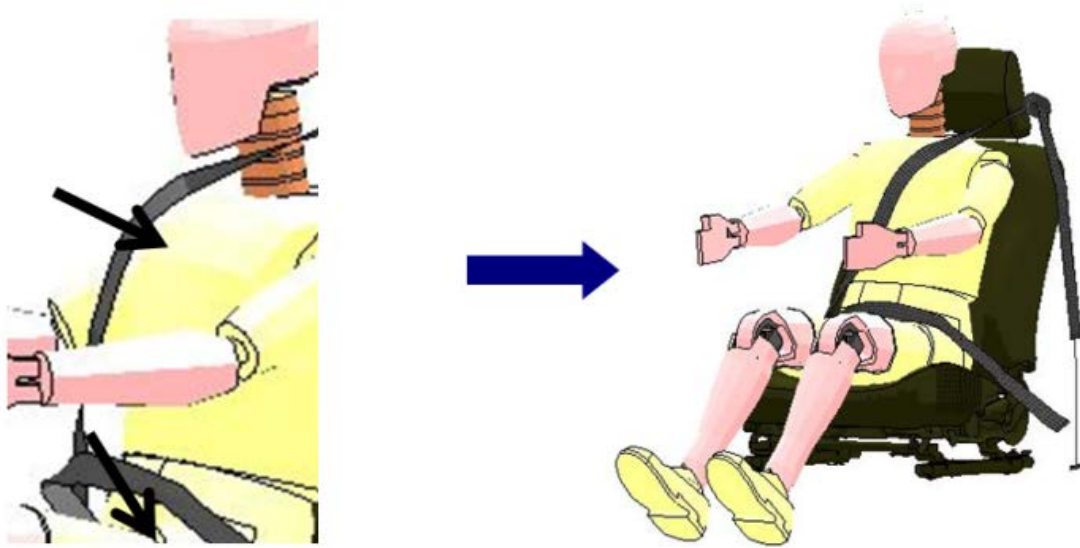


Seat Squash: Simulation with Rigidified Dummy and Prescribed Motion into final Seating position is used to create “squashed” Seat

Figure 6: Seat squash

1.2.4 Belt fit

"Belt fit" was used to put the seat belt around the occupant in the final seating position as depicted in Figure 7.



Belt-Fitting used to put Seatbelt around Dummy and Seat in final Seating Position

Figure 7: Belt fit

1.3 Complete and reduced model methodology

Full and sub models were used to develop the integrated vehicle-occupant models for the respective crash configurations. The full model contains the entire vehicle model, the respective barrier and occupant model, and all interior and restraint system components. A sub model makes use of the so-called component analysis option in LS-DYNA3D. It can be used to replicate the kinematics and intrusion behavior of defined parts of the full model. With respect to occupant analysis it can be used in the following manner: First, the full model is run in the respective load case with all available interior and restraint system components. During this simulation run, "relevant" parts, such as the floor, firewall, as well as the attachments for the seat, the steering column, the seat-belt, and the instrument panel, for example, are defined and the motion over time is being "recorded" in a binary file by LS-DYNA3D. The level of reduction depends on the objective: for many cases it is sufficient to record the behavior of the seat surface, instrument panel, as well as the steering column behavior in addition to the seat-belt attachments, for example. Second, the sub model is created using the recorded information. In this reduced model, the entire barrier model and the structural model are replaced with the defined few relevant parts (for example, attachments, floor and instrument panel), which are guided and move exactly the same way as in the full occupant-vehicle simulation. Adding the original additional ("deformable") parts (such as the instrument panel, the seat, the steering column with steering wheel and driver air bag, as well as the seat belt and the respective occupant model, the same way as in the full model) results in a much smaller model, which can be considered an advanced sled test model. Kinematics and intrusion behavior of the defined parts that are relevant for the occupant analysis behave exactly the same way as in the full occupant-vehicle simulation run. Being much smaller in size, (since the entire vehicle and barrier is replaced by only a few parts) it runs much faster and can still be used to evaluate the effects of modified seat belt or air bag characteristics, for example. Third, the sub model is used to optimize or validate the air bag or seat belt models, for example, in many simulation runs. Due to its smaller size, many simulation runs and parameter studies can be performed efficiently. Fourth, the optimized component models are integrated into the full occupant-vehicle model, once a satisfying status is being reached. This is necessary because changes in restraint system characteristics and consequently occupant kinematics can affect the movement of the parts and attachments, which have been defined before and used for the so-called prescribed motion. Having a modular LS-DYNA3D input deck, as explained in the next section, allows an easy iteration and switch between the full and the reduced models. Therefore, the modular LS-DYNA3D input deck provides an efficient way of validating or optimizing occupant and component models.

1.3.1 Modular input deck using include option

Figure 8 shows the modular structure of the LS-Dyna3d input decks. As shown in the figure, the modular structure is taking advantage of the available “include” option within LS-Dyna3d. The vehicle structure model, barrier, occupant, air bag, seat belt, and other interior components were included into the main input deck. With this technique, the various components can be replaced or modified in an efficient manner without having to rebuild the entire integrated occupant-vehicle model.

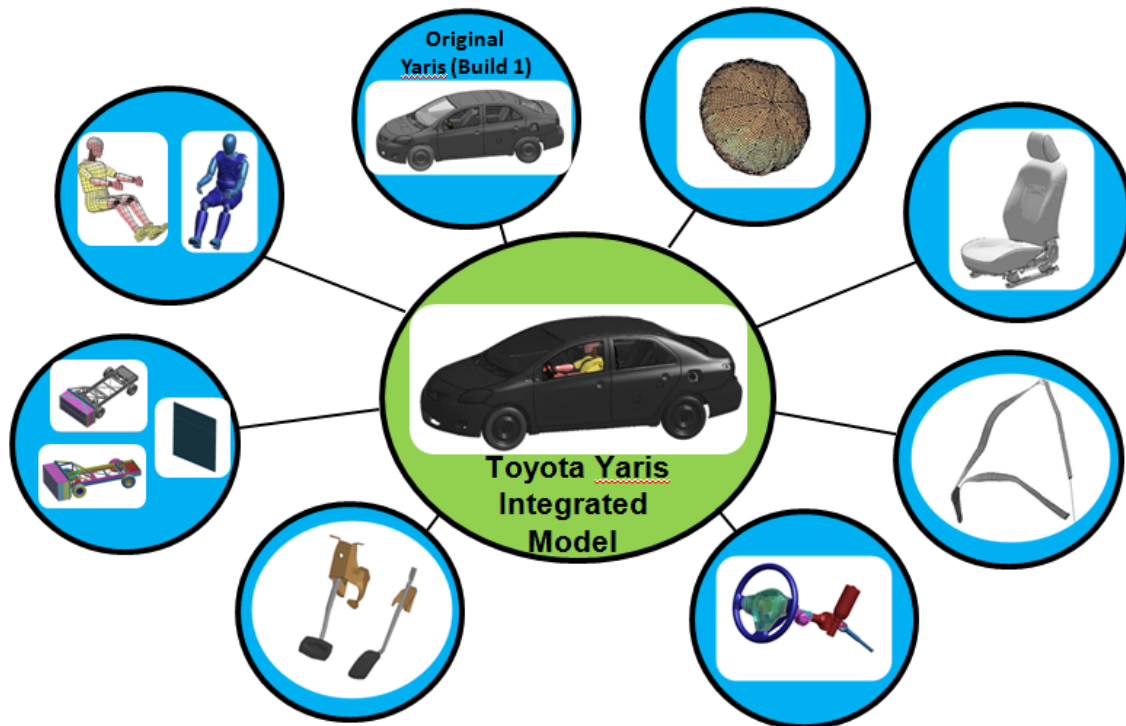
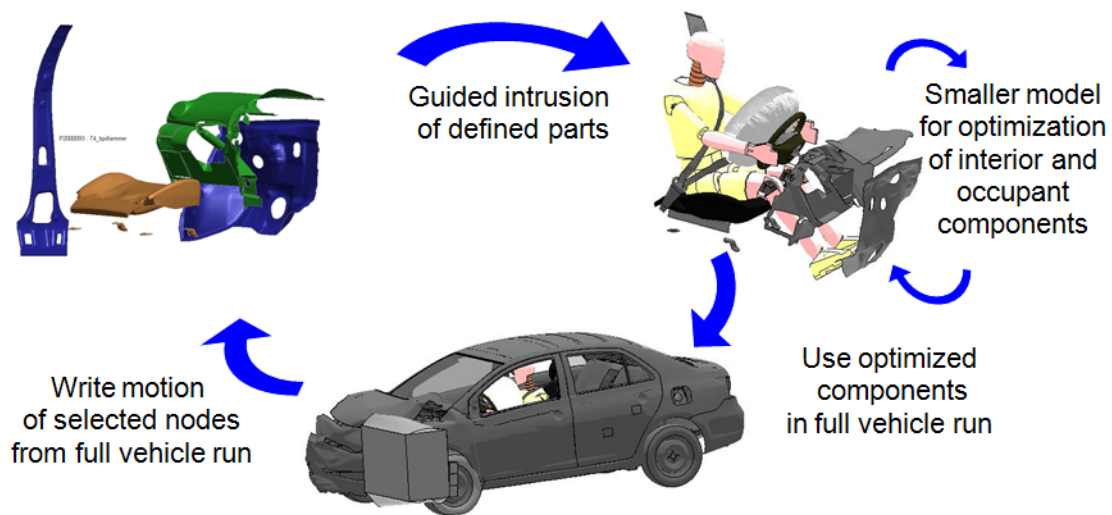


Figure 8: Modular input deck

1.3.2 Reduced model technique

As shown in Figure 9 and described in section 1.3, reduced or sub model techniques were used for the model development. Defined output from a full vehicle run was used to create a sub model with prescribed motions of the occupant environment. Occupant and restraint systems were included to the sub model in a similar manner as in the full occupant-vehicle model. The smaller model replicates the realistic intrusion behavior and vehicle kinematics from the full model and could be used for optimization of interior components and for validation purposes. The "turnaround time" of sub models was reduced by up to 90 percent when compared to that of the complete model and allowed a more efficient model creation and validation process.

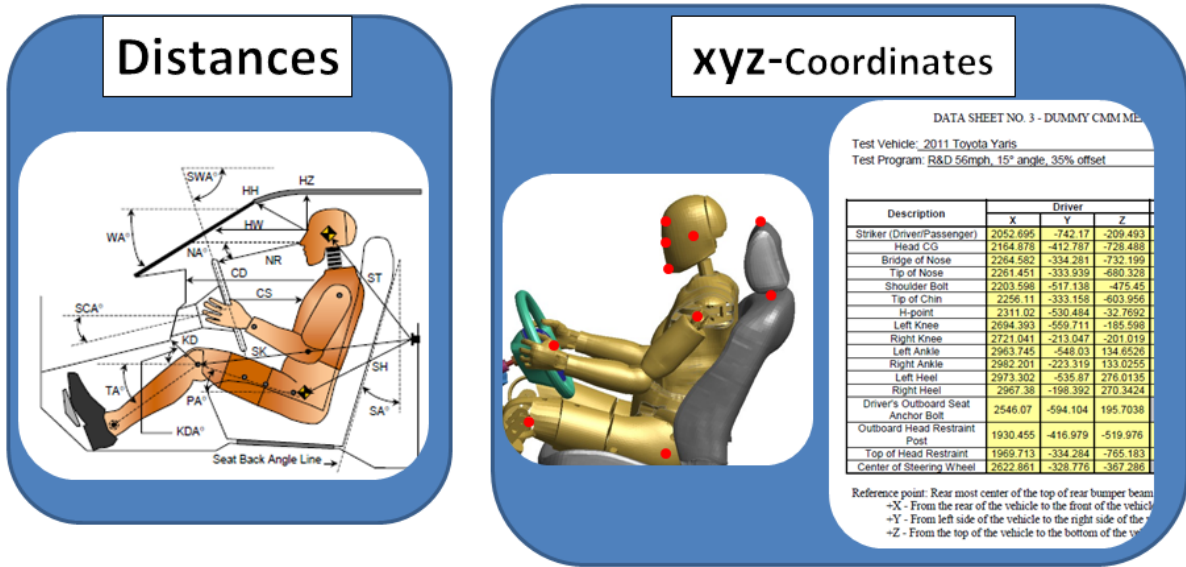


Reduced model is used to verify and optimize components such as belt, airbag, seat, and dummy using realistic intrusion behavior and vehicle kinematics. Reduced model runs about 90% faster than full vehicle model.

Figure 9: Sub model technique

1.3.3 Positioning

Documentation of available full-scale crash test data, such as that shown in Figure 10, was used to position occupants according to different laboratory crash configurations.



XYZ Coordinates of characteristic Points (Face, Steering Wheel middle ..) from Oblique Test especially helpful

Figure 10: Occupant positioning

1.4 Crash configurations

Models for three different load cases were developed and evaluated using full-scale crash test data for full frontal, frontal offset, and oblique frontal impact configurations.

1.4.1 IIHS frontal offset

Using full-scale crash test data of a 2007 Toyota Yaris test from September 14, 2006 (reference number CEF0610), a model for simulating the IIHS 64km/h 40-percent offset impact into a fixed deformable barrier with a 50th percentile Hybrid III dummy in the driver seat was developed and evaluated, as shown in Figure 11.

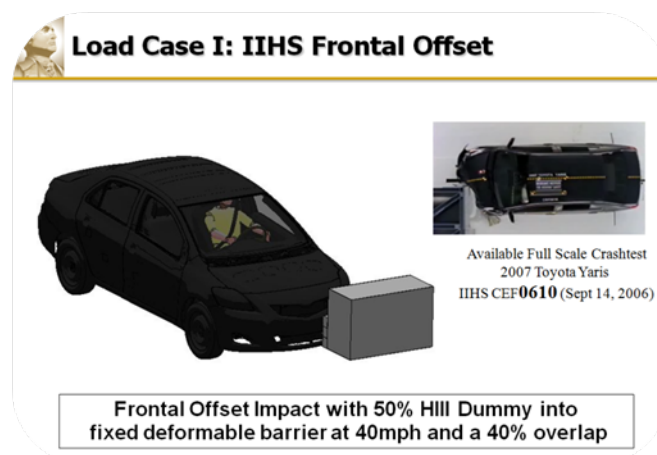


Figure 11: IIHS frontal offset configuration

1.4.2 NCAP full overlap frontal impact

As a second load case, a model for simulating the 35 mph NCAP full overlap crash with a 50th percentile Hybrid III dummy in the driver seat was developed. Two available full-scale crash tests for the Toyota Yaris were used to evaluate the integrated vehicle-occupant model as shown in Figure 12. The first test used a 2007 sedan vehicle version described in ⁵. The second test used a 2008 3-door hatchback version described in ⁶.

⁵ Final Report of New Car Assessment Program Testing of a 2007 Toyota Yaris

⁶ Final Report of New Car Assessment Program Testing of a 2008 Toyota Yaris 3-Door Liftback

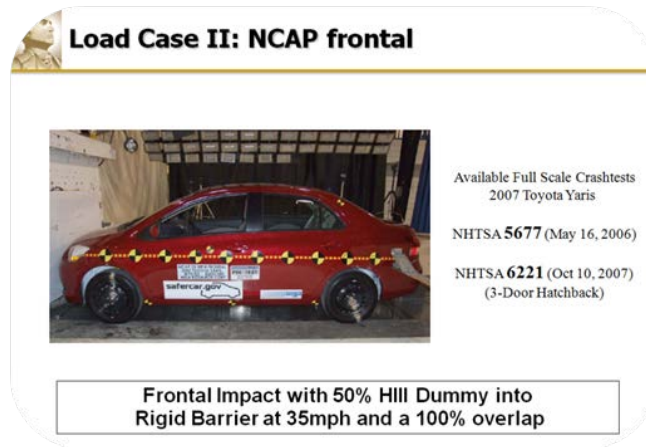


Figure 12: NCAP full overlap configuration

1.4.3 Oblique offset frontal impact

The third load case was an oblique impact at 90km/h, configured at a 15-degree angle with 35-percent overlap, and a 50th percentile THOR dummy in the driver seat. This model was developed and evaluated using full-scale crash test data of the Toyota Yaris NHTSA test no. 7441 from August 16, 2011, as shown in Figure 13.



Figure 13: Oblique offset frontal configuration

1.5 Evaluation procedure of test and simulation results

Test and simulation results were compared using three levels of comparison: overall comparison, qualitative comparison including an objective curve correlation tool called "CORA" (CORrelation and Analysis),⁷ and quantitative comparison.

1.5.1 Overall comparison of test and simulation

First, a visual analysis of test pictures, test movies, and simulation animations were used to compare overall vehicle, occupant, and restraint system kinematics and characteristics of the various crash events as shown in Figure 14.

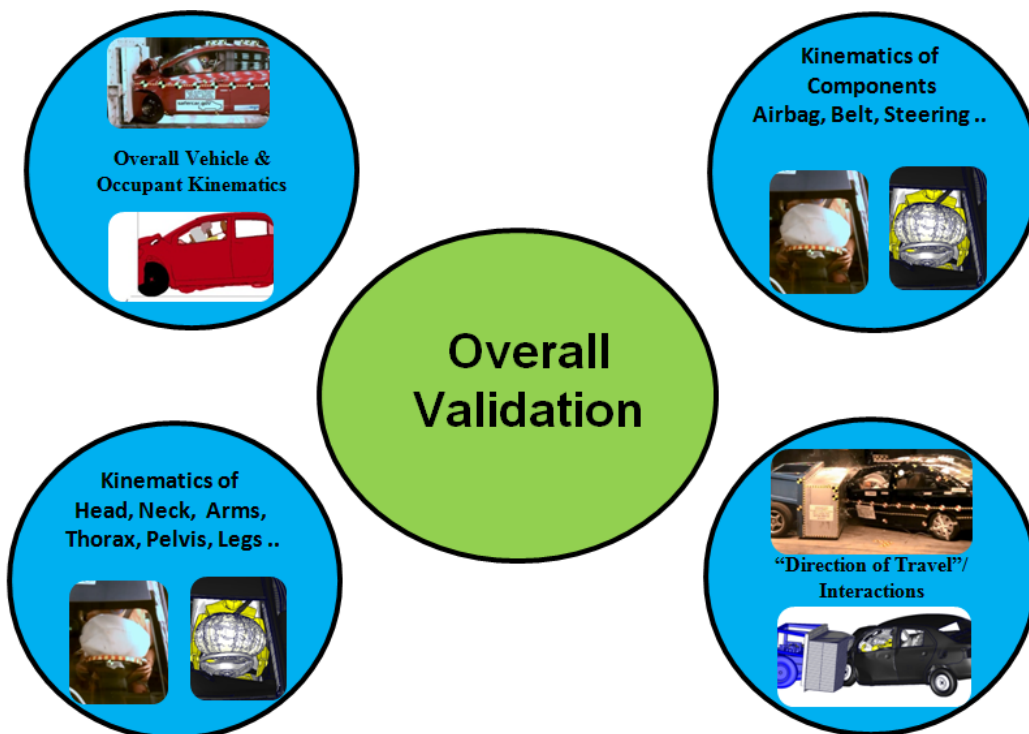


Figure 14: Overall validation

1.5.2 Qualitative comparison

Time history plots in combination with test videos and simulation animations were used to evaluate characteristic injury mechanisms and occupant loads. General examples of qualitative comparisons, such as air bag bottoming out and acceleration peaks caused by first air bag

⁷ CORA Release 3.6 Users Manual by "GNS mbH" on behalf of PDB - Partnership for Dummy Technology and Biomechanics

occupant contacts, are shown in Figure 15. In addition, injury limits and research goals were taken into account, and more emphasis was given to body regions and occupant loads that were close to biomechanical limits, regulatory, and consumer information (i.e., NCAP) requirements. In addition to rate how two curves compared to each other, the software tool "CORA" was used. CORA is explained in more detail in the following chapter. Furthermore, engineering judgment and experience were used to compare, understand and validate the different injury mechanisms in the test and simulation.

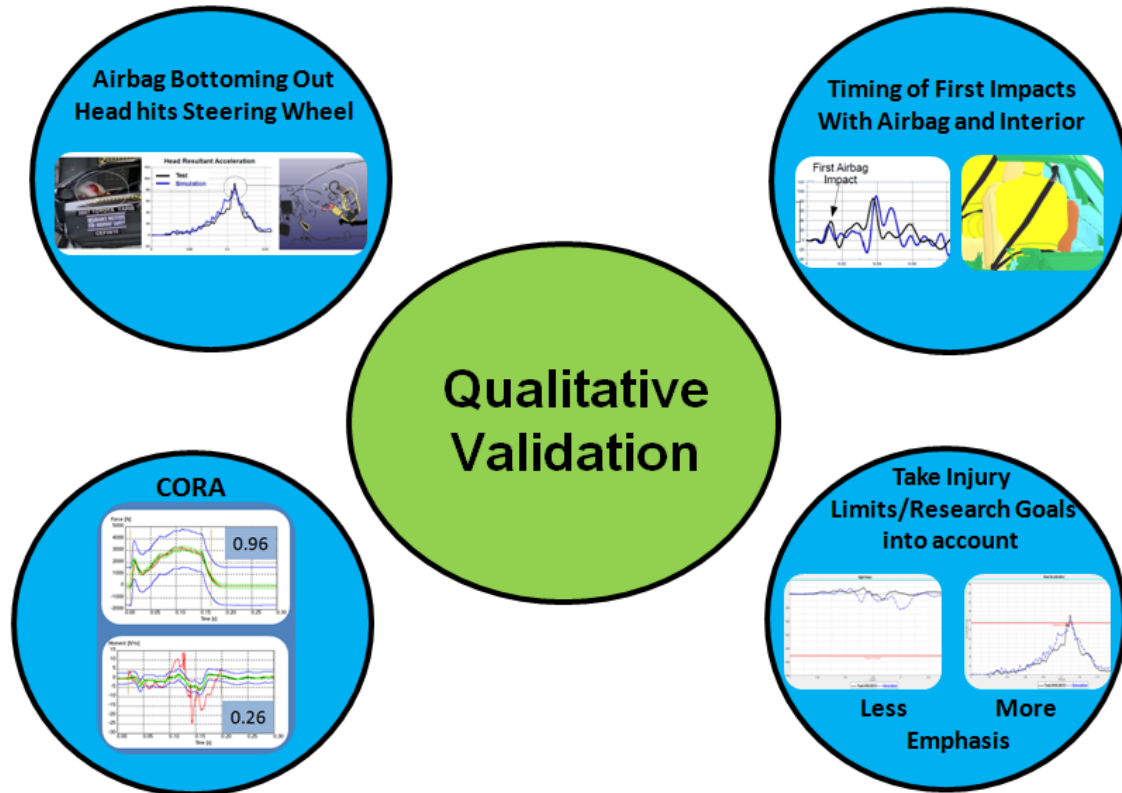
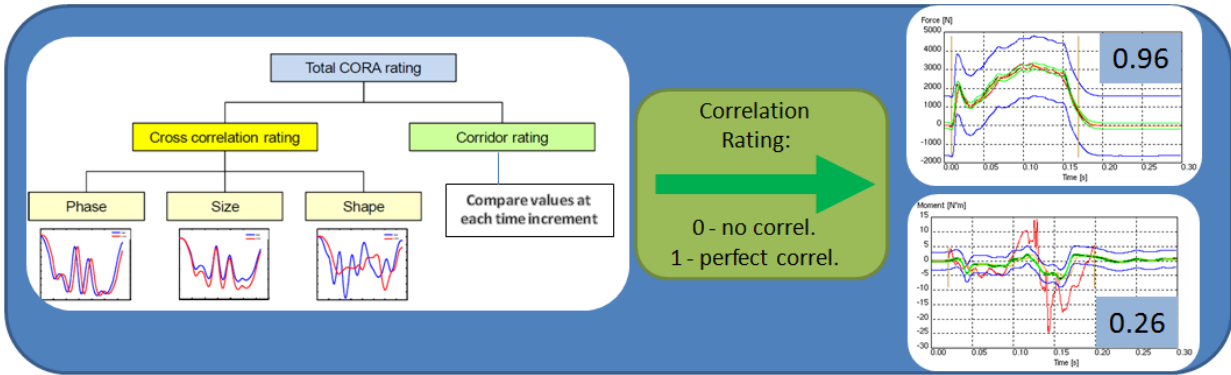


Figure 15: Qualitative validation

1.5.3 CORA

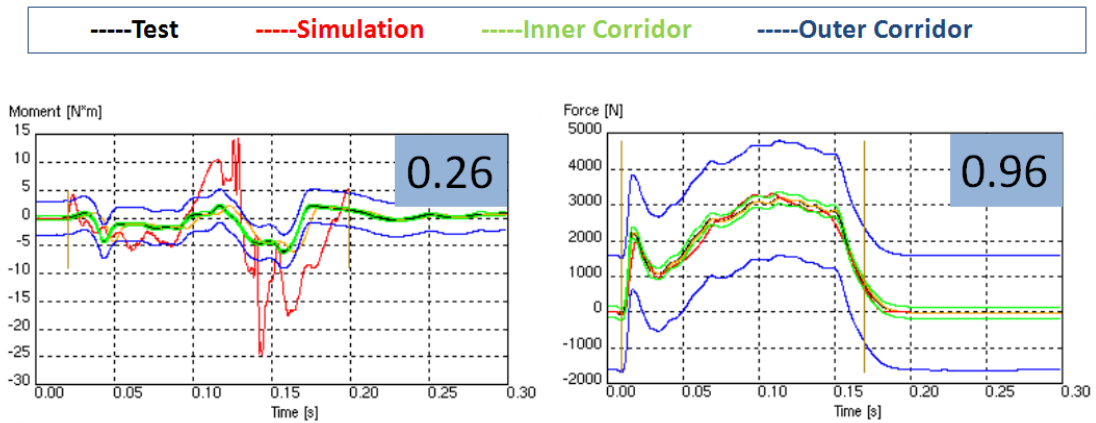
Figure 16 below shows how the software tool CORA compares and rates two curves. CORA was developed by the Partnership for dummy technology and biomechanics (PDB) and takes phase shift, size, shape, as well as the comparison of values at each time increment into account. Using these techniques, an "objective rating" is given which indicates how well a curve (e.g., simulation) compares to a reference curve (e.g., test). Rating results range between 0 and 1, where 0 means no correlation and 1 means (close to) perfect correlation.



CORA can be used to give an “objective Rating” how a curve (e.g. simulation) compares to a reference curve (e.g. test)

Figure 16: CORA rating

Figure 17 shows two general examples of curve comparisons using CORA. Inner and outer corridors are depicted in green and blue, respectively. The example on the left shows a test result in black and a simulation curve in red. A correlation rating of 0.26 was given by CORA, and therefore the correlation can be judged as poor. The example on the right shows an example where test in black and simulation in red correlate very well and a close-to-perfect rating of 0.96 was given.



Example of a poor (left) and close to perfect (right) correlation

Figure 17: CORA examples

CORA also can be used to evaluate how well results from one test compare to results from another test. Figure 18 below shows how the two available NCAP full overlap tests compare for the different body regions'

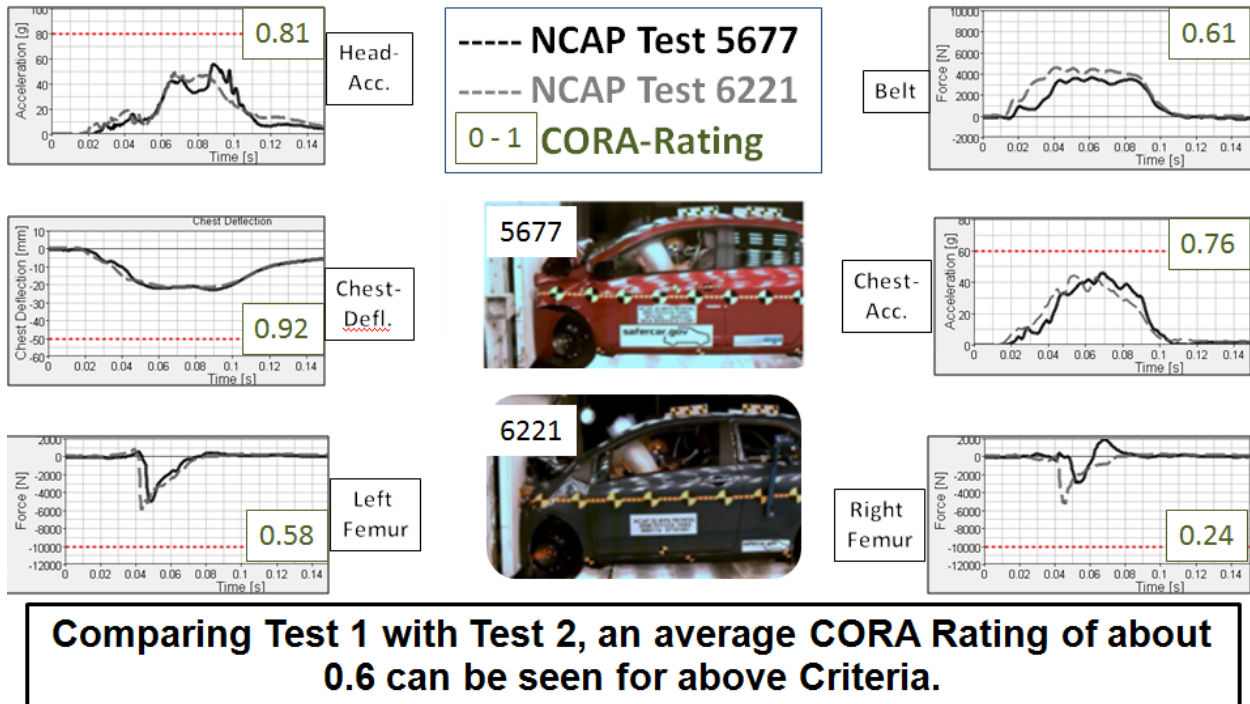


Figure 18: CORA evaluation of two NCAP tests

1.5.4 Quantitative comparison

In addition to overall and qualitative comparison of test and simulation results, quantitative comparison was used. General examples of quantitative evaluation of test and simulation results are shown in Figure 19. The IIHS Rating chart which normalizes the absolute injury values of the different body regions is one example of comparing the peak numbers for a test and simulation. NHTSA regulation and rating summary tables with the most important occupant results next to the respective simulation results also can be used for this purpose. Finally dummy plots using colors for the different body regions according to the occupant results and the defined injury thresholds, as used by Euroncap, can be used to compare test and simulation results.

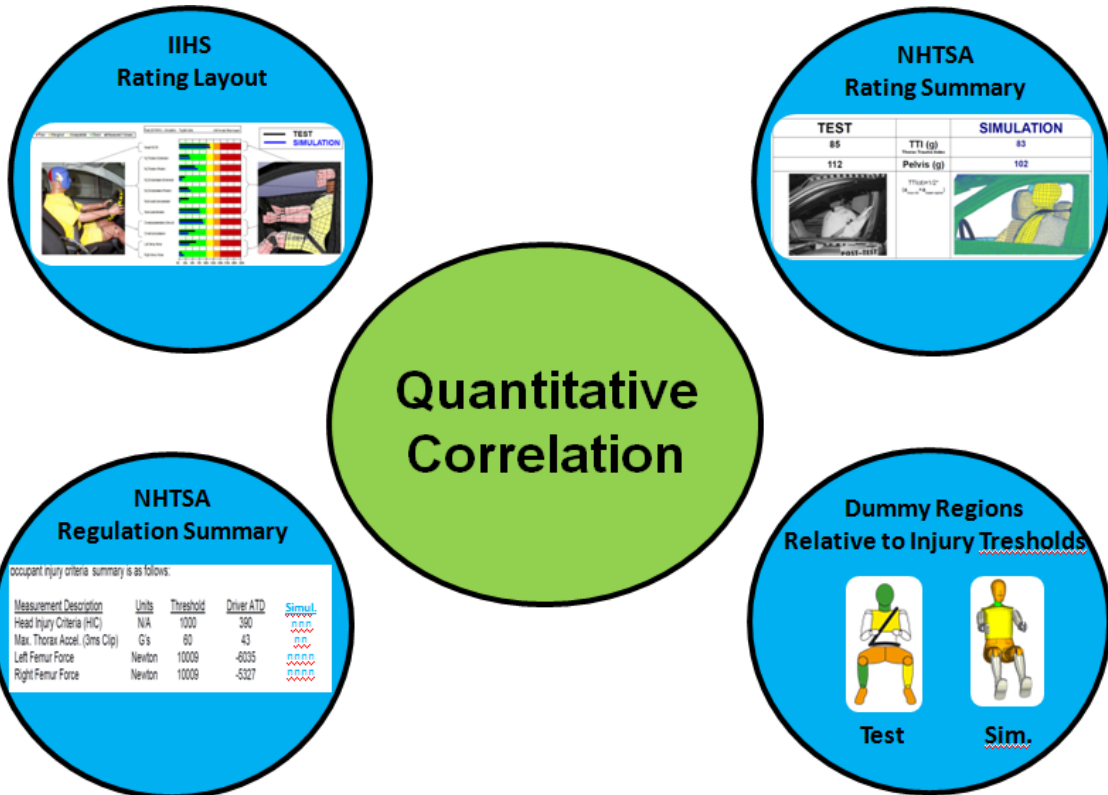


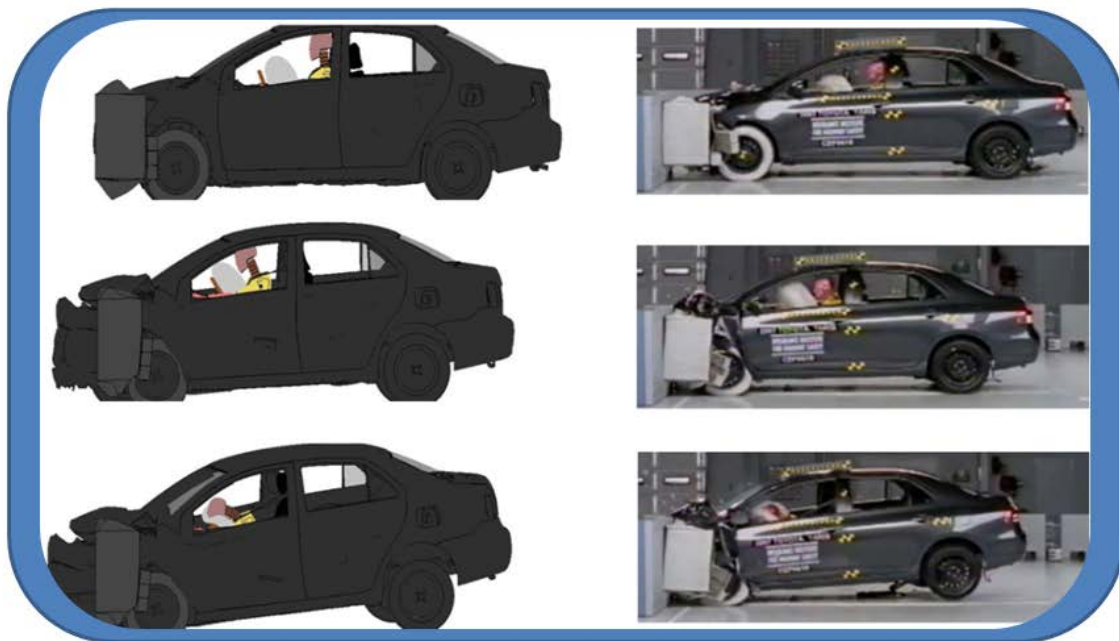
Figure 19: Quantitative validation

1.6 IIHS frontal offset configuration results

Simulation results of the 64km/h 40-percent overlap IIHS load case and comparison with results from the available full-scale crash test are described in this chapter.

1.6.1 IIHS overall comparison of test and simulation

Figure 20 shows a portrayal of the overall evaluation. Finite-element simulation results can be seen on the left and test results on the right. After the occupant interacts with the restraint systems, air bag bottoming out (i.e., a contact of the head with the steering wheel through the air bag occurred) can be observed in both the simulation and test.



Overall Comparison of Simulation with Test-0610

Figure 20: Overall validation

1.6.2 IIHS qualitative comparison of test and simulation

Figure 21 shows the qualitative comparison of test and simulation results together with the corresponding CORA rating values. Head and chest acceleration, which are the most critical injury values, have the highest correlation of 0.84 and 0.82, respectively. Chest deformation, neck, and femur have lower correlation ratings. At the same time, values for both test and simulation are clearly below critical injury thresholds as defined by the IIHS rating.

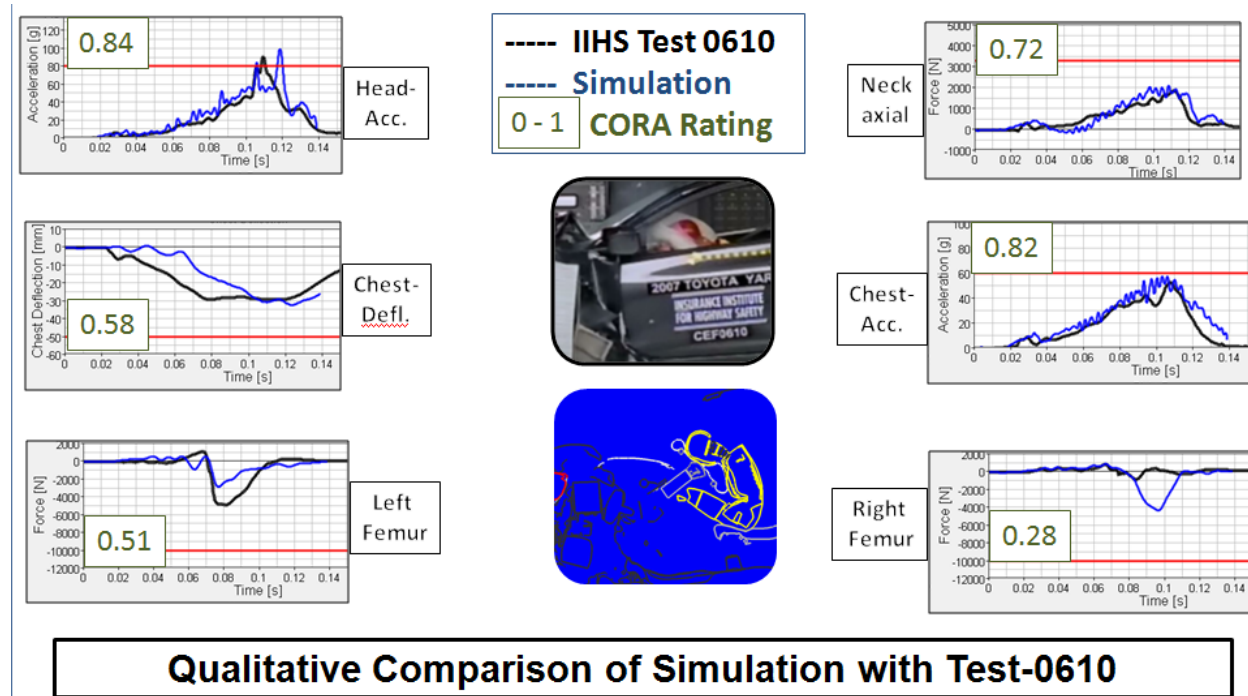
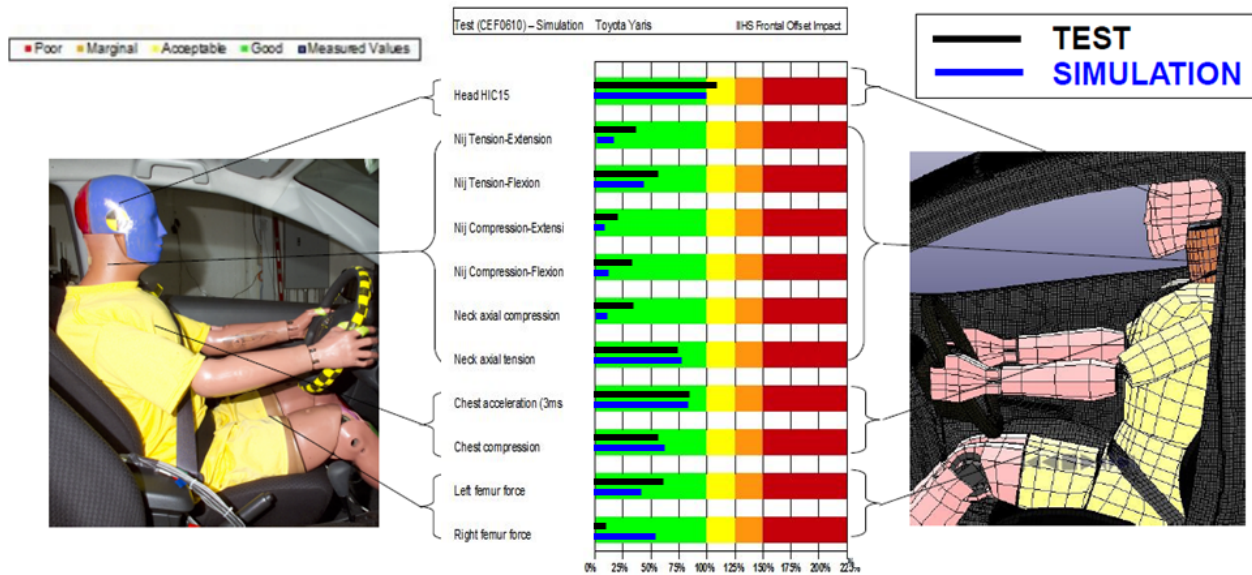


Figure 21: IIHS qualitative evaluation

1.6.3 IIHS quantitative comparison of test and simulation

Figure 22 shows the quantitative comparison of test and simulation results according to a normalized rating chart used by the IIHS. Test values are shown in black and simulation values are shown in blue for the different injury criteria. Again, it can be seen that the correlation between test and simulation is best for the most critical body regions, and less emphasis was placed on values that are clearly below the border between a good (green) and an acceptable rating (yellow).



Quantitative Comparison of Simulation with Test-0610

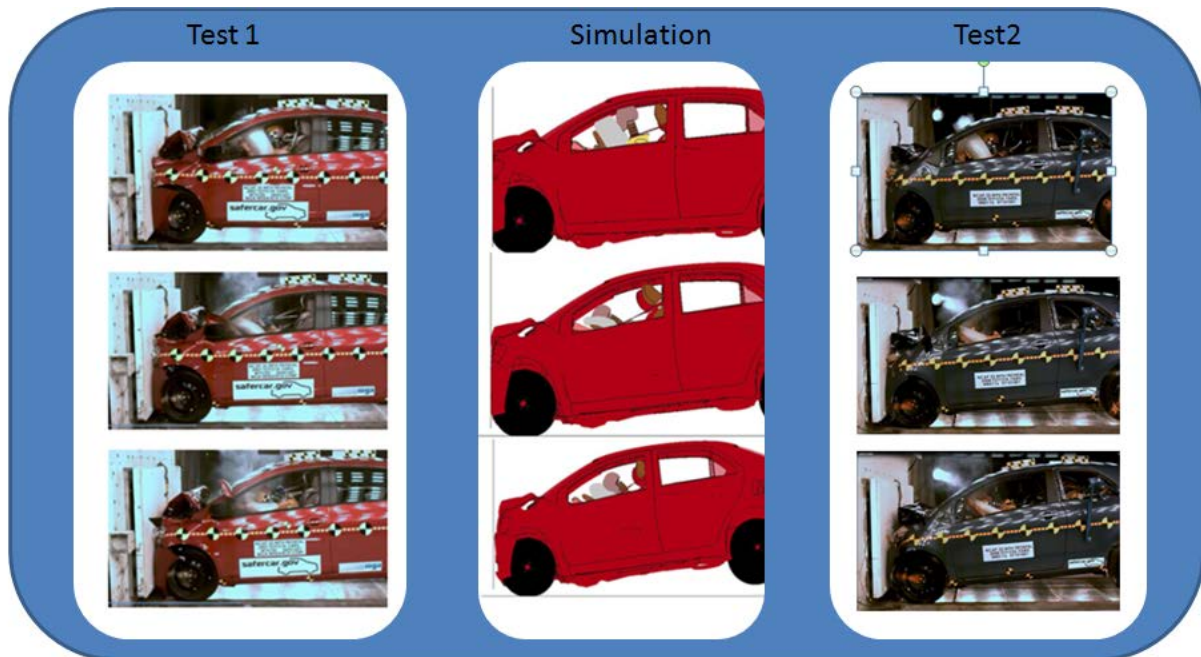
Figure 22: IIHS quantitative evaluation

1.7 NCAP frontal full overlap results

Simulation results for the 56km/h full overlap NCAP load case and comparison with results from available full-scale crash test results are described in this chapter.

1.7.1 NCAP overall comparison of test and simulation

Figure 23 shows a sequence of pictures of the NCAP full overlap crash event. Test 1 is shown on the left; simulation results are shown in the middle; and Test 2 is shown on the right. Vehicle and occupant kinematics compare well between the two tests and the simulation.



Overall Comparison of Simulation with Tests 5677 & 6221

Figure 23: NCAP overall evaluation

1.7.2 NCAP qualitative comparison of test and simulation

Figure 24 shows the qualitative comparison of test and simulation results. The average of the two available test results was used as a reference to calculate the CORA rating for the simulation time history plots. Head and chest ratings are around 0.7, and belt force characteristics are rated about 0.9. Femur loads which showed clear differences when compared with Test 1 and Test 2 consequently resulted in lower correlation rating. It must be noted again that femur loads for both tests and simulation are far below critical values as defined by NCAP risk curves.

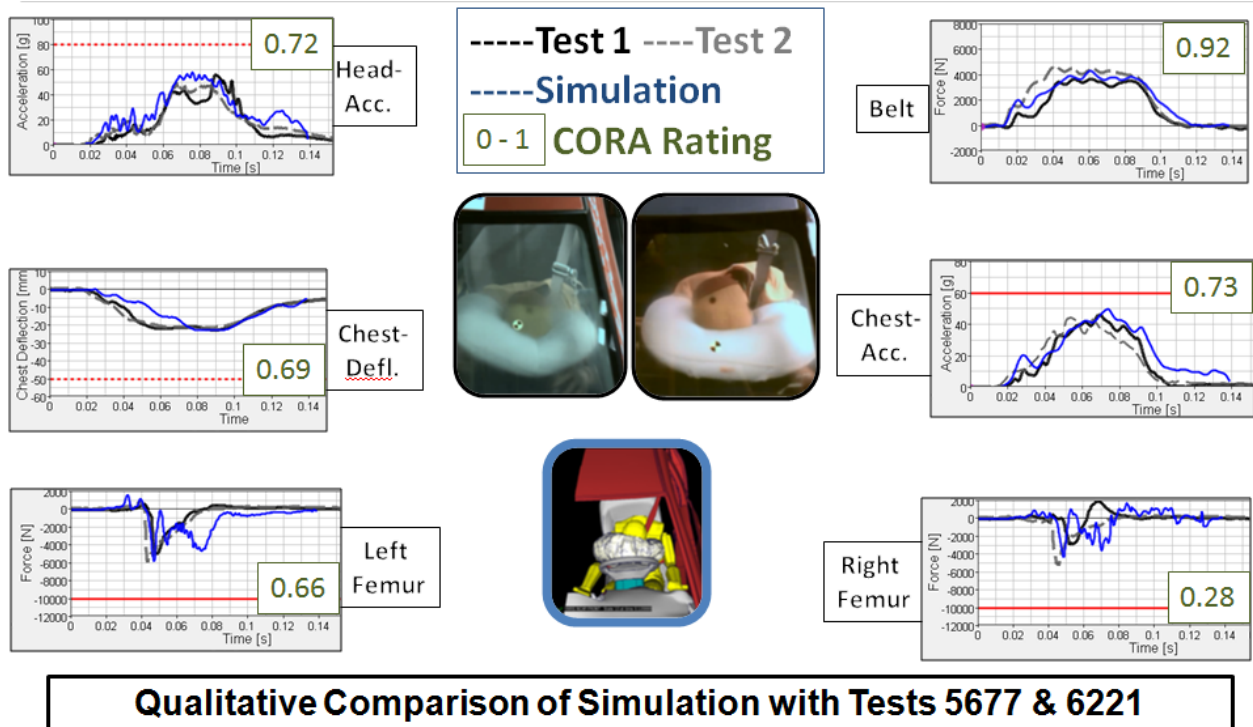
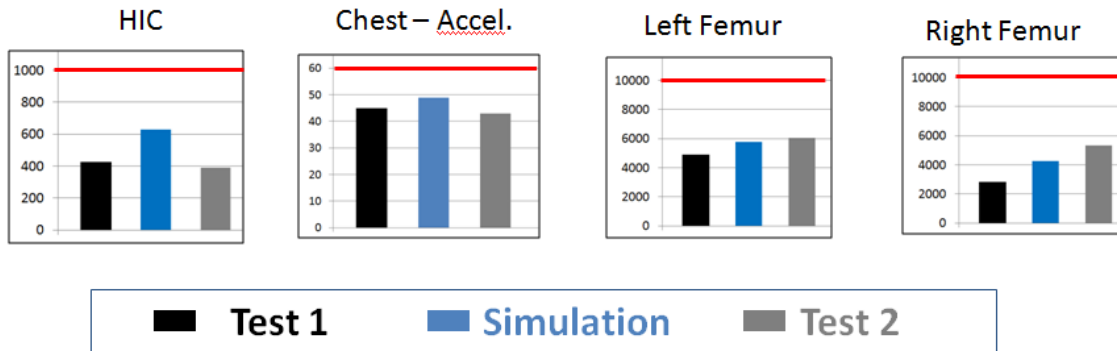


Figure 24: NCAP qualitative evaluation

1.7.3 NCAP quantitative comparison of test and simulation

Figure 25 shows the quantitative comparison of test and simulation results for the 56km/h full overlap crash into a fixed rigid barrier. Thresholds and absolute values for the different body regions in the two tests and the simulation can be seen in the first table. We note that the values for all body regions are below the red line representing the injury thresholds in the graphs below. While maximum femur loads in the simulation lie between the two test results, the simulation results for the chest and head are slightly higher than those in the two available full-scale crash tests.

Measurement Description	Units	Threshold	Test 1	Sim.	Test 2
			Driver ATD		Driver ATD
Head Injury Criteria (HIC)	N/A	1000	427	627	390
Max. Thorax Accel. (3ms Clip)	G's	60	45	49	43
Left Femur Force	Newton	10009	-4893	-5786	-6035
Right Femur Force	Newton	10009	-2829	-4261	-5327



Quantitative Comparison of Simulation with Tests 5677 & 6221

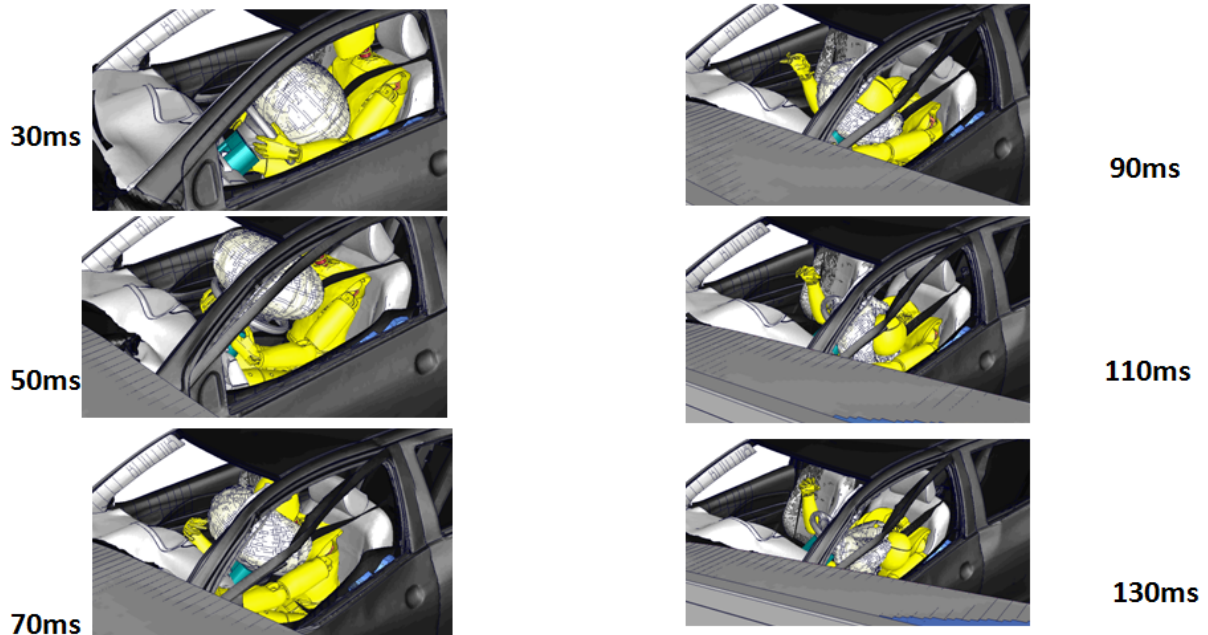
Figure 25: NCAP quantitative evaluation

1.8 Oblique load case results

Simulation results for the oblique frontal impact with a 50th percentile THOR dummy impacted by a moving deformable barrier at 90km/h, a 15-degree angle with a 35-percent overlap are described in this chapter. A model of the THOR dummy was used and positioned in the vehicle model according to the full-scale crash test. Results described in this chapter have been created using the original Toyota Yaris model. An updated structural model according to the vehicle used in the full-scale crash test and its effect on occupant kinematics and results are shown in Chapter 2 (sensitivity analysis). Structural failure of relevant parts was incorporated as described in Section 5.2.

1.8.1 Oblique load case overall evaluation

Figure 26 shows a sequence of simulation results capturing the tendency of the driver to move towards the space between the steering wheel/air bag and the door. The same kinematics can be observed in the available full-scale laboratory crash test.



The drivers head has a tendency to move towards the space between the steering wheel and the door.

Figure 26: Oblique load case overall evaluation

1.8.2 Oblique load case qualitative comparison of test and simulation

Figure 27 shows the qualitative comparison of the test and simulation results for the oblique frontal load case. A high peak in the head acceleration curve can be observed in the test at around 109ms. This peak occurred a little later and to a lesser extent in the original simulation. It is seen later in this report that when using the modified structural vehicle model, the timing of this peak was captured very closely. Using the test and simulation results, it was determined that this peak was caused by an interaction of the head of the THOR dummy with its upper left arm. Correlation ratings using CORA for the different body regions and seat belt forces can also be seen in the figure below.

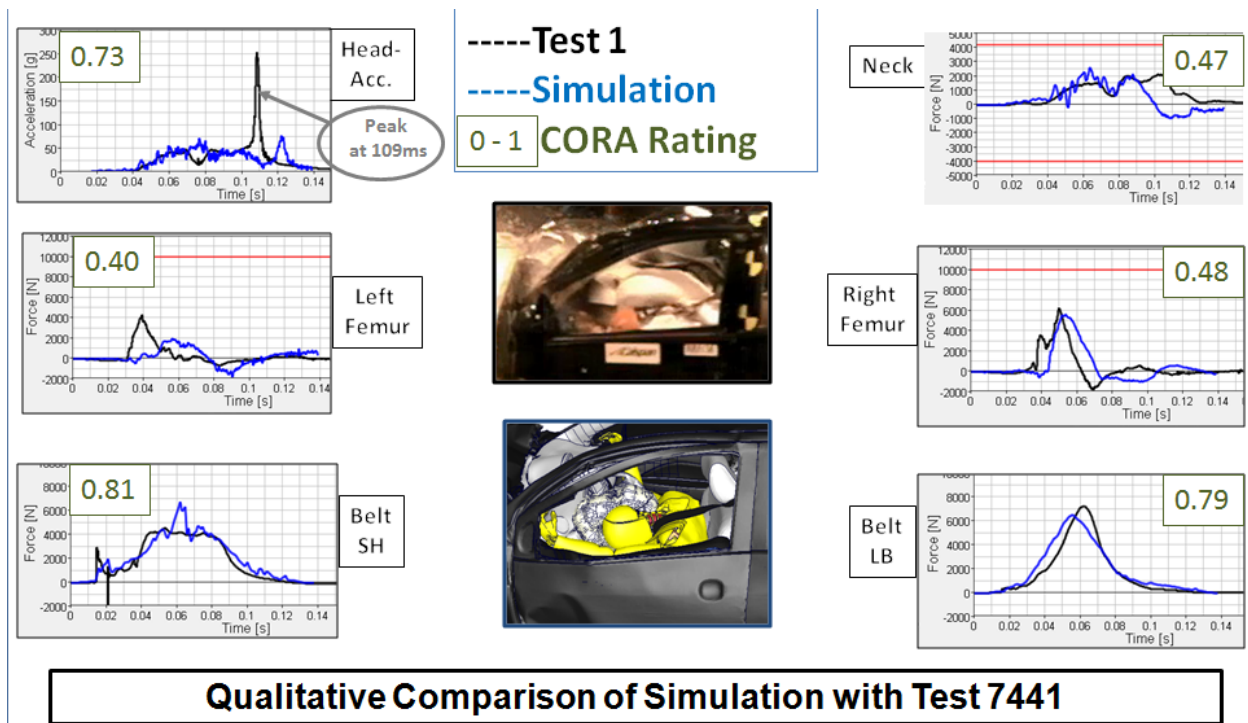


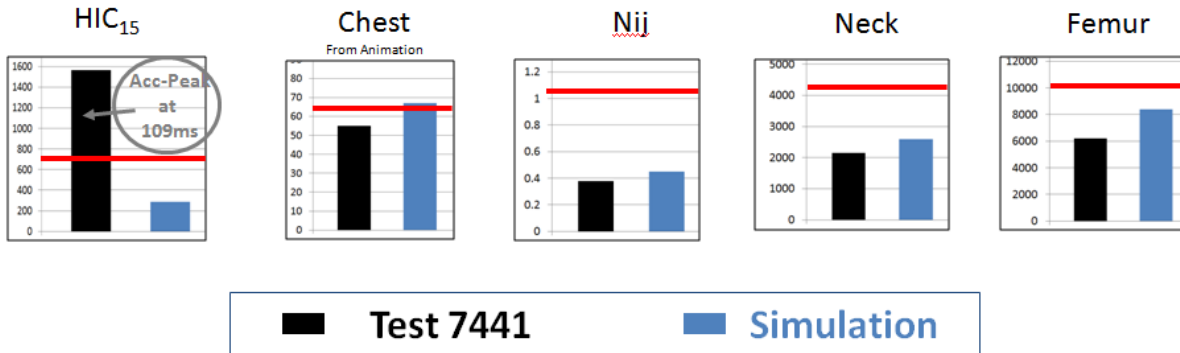
Figure 27: Oblique load case qualitative evaluation

1.8.3 Oblique load case quantitative comparison of test and simulation

Figure 28 shows the quantitative comparison of test and simulation results. The first table includes the thresholds for the different body regions, as tabulated in the test report summary, and the respective occupant loads as seen in the full-scale crash test and in the simulation. We note that chest, neck, and femur loads are clearly below the threshold values for both test and simulation. Although a contact of the head with the upper arm occurred in the simulation, the head HIC value which was clearly above the limit (depicted as a red line in the graph below) in the available full-scale crash test was not captured in the simulation using the original Yaris

model. A much closer correlation of the head using a modified structural model of the Yaris is described in Chapter 2 of this report.

Measurement Description	Driver A		Test	Simulation
	Units	Threshold		
Head Injury Criteria (HIC ₁₅)	N/A	700	1563.50	289
Maximum Chest Compression	mm	63	54.94	67
Nij	N/A	1.113	0.38	0.45
Neck Tension	N	4,170	2149.15	2602
Neck Compression	N	4,000	-393.95	-959
Left Femur Force	N	10,008	-4351.16	-1969
Right Femur Force	N	10,008	-6221.03	-8391



Quantitative Comparison of Simulation with Test 7441

Figure 28: Oblique load case quantitative evaluation

1.9 Conclusion Subtask I

In Subtask I, an integrated vehicle-occupant model for occupant safety analysis was developed with relevant interior components, generic restraint system components, and respective occupant models.

The developed model was extensively validated using three different load cases — IIHS 40-percent offset, NCAP full overlap, and 15-degree oblique 35-percent offset impact — using full-scale test data. Eleven accomplishments are summarized below:

1. Development of relevant interior and restraint system models: air bag, belt, collapsible steering column;
2. Enhancement and adaption of available occupant models;
3. Use of seat squash, belt fit, and tree file for positioning;
4. Available THOR model successfully used in full vehicle environment;
5. Outline of 3 level validation procedure;
6. Use of objective correlation tool (CORA);
7. Full vehicle-occupant simulation as well as sub-model procedure developed;
8. IIHS: evaluation of simulation results using full-scale test data used;
9. NCAP: evaluation of simulation results using full-scale test data;
10. Oblique: evaluation of simulation results using full-scale test; and
11. Results of IIHS, NCAP, and 90km/h oblique offset load case.

V Subtask II

2. Sensitivity Analysis

2.1 Methodology

Relevant parameters regarding the vehicle environment, seating position, seat belt, air bag, and steering column attributes were defined and examined one parameter at a time (i.e. when changing the seating position, all other parameters, such as original impact speed were unchanged), as shown in Figure 29. Sensitivity analyses were performed for all three load cases (NCAP, IIHS, and oblique) with the respective occupant models (HIII and THOR). Fully integrated occupant-vehicle models were used for all sensitivity analyses. The objective of this subtask was to evaluate and understand how sensitive and robust the occupant results were to the variation of the defined parameters, which go beyond the boundary conditions that have been defined during the validation process using results from available full-scale crash tests. The intent of the sensitivity analyses was to show that the developed models produce realistic results for these parameter variations. For example when changing the vehicle impact speed, higher occupant loads would be expected for higher impact speeds. Results for other parametric studies sometimes are not as intuitive in both test and simulation. However, possible relationships of cause versus effect were analyzed and discussed for all studied parametric studies. An additional sensitivity analysis using the THUMS model is described in Subtask III (use and evaluation of different occupant models).

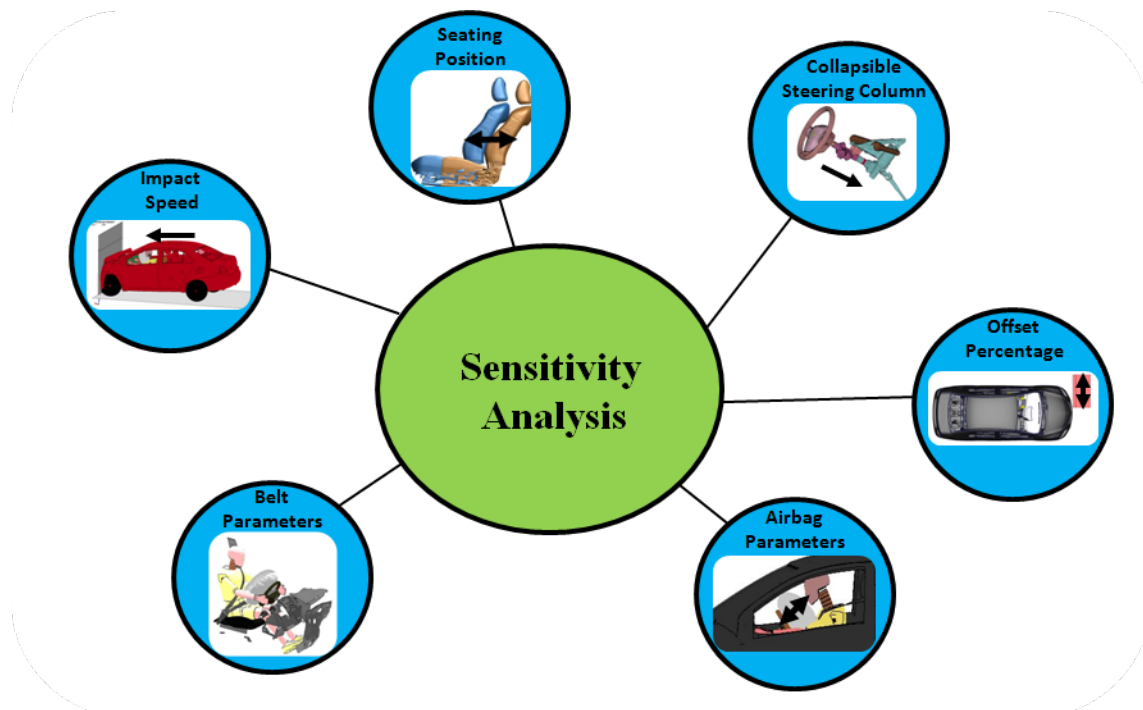


Figure 29: Sensitivity analysis parameters

Effects due to the variation of defined parameters were analyzed using overall evaluation, qualitative evaluation, and quantitative evaluation as depicted in Figure 30.



Figure 30: Sensitivity analysis methodology

In the overall evaluation, differences in vehicle and occupant kinematics as well as changes in restraint system characteristics were analyzed. The qualitative evaluation compared injury curve characteristics and timing of distinct crash events for the various parameter studies. Finally, absolute values for the head, neck, chest, and femur were analyzed in the quantitative evaluation. The risk functions⁸ used to calculate the probabilities for AIS > 3 and AIS > 2 injuries for the respective body regions are documented in Figure 31.

⁸ NHTSA, “New Car Assessment Program,” Docket No. NHTSA-2006-26555, 120 pp., July 11, 2008

Body region	Risk function
Head	$P_{\text{head}}(\text{AIS} \geq 3) = \Phi\left[\frac{\ln(\text{HIC}_{15}) - 7.45231}{0.73998}\right]$ <p>where Φ = cumulative normal distribution (e.g., use NORMDIST(LN(cell), 7.45231, 0.73998, 1) in Excel)</p>
Neck	$P_{\text{neck}}(\text{AIS} \geq 3) = 1/[1 + e^{(10.9745 - 2.375 * F)}]$ <p>where F = either axial tension or axial compression in kN</p>
Chest	$P_{\text{chest}}(\text{AIS} \geq 3) = [1 + \exp(12.597 - 0.05861 * 35 - 1.568 * \delta^{0.4612})]^{-1}$ <p>where δ = Hybrid III 50th % male chest deflection in mm</p>
KTH	$P_{\text{KTH}}(\text{AIS} \geq 2) = [1 + \exp(5.7949 - 0.5196 * F_{\text{femur}})]^{-1}$ <p>where F_{femur} = femur force in kN</p>



Risk functions used to evaluate injury risks for the head, neck, chest, and femur/KTH of the Hill dummy

Figure 31: Injury risk functions

2.2 Sensitivity analysis using NCAP load case

Figure 32 shows the different parameter variations simulated and evaluated using the NCAP full overlap load case. Sensitivity analyses regarding the variation of impact speed, different seating position modifications, air bag, seat belt, and steering column characteristics were performed.

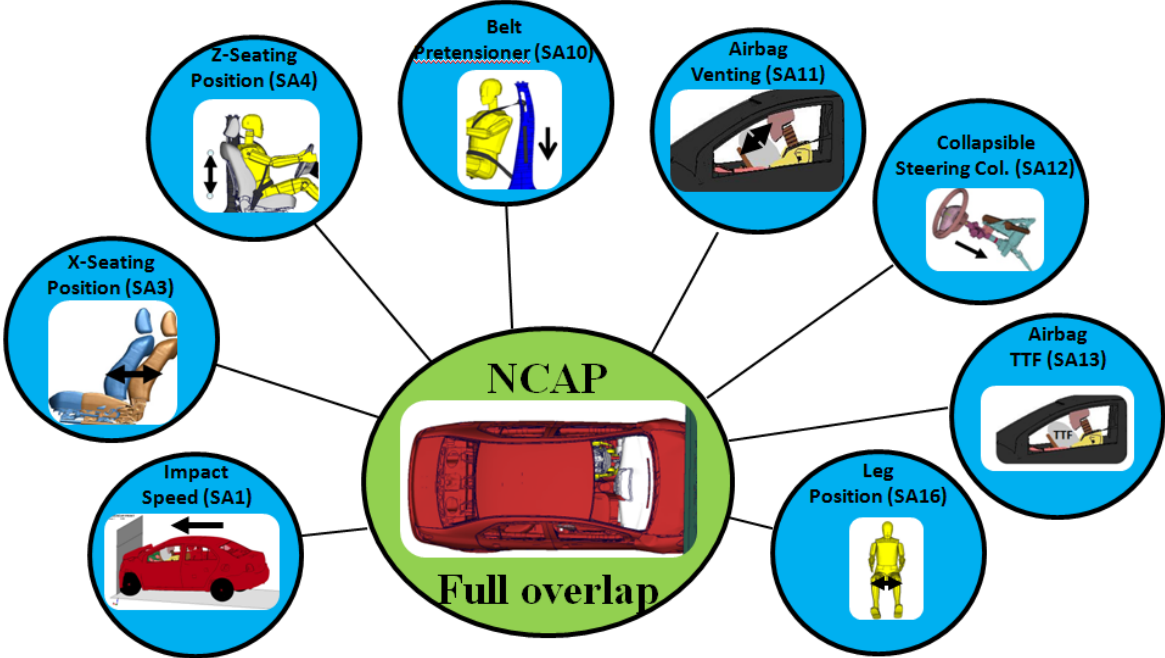


Figure 32: NCAP parameters

2.2.1 Variation of impact speed

In the first sensitivity analysis, the vehicle impact speed was reduced from 56 km/h to 48km/h and 40km/h. Figure 33 shows a time history plot of the chest deflection and the absolute values for head, chest, neck, and femur loads together with the respective injury risk probabilities using the risk function described in Figure 31 above. As expected, the developed integrated vehicle-occupant model predicts that the higher the impact speed the higher the occupant loads for all body regions.

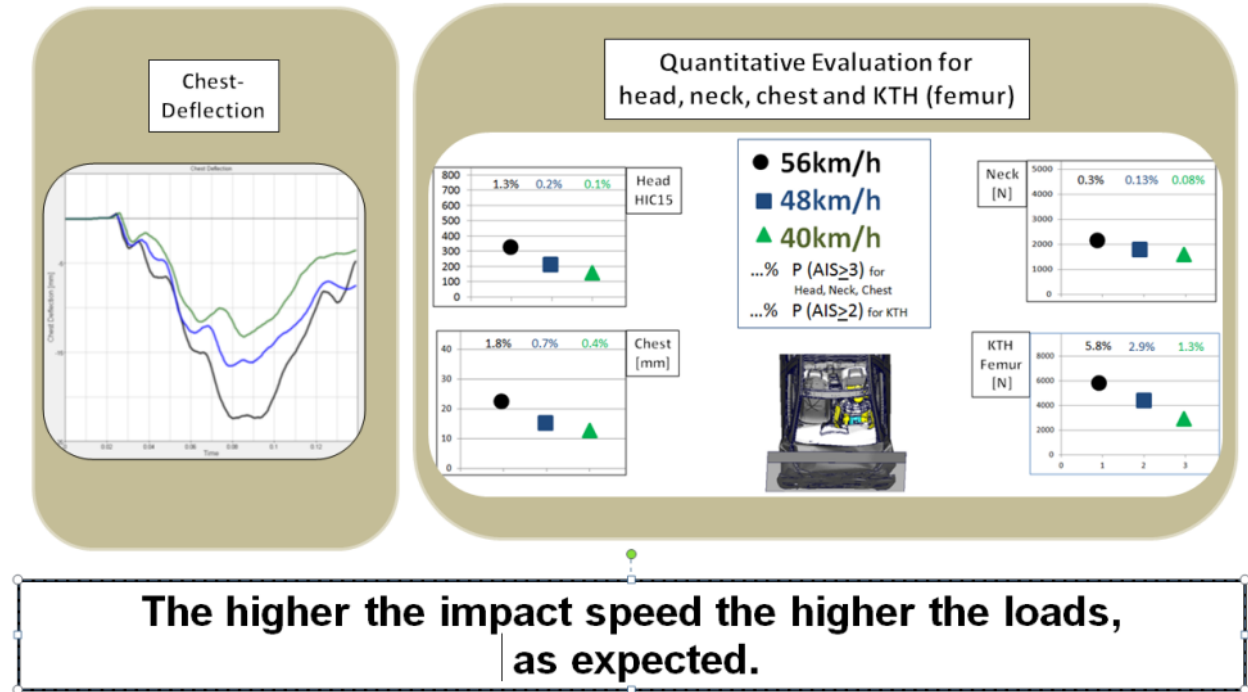


Figure 33: NCAP variation of impact speed

2.2.2 Variation of x-seating position

The effect of variation of the longitudinal seating position was studied. Using the NCAP seating position test procedure, where the occupant was positioned 25mm further aft and a seating position where the occupant was sitting 25mm more forward (or closer) to the instrument panel were compared to the original seating position. All other parameters, such as original NCAP speed were unchanged. Figure 34 shows the comparison depicting the further aft (or "more back") position in blue, the original seating position in black, and the "closer to IP" position in green. Note that occupant loads were similar for all body regions with slightly higher values for the further aft position where the dummy could reach a little higher momentum before interaction with the air bag, steering wheel, and instrument panel.

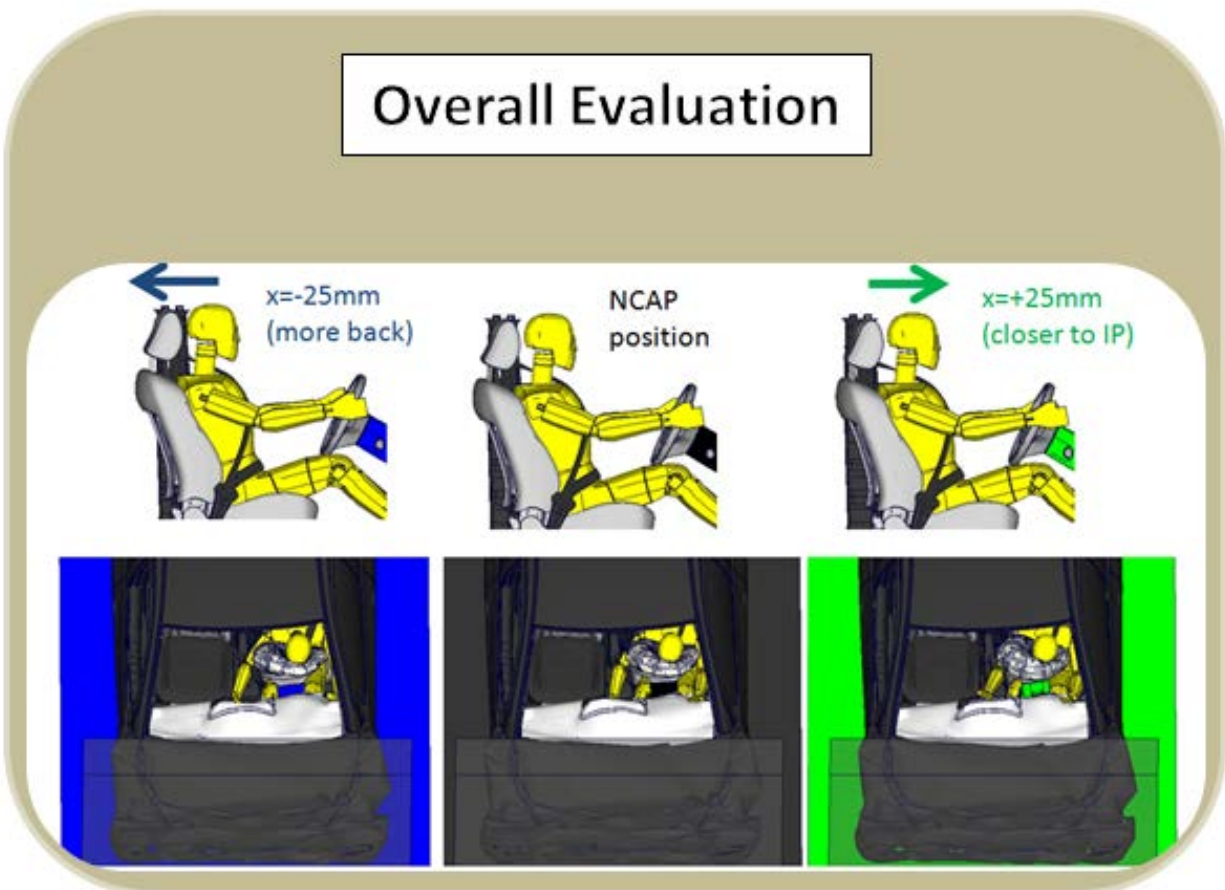
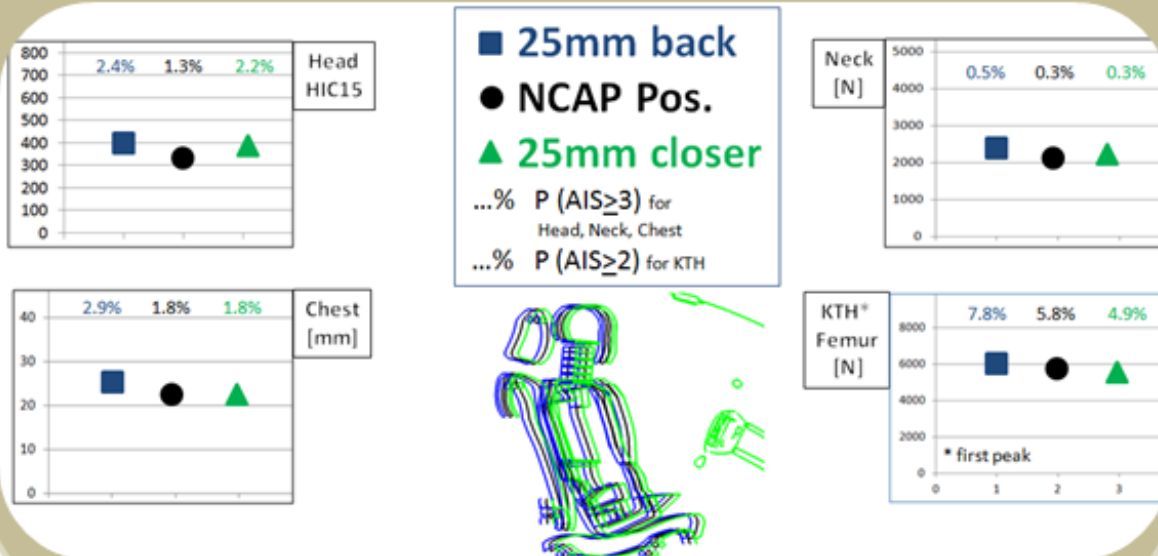


Figure 34a: NCAP variation of x-seating position - overall evaluation

Quantitative Evaluation for head, neck, chest and KTH (femur)



Similar values with slightly higher peaks for “back” position where occupant can reach higher momentum.

Figure 34b: NCAP variation of x-seating position - quantitative evaluation

2.2.3 Variation of seating height

The effect of variation of vertical seating height was studied for the NCAP full overlap load case. The original seating height was compared to a 5mm higher and a 20mm higher seating position. While the 5mm difference can be considered as a very small variation, which is within the tolerance when positioning a dummy in a full-scale crash test, the 20mm higher seating position is of a magnitude where effects to the occupant results can be expected. Figure 35 shows the original seating position in black, the 5mm higher position in blue, and the 20mm higher position in green. As expected almost no differences in occupant loads were caused by changing the seating height by a small amount of 5mm. However, differences can be noticed for the 20mm higher position due to different occupant-seat-belt-air-bag-IP interactions.

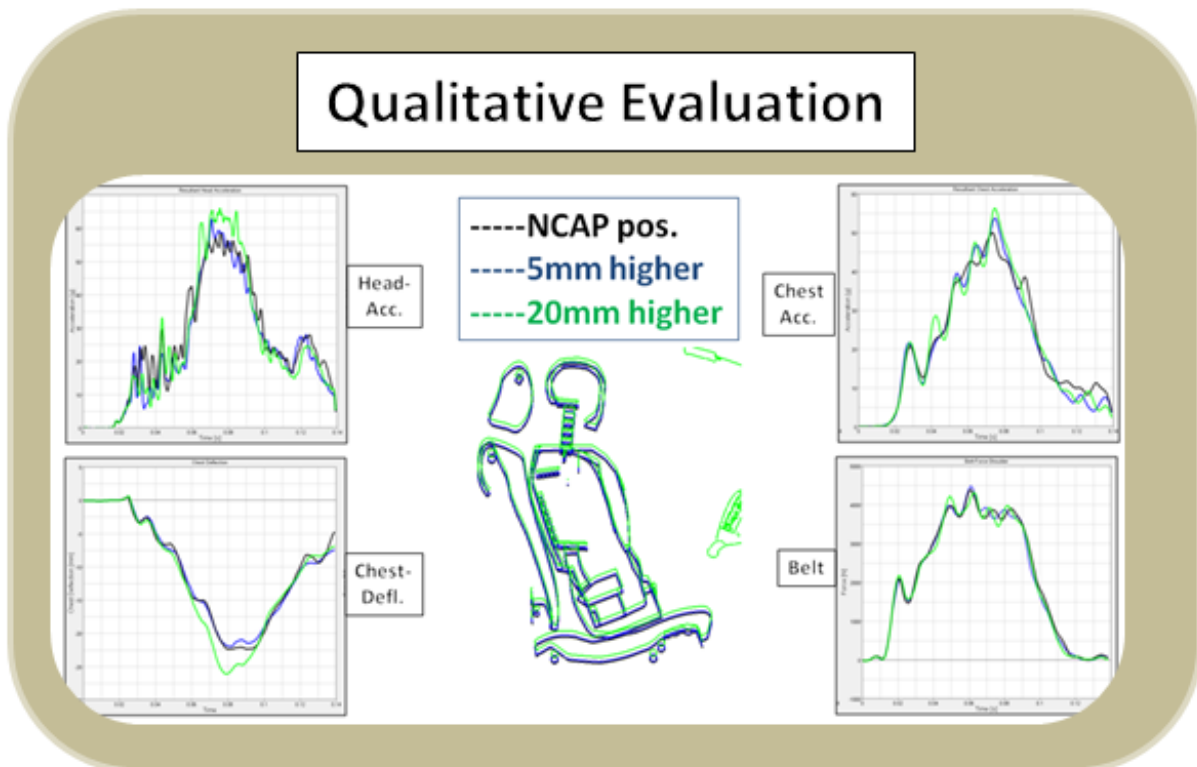
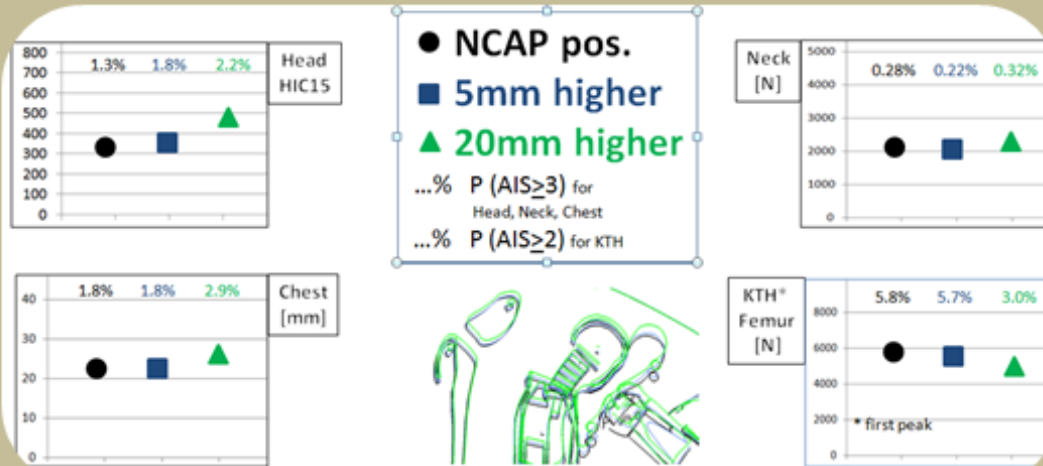


Figure 35a: NCAP variation of seating height - qualitative evaluation

Quantitative Evaluation for head, neck, chest and KTH (femur)



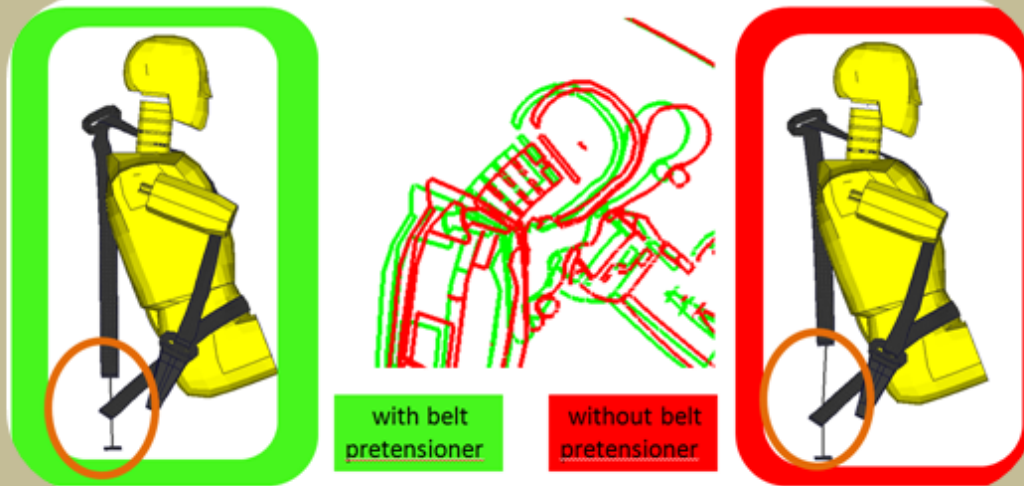
Almost identical values for 5mm higher seating position. 20mm higher position shows effects due to different occupant - seat belt - airbag interactions

Figure 35b: NCAP variation of seating height - quantitative evaluation

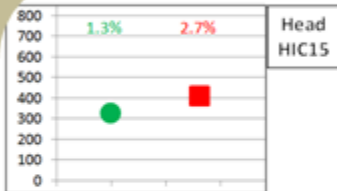
2.2.4 Seat belt with and without pre-tensioner

Figure 36 shows the effect of the pre-tensioner in the NCAP load case. While the seat belt is tightened in the early phase of the crash event in the simulation with a pre-tensioner, shown in green, no belt is being reeled in when the pre-tensioner is not fired, depicted in red. As expected, higher occupant loads can be noticed without a pre-tensioner where the seat belt dummy coupling (i.e., vehicle ride down) is not as effective. Consequently, without the pre-tensioner, more forward displacement occurred. As a result, the head, neck, and femur loads increased without the use of the seat belt restraint system feature.

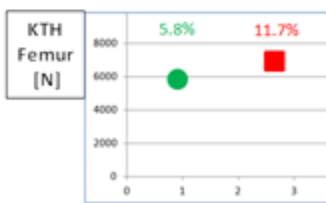
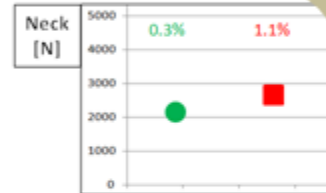
Overall Evaluation



Quantitative Evaluation for head, neck, chest and KTH (femur)



● with belt pretensioner
■ without pretensioner

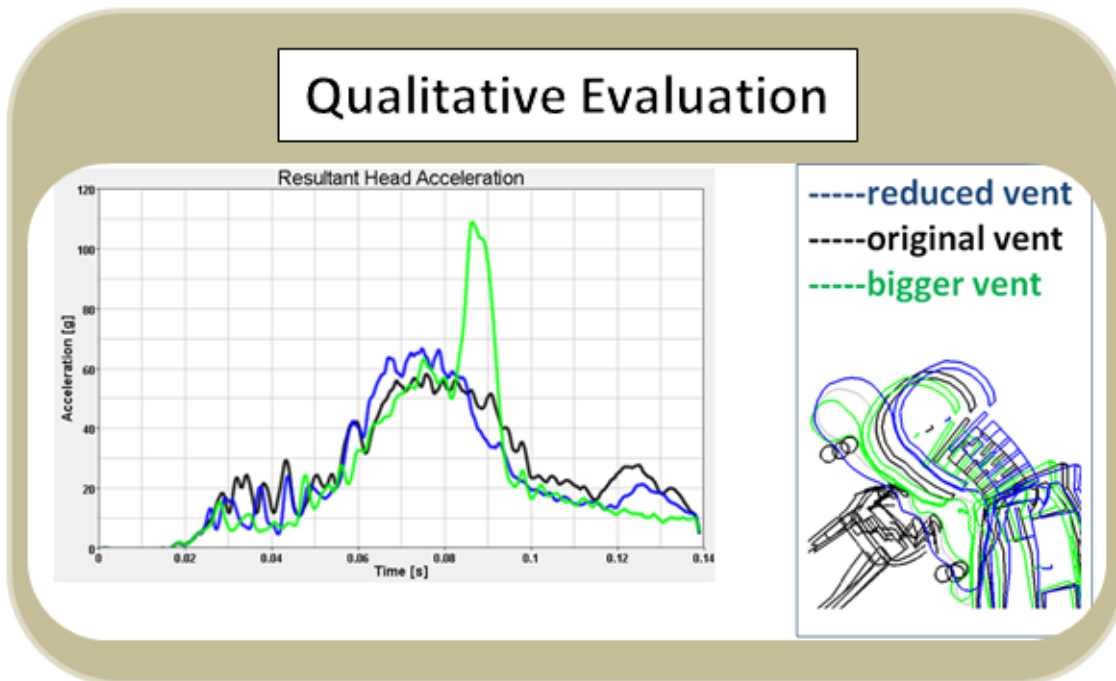


Simulation without pretensioner allows more occupant forward displacement and shows higher head, neck, and femur loads

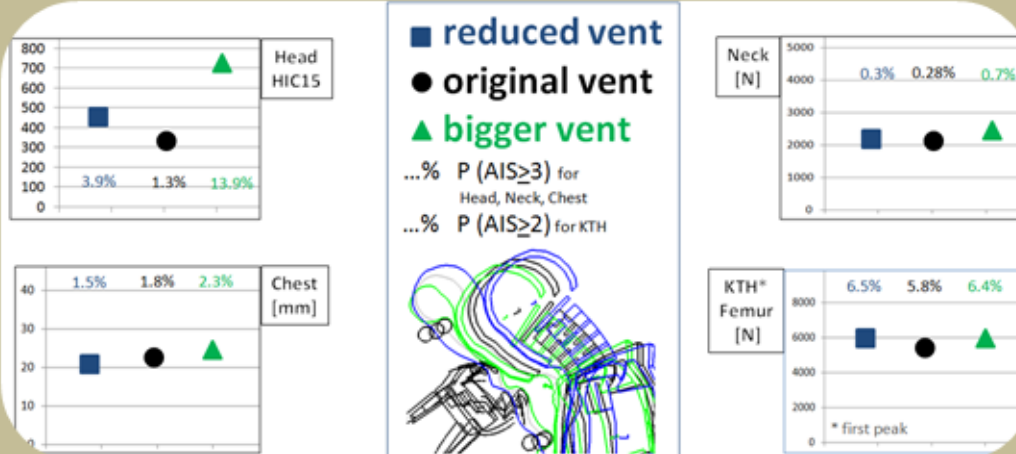
Figure 36: NCAP belt with and without pre-tensioner

2.2.5 Variation of air bag venting

The effect of variation of air bag venting and consequently of different air bag internal pressure characteristics were evaluated using the NCAP load case. The diameter of the vent hole of the original model, which was validated against full-scale crash tests, was both reduced and increased by 5mm. Figure 37 shows the results for the original vent in black, for the reduced vent diameter in blue, and for the bigger vent diameter in green. While injury risks for the neck, chest and femur did not show high sensitivity, the head showed the most interesting response due to the change of air bag venting. The simulations showed that the air bag with the original vent allowed a close-to-perfect forward displacement of the head. Most of the available distance between the occupants head and the steering wheel was used and no air bag bottoming out could be seen in either the test or simulation results. The air bag with the reduced vent resulted in a "stiffer" (i.e., higher pressure) air bag. The available space between the dummies head and the steering column was not used to such an extent as with the original model, and the head did not "dive" (i.e., was not cushioned as much) into to air bag as much. This resulted in a higher HIC15 value and therefore a higher injury risk for the head. The simulation with the bigger air bag vent diameter resulted in a "softer" air bag with less internal pressure during the critical time of impact. The green-colored, head acceleration curve on the left shows a distinct high peak between 80ms and 90ms, which was caused by direct contact of the head with the steering wheel hub due to the air bag bottoming out.



Quantitative Evaluation for head, neck, chest and KTH (femur)



Differences can especially be noticed for the head. Both variations cause higher values. The stiffer airbag because it allows less head forward displacement and the “softer” airbag because it allows bottoming out and contact with the steering wheel.

Figure 37: NCAP air bag venting

2.2.6 Variation of steering column collapse

Besides constructing generic air bag and seat belt restraint system models with a pre-tensioner and belt force limiter, a generic collapsible steering column model was developed for the integrated occupant-vehicle model. In the original simulation run, which was validated using the available information from full-scale crash tests, about half of the available steering column collapse was actuated by the occupant. In the second simulation, the force level was reduced to allow the collapse of a steering column uses the entire available striking distance of about 90mm along the steering column axis away from the occupant, depicted in blue in Figure 38. In the third simulation, the force level was increased to a level where no steering column collapse could be observed at all, shown in green. It can be noticed that the head and chest values were higher for the case where no steering column collapse occurred, and that the sensitivity for the neck and femur loads was rather small (0.31% compared to the original 0.28% for the neck and 6.4% compared to the original 5.8% for the femur).

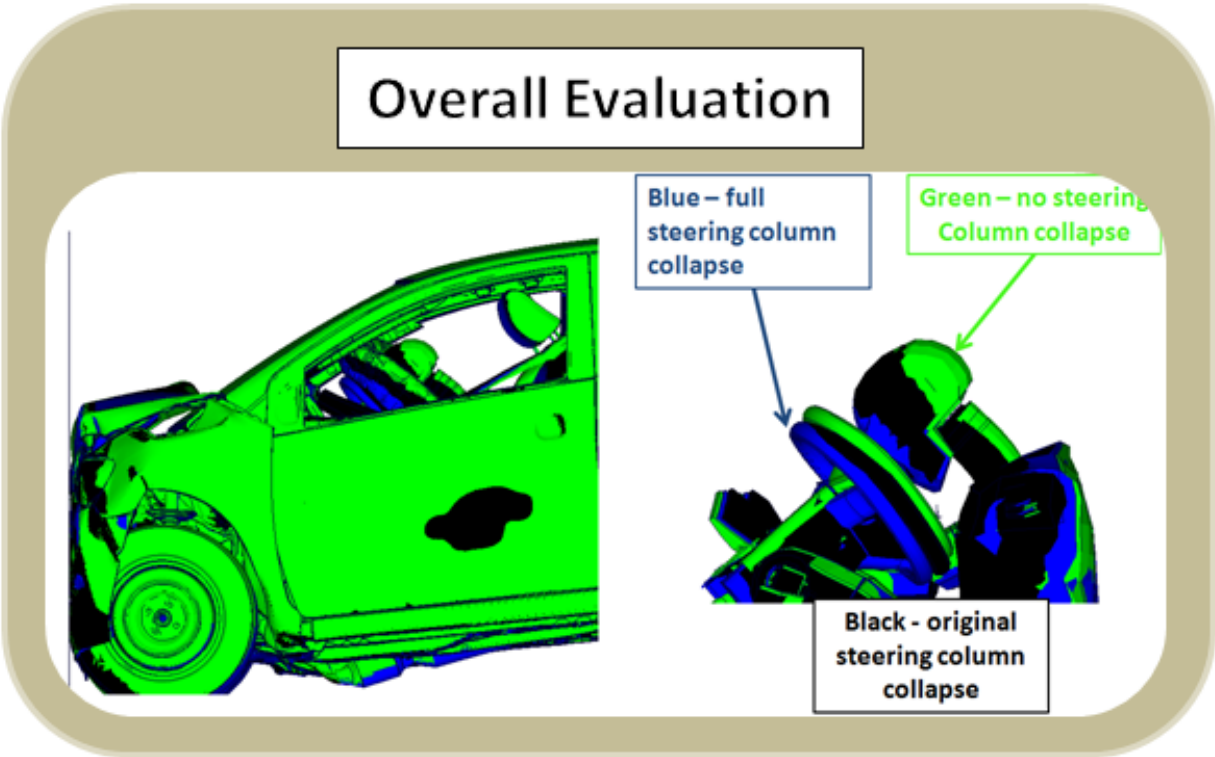
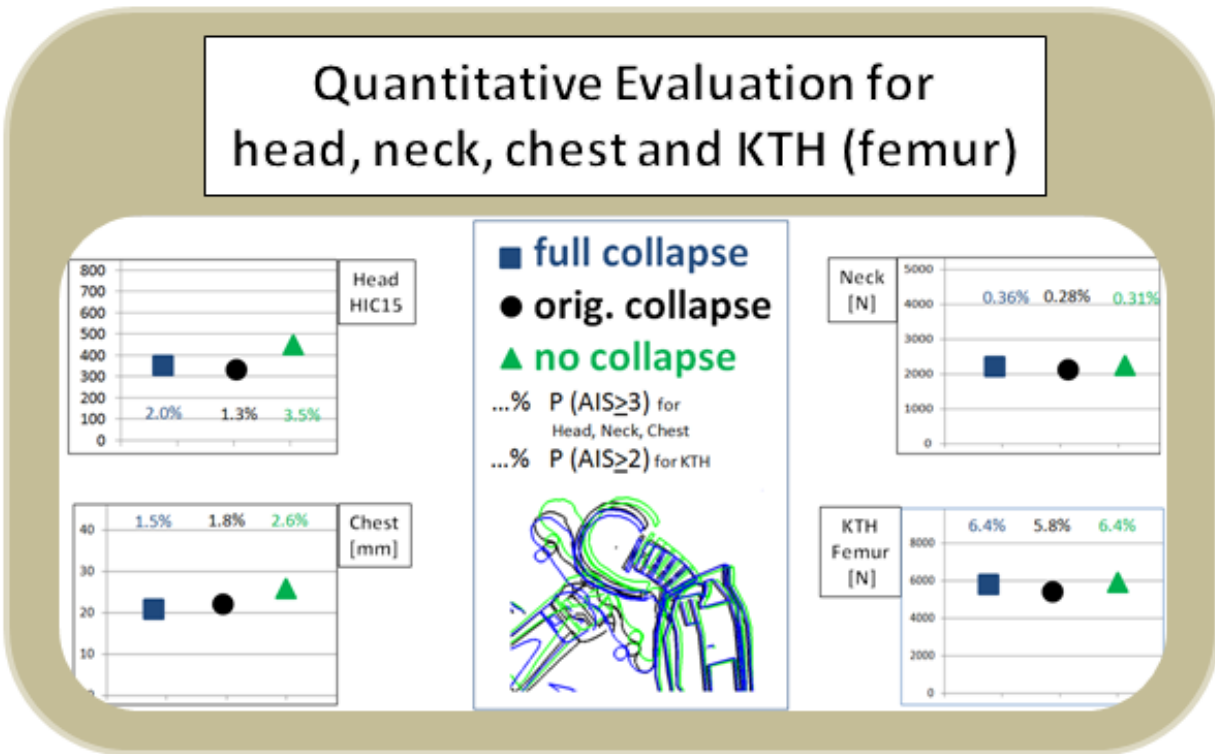


Figure 38a: NCAP steering column collapse - overall evaluation

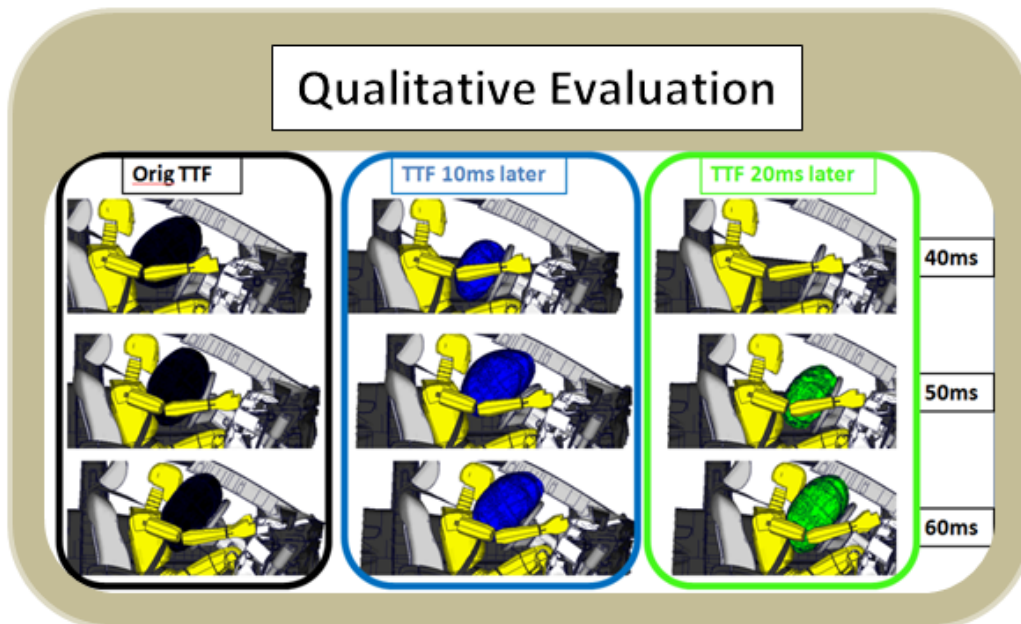


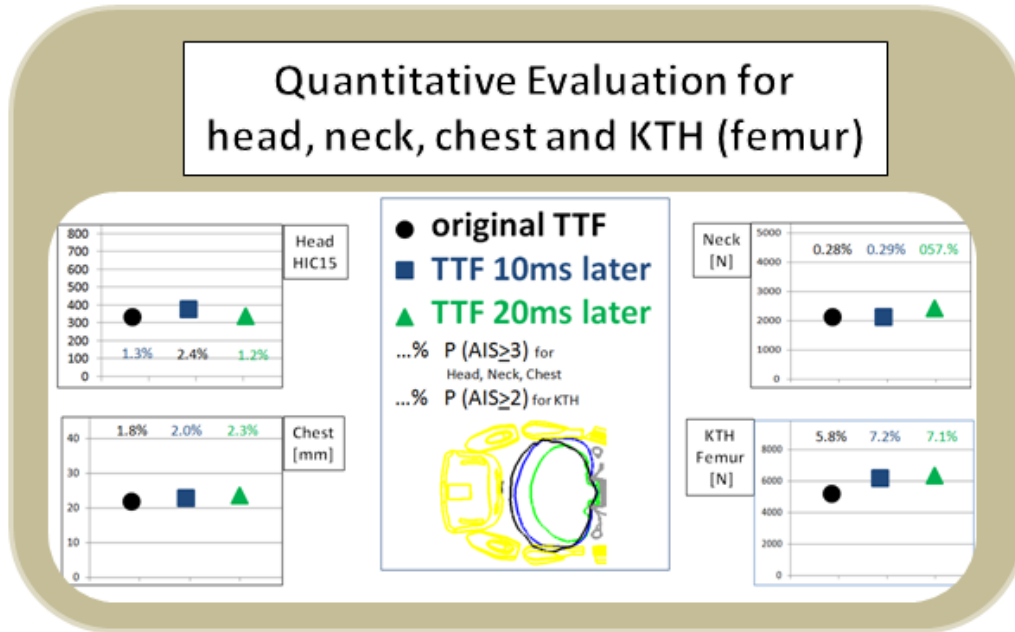
Main differences due to different amount of steering column collapse can be noticed in the head and chest where the values are the highest when no collapse occurs

Figure 38b: NCAP steering column collapse- quantitative evaluation

2.2.7 Variation of air bag time-to-fire

The amount of time between the first contact of the vehicle with the barrier and the beginning of the air bag inflation, called time-to-fire (TTF) was used as another parameter regarding air bag characteristics. The original air bag TTF, which was determined from the available full-scale crash tests, was used in the original simulation run, shown in black in Figure 39. Two more simulations were run using a TTF that was 10ms and 20ms later than that used in the original case, shown in blue and green, respectively. The effect of the different TTF can be clearly seen in the overall evaluation, as shown in the left picture of Figure 39. It can be noticed that femur loads were higher with a later air bag TTF due to the later coupling/interaction of the air bag with the occupant, and consequently a slightly more forward displacement and more severe interaction with the instrument panel and interior resulted.





Occupant loads are similar for all body regions. Femur loads are slightly higher in the simulations with later time to fire and consequently later coupling of the airbag with the occupant

Figure 39: NCAP air bag time-to-fire

2.2.8 Variation of leg position

In the final sensitivity analysis using the NCAP full overlap load case, the leg position was modified. The original leg position according to the available full-scale crash tests can be seen in black in Figure 40a. The distance of the left to the right knee in the two available full-scale crash tests was 320mm and 322mm, respectively. It is noted that the femur loads in the two tests showed different qualitative and quantitative characteristics, as described in section 1.7, which suggests that the underlying stiff structure was impacted differently. As a variation to the original leg position, the knees were moved 80mm closer together, shown in green. Differences in occupant kinematics and loads were observed. The pelvis moved not as much forward during right down. As a result head values were higher for the modified leg position. In addition, the femur loads reacted very sensitively to the modified leg position. Similarly, when comparing the two available NCAP full-scale crash tests where leg position was different within the occupant positioning tolerance, the two crash tests showed major differences in femur loads. This was due the different interaction points of the femur with the instrument panel, the steering column interior, and the underlying stiff structural parts, as shown in red below.

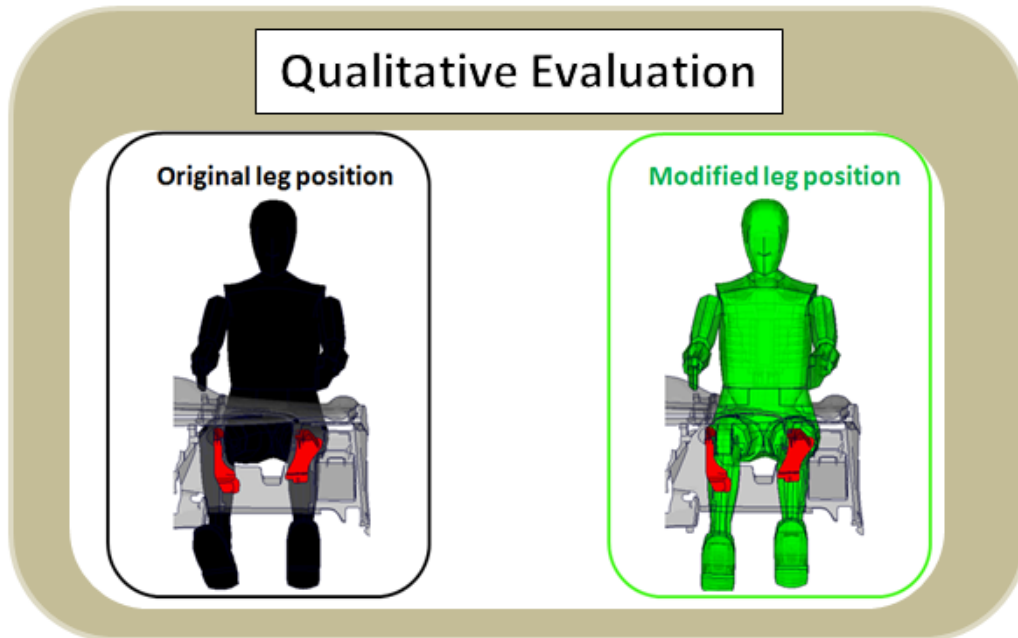
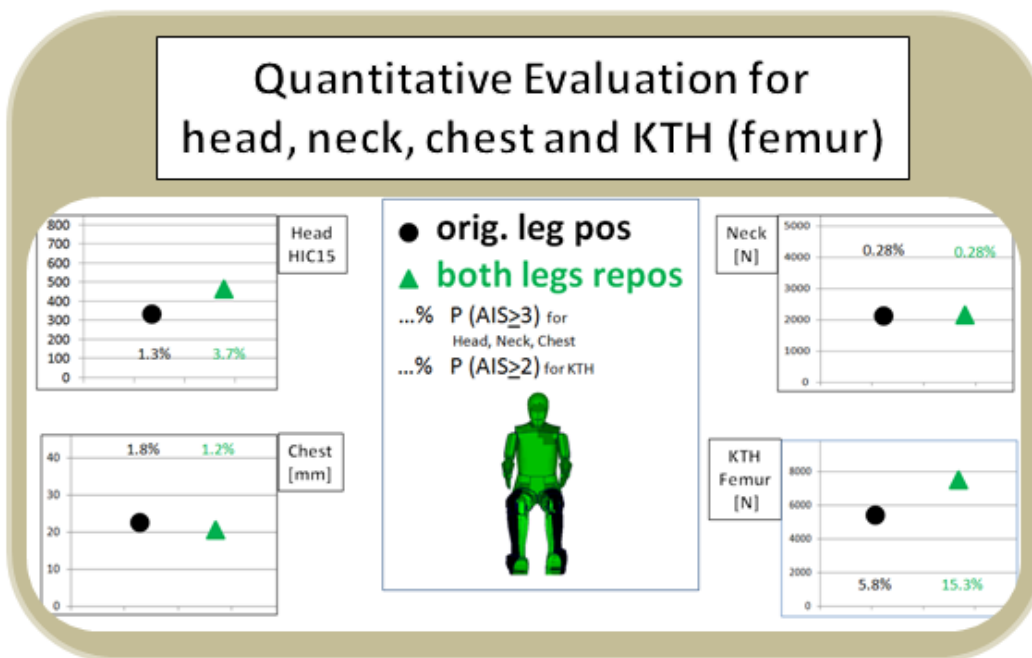


Figure 40a: NCAP leg position - qualitative evaluation



Femur loads and occupant kinematics are influenced by the leg position and their interaction with the instrument panel and the underlying structure.

Figure 40b: NCAP leg position - quantitative evaluation

2.3 Sensitivity Analysis using IIHS load case

Figure 41 shows the different parameter variations simulated and evaluated using the IIHS 40-percent frontal overlap load case. Sensitivity analyses regarding the variation of overlap percentage, impact speed, different seating position and occupant torso angle, air bag, and seat belt characteristics were performed.

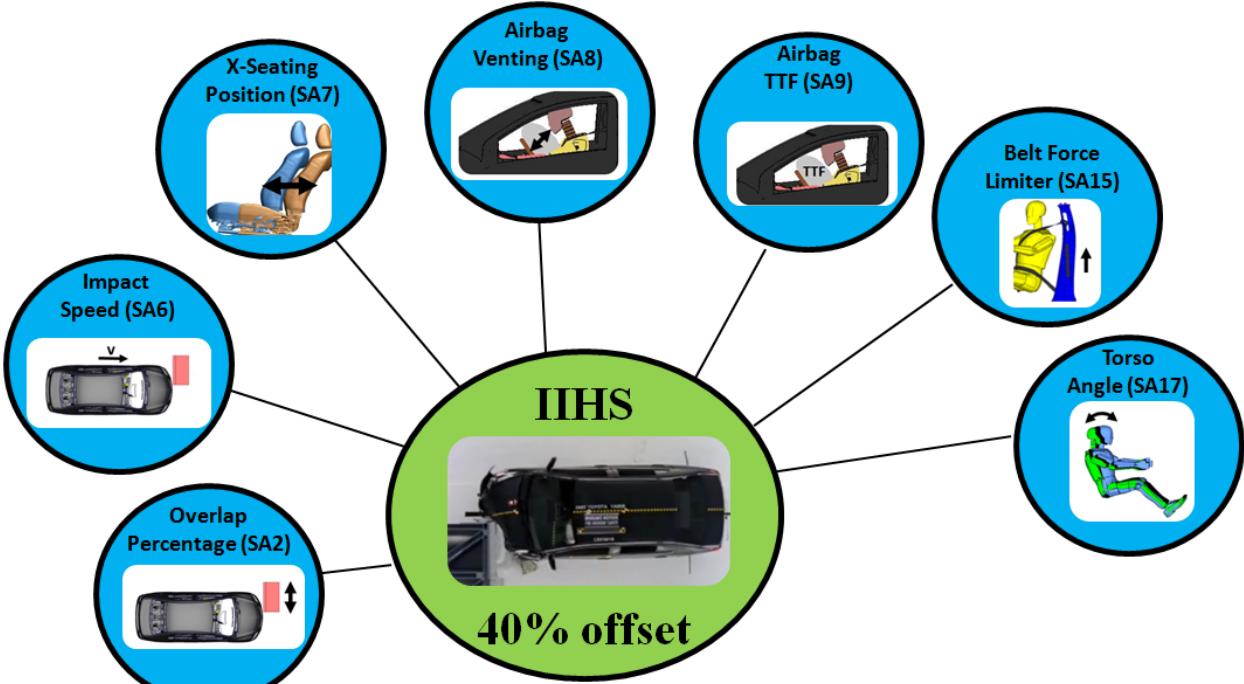
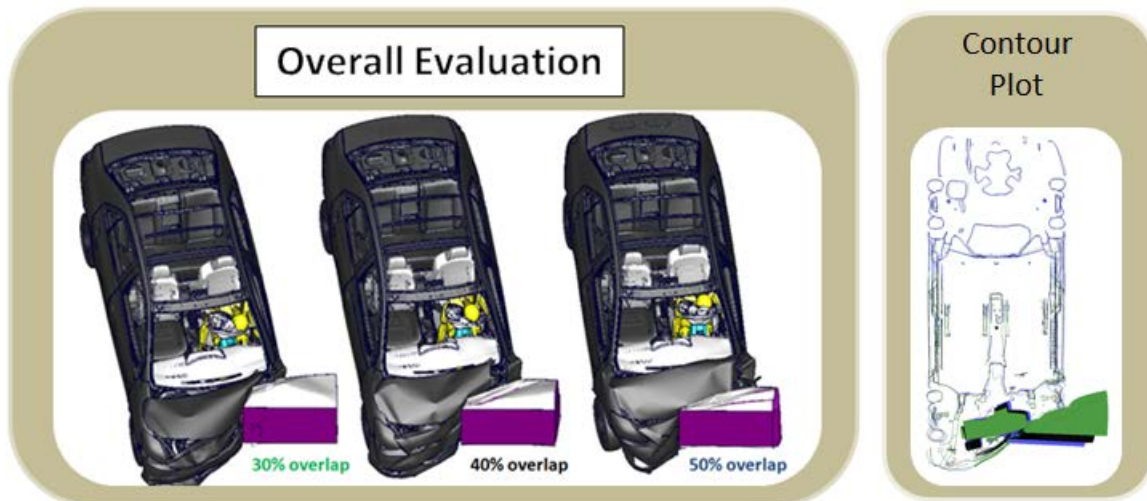


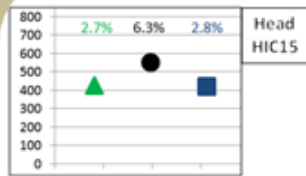
Figure 41: IIHS parameters

2.3.1 Variation of overlap percentage

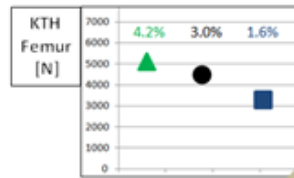
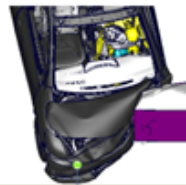
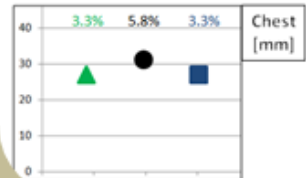
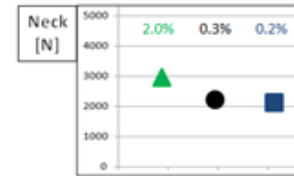
While the original IIHS simulation run used an overlap percentage of 40 percent of the vehicle with the deformable barrier according to the IIHS test protocol, a smaller overlap percentage of 30 percent (shown in green) and a bigger overlap percentage of 50 percent (shown in blue) in Figure 42 were performed. The differences in the overall vehicle kinematics can be seen in the left picture documenting the top view at around 120ms. In viewing Figure 42, it can be seen that the smaller the overlap percentage, the higher the rotation around the z-vehicle axis/ yaw motion. The picture on the right shows a contour plot of the structural deformation using a tracked view where the rear of the vehicle is overlaid. Again the 30-percent case is shown in green, the 40-percent case is shown in black, and the 50-percent case is shown in blue. Head and chest values were the highest for the 40-percent overlap case due to the respective vehicle and occupant kinematics causing different interactions of the HIII dummy with the belt, air bag, steering wheel, and instrument panel. Neck and femur loads were the highest for the smaller overlap percentage of 30 percent due to the different intrusion characteristics and occupant kinematics. From the left picture of Figure 42, it can be noticed that the head drifts more off the center of the steering wheel the smaller the overlap percentage is. This results in a higher forward head displacement and higher neck-tension forces.



Quantitative Evaluation for head, neck, chest and KTH (femur)



▲ 30% overlap
● 40% overlap
■ 50% overlap
 ...% P (AIS_{≥3}) for Head, Neck, Chest
 ...% P (AIS_{≥2}) for KTH



While the 30% offset run shows highest neck and femur loads, head and chest loads are the highest in the 40% IHS load case. Variation of overlap causes differences in vehicle & occupant kinematics and loads resulting in different interactions of HIII with belt, airbag, steering wheel, and IP.

Figure 42: IHS overlap percentage

2.3.2 Variation of impact speed

Figure 43 shows the effect of different vehicle impact speeds using the original 40-percent overlap IIHS load case. In addition to the impact speed of 64km/h according to the test protocol and available full-scale crash test, a 56km/h and a 48km/h scenario also were evaluated. The left picture shows the qualitative comparison of the three simulations and the right picture shows the quantitative evaluation, using black for the highest, blue for the middle and green for the lowest impact velocity. As expected, loads for all body regions were larger for the higher the impact velocities. It can be noticed that the high head acceleration peak in the original simulation, which was caused by a contact of the head with the steering wheel hub through the air bag (air bag bottoming out), did not occur anymore when reducing the impact velocity by 8km/h. In addition, as expected, the head contact with the steering wheel did not occur by the 16km/h reduced impact speed. The differences can also be observed by looking at the timing of the different body loads. The later "onset" of the time history curves for lower impact speeds can be noted in this context as well.

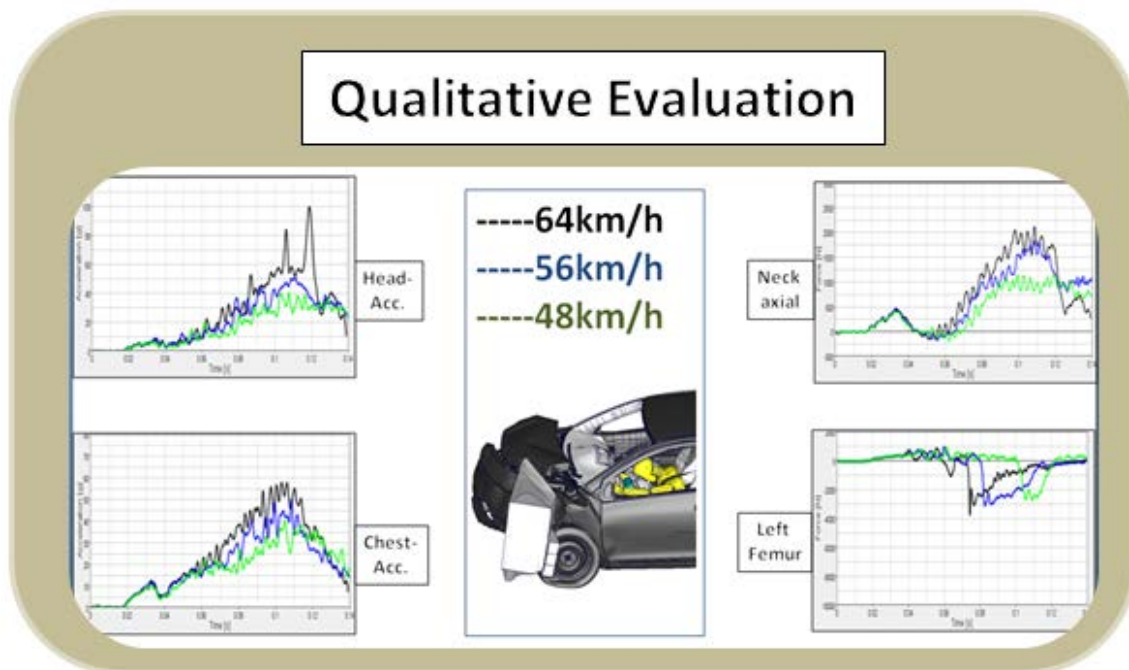
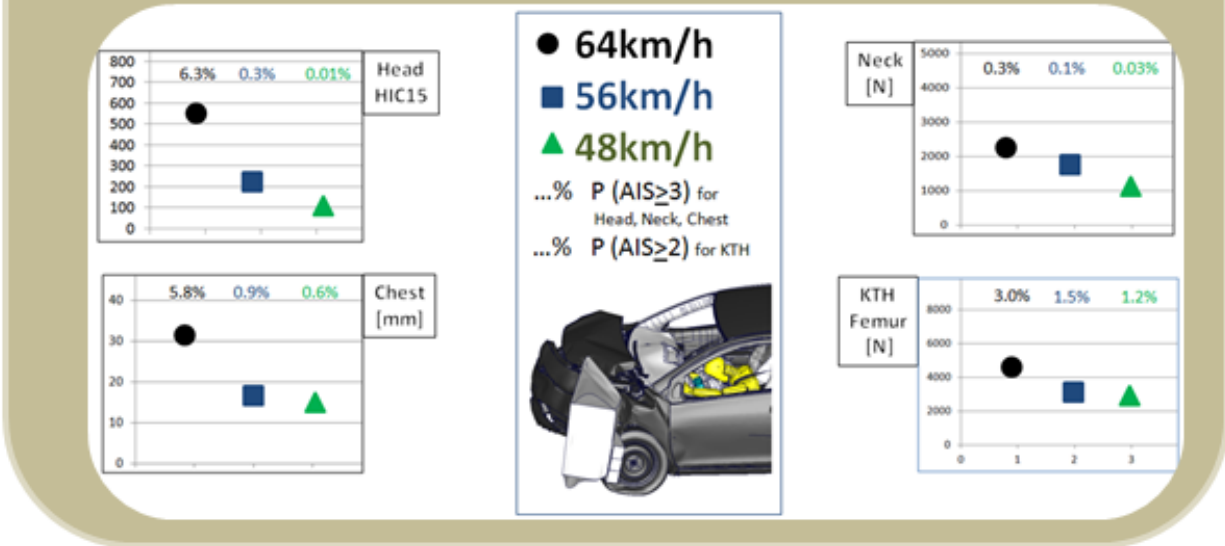


Figure 43a: IIHS impact speed - qualitative evaluation

Quantitative Evaluation for head, neck, chest and KTH (femur)



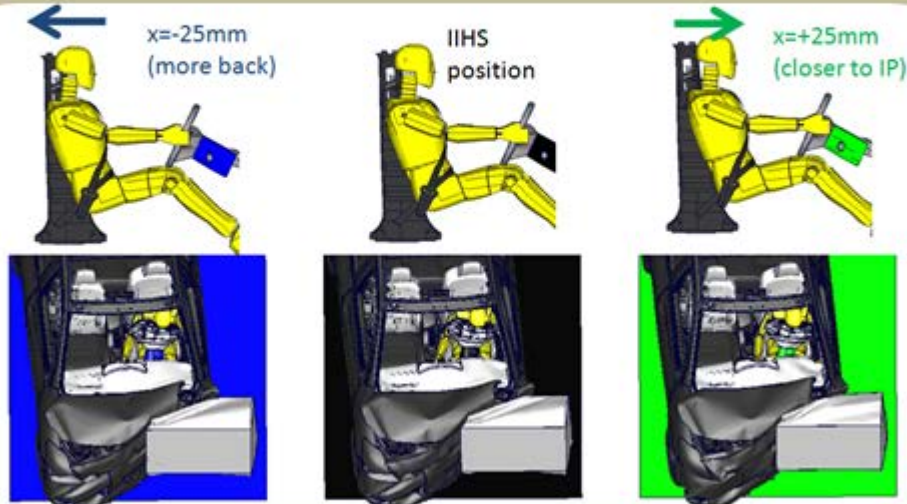
**Comparison of the IIHS load case with different impact velocities:
the higher the impact speed the higher the loads, as expected**

Figure 43b: IIHS impact speed - quantitative evaluation

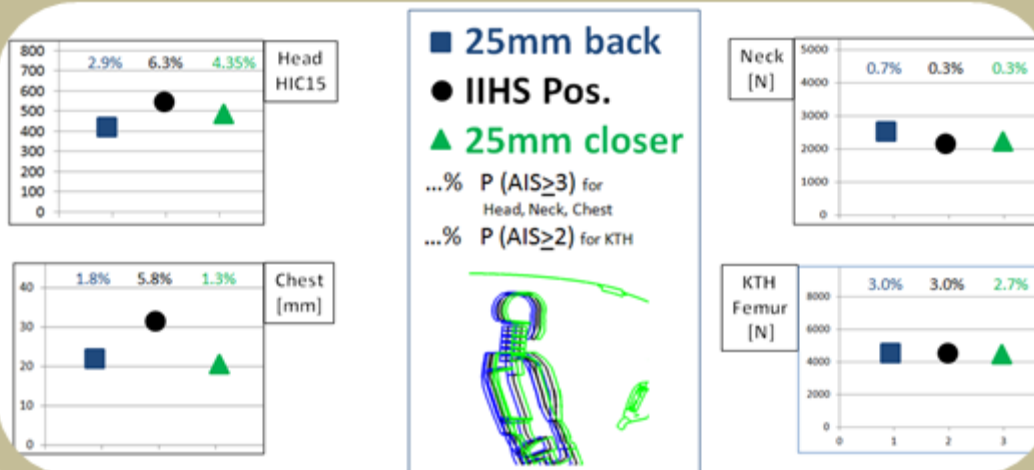
2.3.3 Variation of x-seating position

Figure 44 shows the variation of longitudinal seating position. A position 25mm further away from the instrument panel, shown in blue, and a position 25mm closer to the instrument panel, shown in green, were compared to the original IIHS seating position, depicted in black. Neck values were highest for the further aft seating position, where the occupant could reach higher momentum and thereby recorded a higher tension. The higher tension is similar to the observations from the NCAP sensitivity analysis for the same parameter. Femur load showed a similar trend but to a much smaller extent.

Overall Evaluation



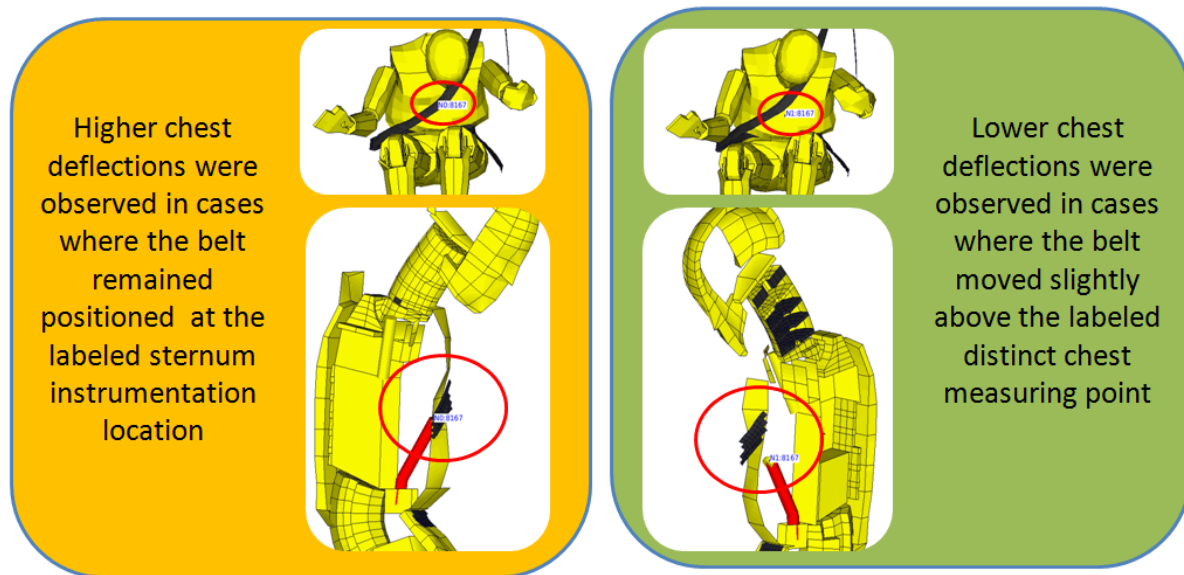
Quantitative Evaluation for head, neck, chest and KTH (femur)



HIC15 and chest deflection are the highest for the IIHS seating position because of the characteristics of the acceleration curve and different interaction with the belt, respectively. Neck tension is the highest for the back position, maximum femur loads are similar for all three seating positions.

Figure 44: x-seating position

Head and chest values were the highest for the original IIHS seating position mostly because of different interaction of the belt with the occupant. Figure 45 shows the one point chest deflection measuring device in the middle of the sternum (for the Hybrid III dummy), which is sensitive to the belt location across the chest. While the belt was located very close to the sternum during the time of high occupant loads for the original IIHS seating position, the belt moved away from that point of measurement for the other two seating positions due to different occupant kinematics and occupant restraint system interactions, which thereby caused lower chest deflection measurements for these cases.

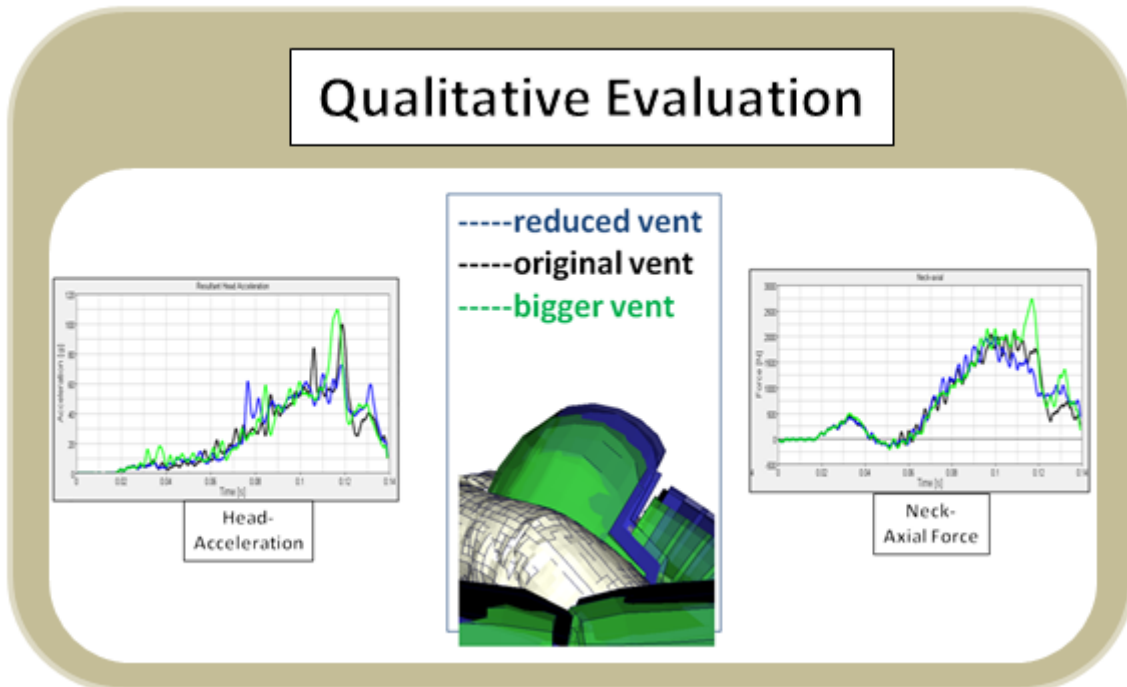


Some sensitivity analysis simulations showed differences in chest deflection. Most of the time they were influenced by the position of the belt relative to the one point sternum deflection measurement location during the impact.

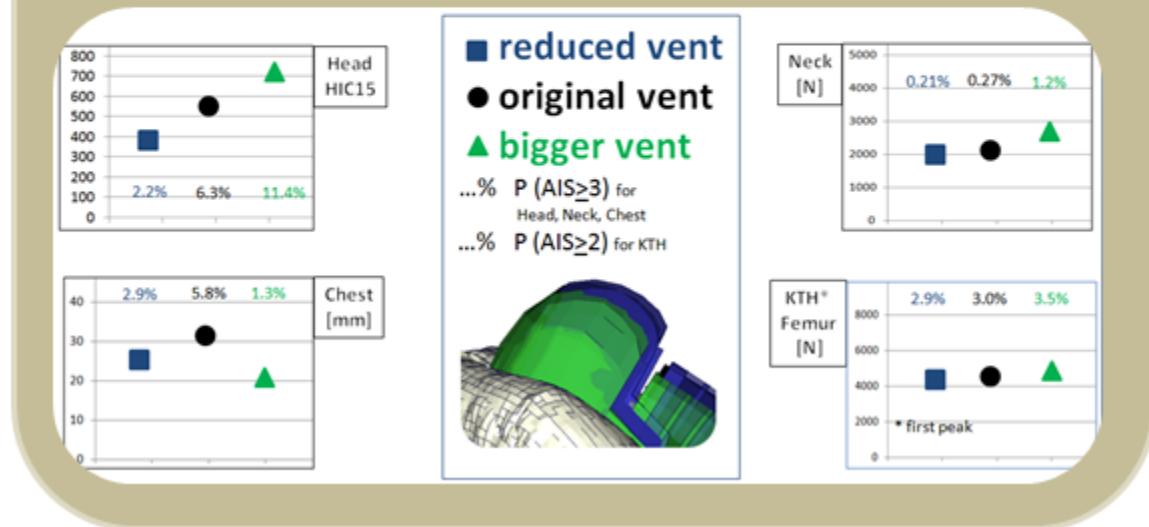
Figure 45: H3 Chest deflection analysis

2.3.4 Variation of air bag venting

Figure 46 shows the sensitivity of occupant results with respect to air bag internal pressure characteristics. As discussed for the NCAP load case, the original simulation run, shown in black below, contained the air bag model, which was validated using available full-scale crash tests for NCAP, IIHS, and oblique crash configurations. The second simulation with an air bag vent that was reduced by 5mm in diameter and the third simulation using an air bag vent that was increased by 5mm in diameter were performed and evaluated. Other than in the NCAP load case, a high head acceleration peak could be observed in the baseline simulation as well as in the corresponding full-scale crash test due to a direct interaction of the head with the steering wheel because of air bag bottoming out. Reducing the vent size resulted in a "stiffer" air bag with a higher internal pressure. Looking at the blue curves and values below, it can be noticed that the reduced air bag vent diameter prevented bottoming out and therefore a relatively high acceleration peak does not occur in the head time history curve anymore. Consequently, HIC15 values also were reduced in this case. Using a bigger air bag vent diameter and therefore a "softer" air bag, the lower internal air bag pressure allowed head to steering wheel interaction and air bag bottoming out. HIC15 values were consequently higher for the larger air bag vent diameter. Chest values were again strongly influenced by the seat belt chest interaction, and the values were influenced by the method of measuring chest deformation at the one point sternum location of the Hybrid III dummy. The highest values could be observed for the simulation case with the original air bag vent where the occupant's kinematics was such that the seat belt remained close to the instrumentation device. The neck and femur loads were not as sensitive to the air bag vent variation. However, a trend of higher occupant readings for the softer air bag characteristics due to a slightly higher occupant forward displacement could be observed.



Quantitative Evaluation for head, neck, chest and KTH (femur)



The bigger the vent the higher the HIC15 values because of stronger bottoming out. The bigger the vent the higher the neck tension values because of higher forward displacement of the head. Chest readings are again caused by local effects at the sternum. Femur values are very similar for all three cases.

Figure 46: IIHS air bag venting

2.3.5 Variation of air bag time-to-fire

Figure 47 shows the sensitivity of occupant loads to the variation of air bag time-to-fire (TTF) in the IIHS load case. In the left picture, the head acceleration and air bag internal pressure are shown for the original TTF in black, a 10ms later TTF in blue, and a 20ms later TTF simulation in green. The resulting different air bag internal pressure characteristics caused different head acceleration and HIC15 values. While the case with the original TTF shows the high peak due to air bag bottoming out in the test and simulation, as discussed before, the later TTF simulation show reduced and no bottoming out at all for the 10ms and 20ms later delays, respectively. The reason was the shifted internal pressure curves, which resulted in a slightly stiffer air bag during the relevant time of head air bag interaction, as seen in the left picture below. Consequently, air bag bottoming out was reduced and prevented, as shown in the blue and green time history curves, respectively. While almost no differences could be observed for the maximum neck tension values, the chest and femur loads showed some sensitivity caused again by the local effects of the seat belt and thorax interaction regarding the chest deflection and by local effects during the femur interior interactions.

Qualitative Evaluation

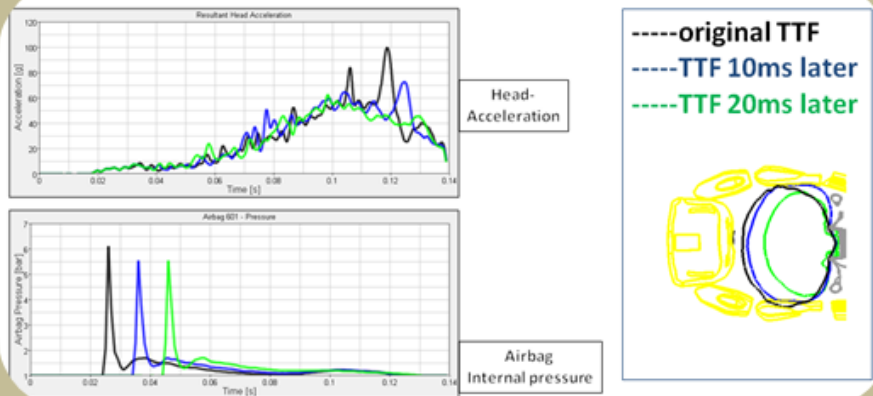
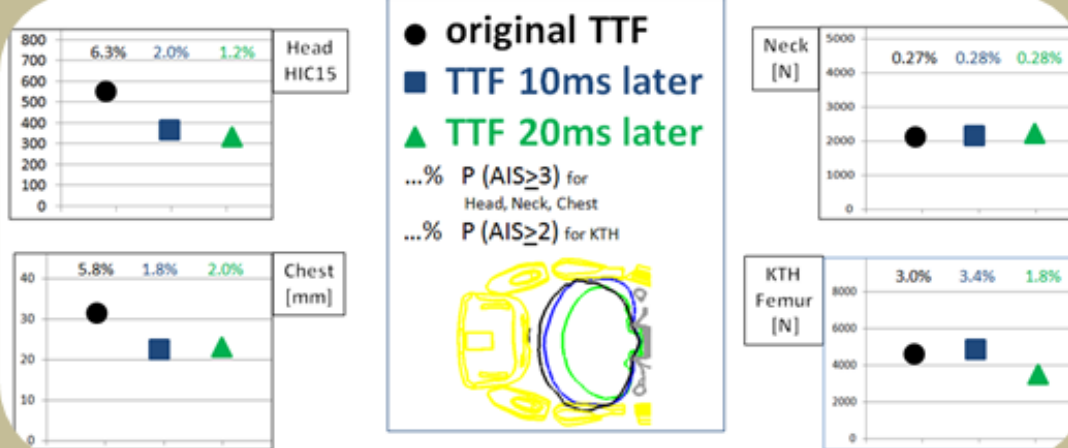


Figure 47a: IIHS air bag venting - qualitative evaluation

Quantitative Evaluation for head, neck, chest and KTH (femur)



Head and Chest values are lower using a later airbag TTF due to different internal pressure characteristics. Neck results are about the same and the right femur shows some differences due to local effects (as seen when comparing 2 tests with each other)

Figure 47b: IIHS air bag venting - quantitative evaluation

2.3.6 Variation of seat belt force limiter

Besides realistic vehicle, air bag, and interior components, a generic seat belt model with a pretensioner and belt force limiter was developed using results and information from the available full-scale crash tests. When evaluating the retractor belt force limit at the upper shoulder belt location, a defined load limit of about 4 kN could be observed in the tests and baseline simulation. The sensitivity of the occupant loads towards the variation of the belt force limit was evaluated using the IIHS load case. First, a load limit of 2kN, implying that the maximum belt force is limited to 2kN rather than 4kN, was examined, shown in blue and black respectively. In this case, more belt-length is being released during the impact allowing higher occupant forward displacement. It can be noticed that this resulted in higher head acceleration and lower chest deflection values, as expected. On the other hand, limiting the allowed shoulder belt force to 6kN, implying that not as much belt material had to be released from the retractor during the impact, reduced the amount of occupant forward displacement and resulted in lower head acceleration and HIC15 values with no air bag bottoming out occurring and with slightly higher chest deflection. Although the sensitivity to neck and femur were rather small, it can be noticed that these values were also slightly higher for the lower belt force limit, which allowed a larger occupant forward displacement.

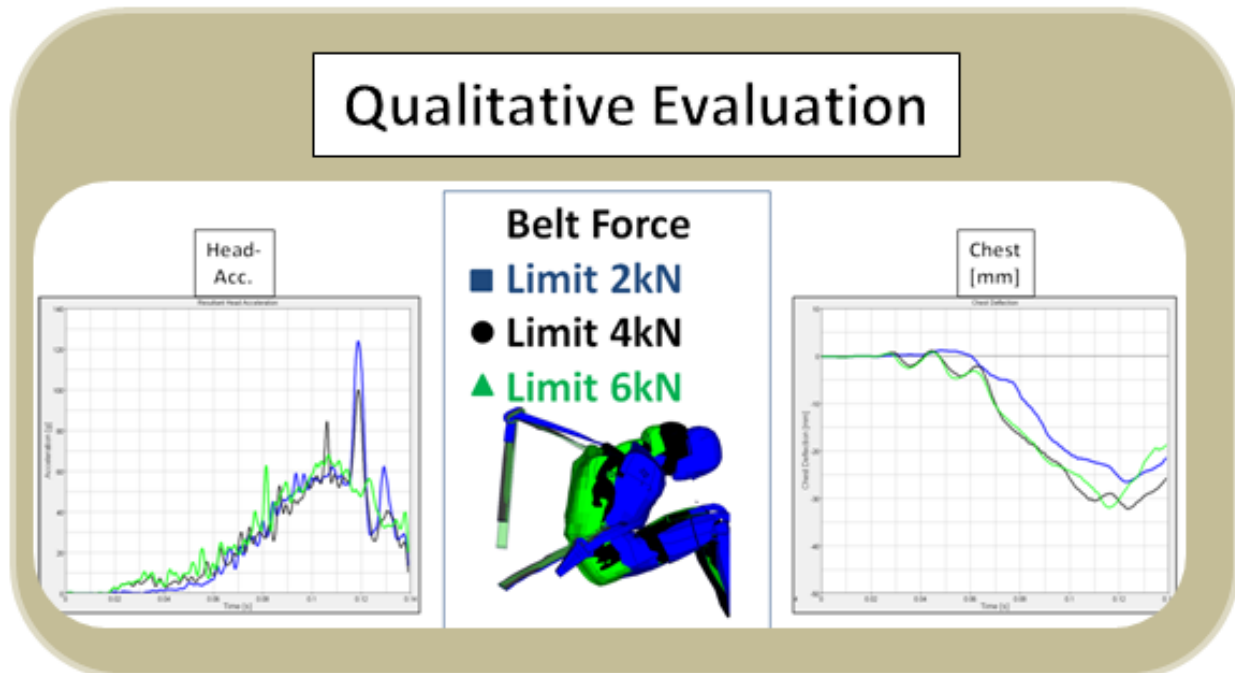
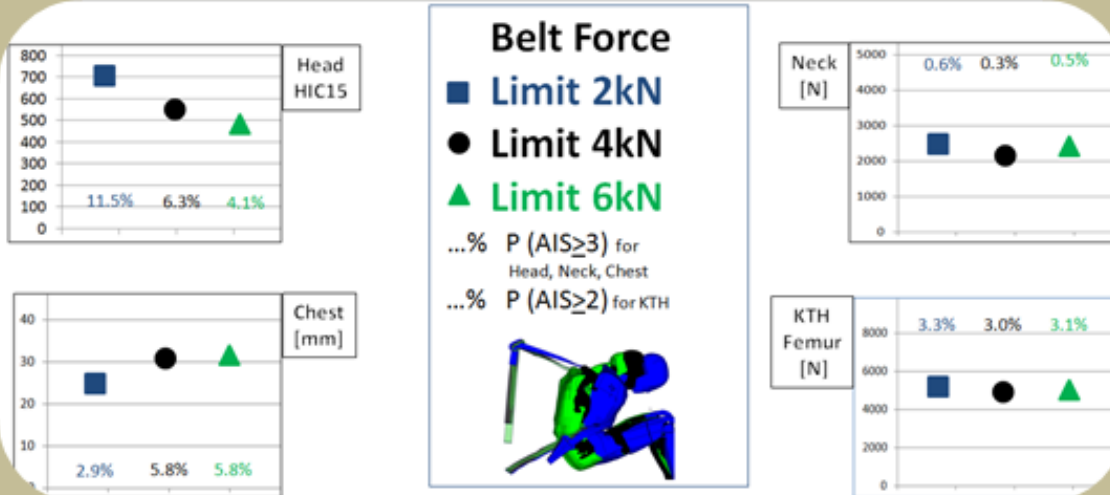


Figure 48a: IIHS air bag venting - qualitative evaluation

Quantitative Evaluation for head, neck, chest and KTH (femur)



The effect of the different belt force limiter values (measured at the shoulder belt) can be clearly seen: The simulation with the lower belt force limit allows more occupant forward displacement, shows lower chest deflection and higher head acceleration, as expected. The simulation where the limit is set higher, before more belt is being released, shows lower occupant forward displacement and no airbag bottoming out occurs.

Figure 48b: IIHS air bag venting - quantitative evaluation

2.3.7 Variation of torso angle

Figure 49 shows the results for simulations with different occupant torso angles. In addition to the baseline simulation, shown in black, a 5-degree more upright seating position, shown in blue, and a 5-degree more reclined seating position, shown in green, were evaluated. It is enlightening that the different torso angles resulted in different seat belt paths between the d-ring and the upper occupant shoulder area. While neck and femur loads were similar in all three cases, different HIC15 values could be observed due to different head steering wheel interaction points. High sensitivity could again be observed for the chest deflection values. While the belt remained well over the sternum for the original seating position, the different torso angles and belt paths caused a small movement away from the chest instrumentation location for the other two torso angles, resulting in lower chest deflection values.

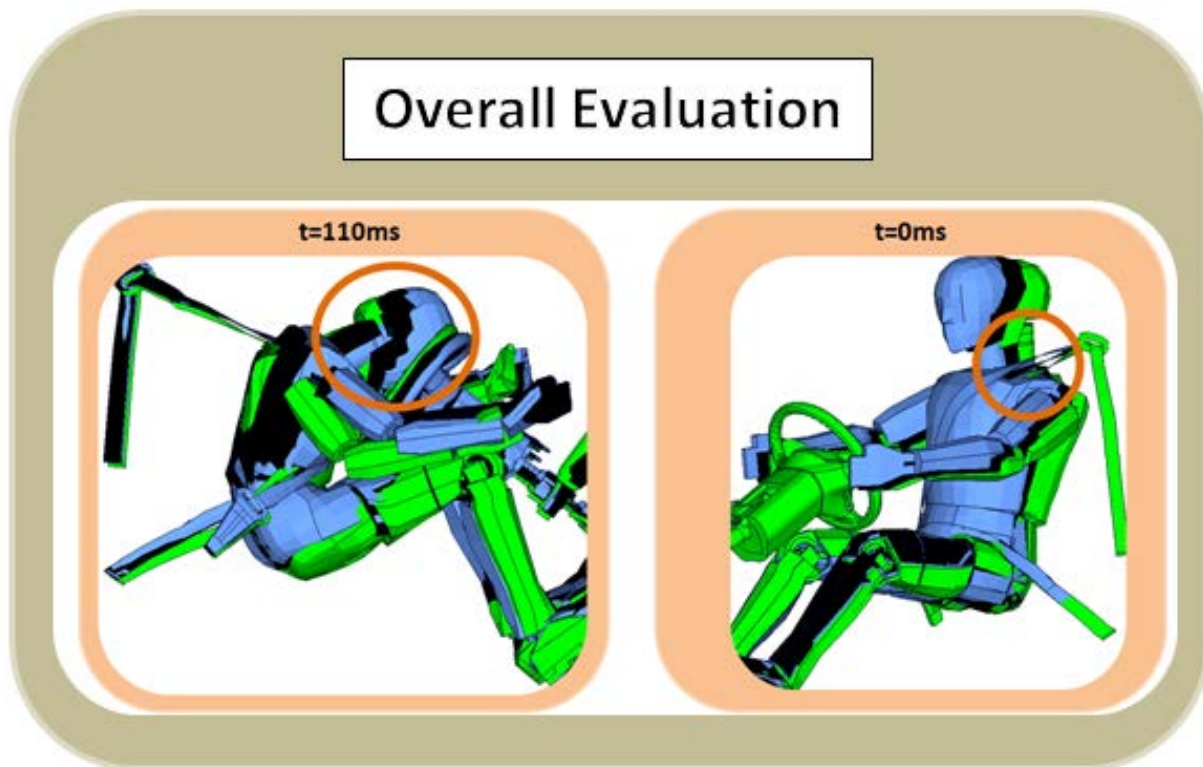
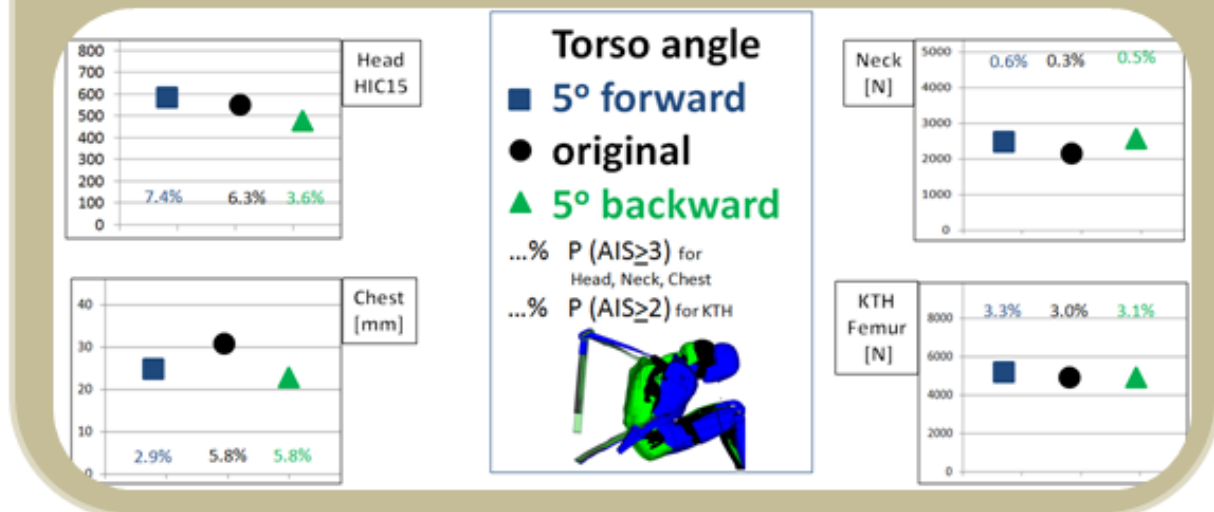


Figure 49a: IIHS torso angle variation - overall evaluation

Quantitative Evaluation for head, neck, chest and KTH (femur)



Neck and Femur show rather small sensitivity towards the different torso angles. Head HIC15 values were the smallest for the 5 degree backward position due to the different impact point at the steering wheel at the time of airbag bottoming out. The different torso angles also resulted in different shoulder belt paths and consequently different chest deflection characteristics

Figure 49b: IIHS torso angle variation - quantitative evaluation

2.4 Sensitivity Analysis using oblique load case

The sensitivity of structural and vehicle modifications to the THOR dummy in the 35-percent offset, 15-degree oblique impact at 90km/h was evaluated. In addition to the results using the original YARIS model, as described in section 1.8, the oblique crash configuration was evaluated using a vehicle structural model that was adapted to the vehicle used in the full-scale crash test, as described in section 5.2.

2.4.1 Differences in vehicle structure

Figure 50 shows differences of the original vehicle model used in section 1.8, shown in blue, and the modified vehicle model, shown in green. It can be noticed that modifications have been made to the front axle and to the engine.

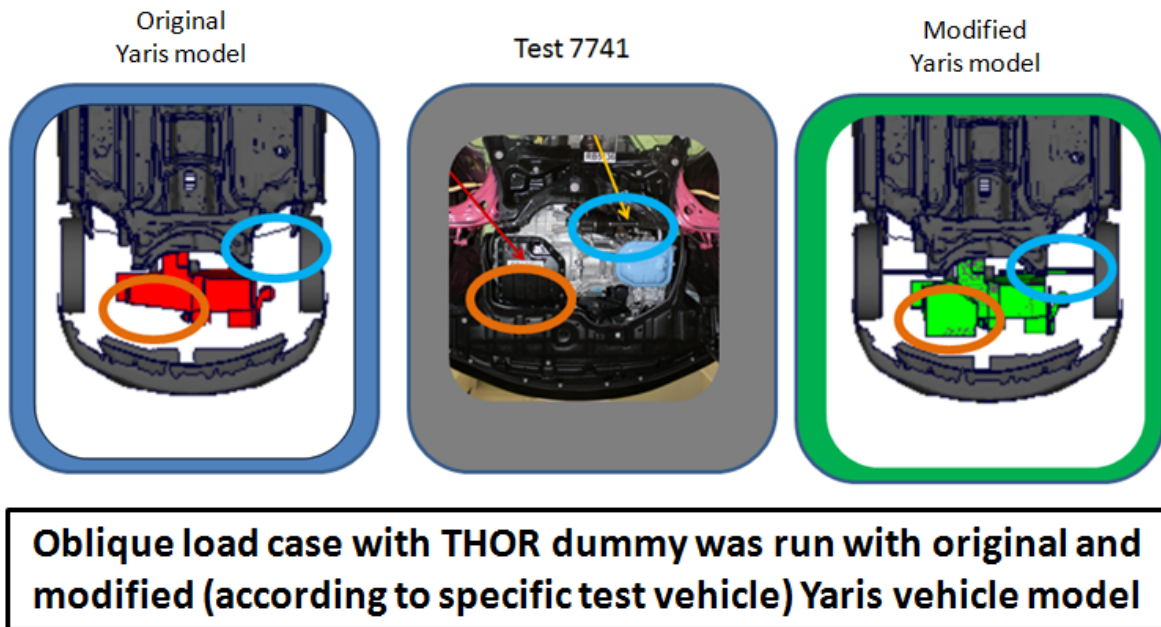


Figure 50: vehicle modifications

2.4.2 Overall evaluation

Figure 51 shows that the modified vehicle model captured the vehicle yaw motion better than the original Yaris model for the specific oblique full-scale crash test. The two top pictures, showing the vehicle from the top at time 0ms and time 120ms, indicate a clear rotation of the vehicle around the z-axis in the full-scale crash test. While the original finite-element model, depicted in blue, showed very little rotation about the z-axis, such yaw motion could be observed for the modified Yaris model, shown in green. The different vehicle kinematics also resulted in different

occupant kinematics and loads. The movement of the occupant towards the area between the steering wheel and the door trim was more distinct for the modified vehicle model.

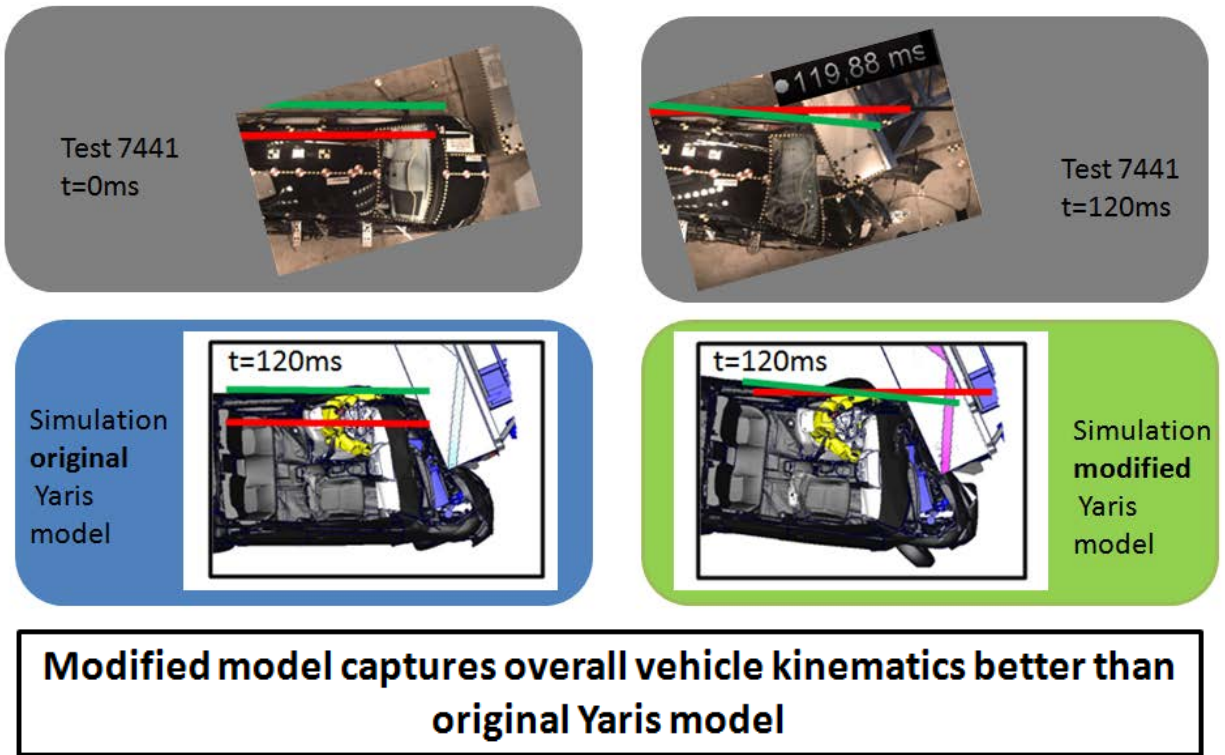


Figure 51: vehicle modifications

2.4.3 Qualitative evaluation

As discussed in section 1.8, the most critical occupant load was the head acceleration, caused by the impact of the head with the upper left arm of the THOR dummy during the rotation of the vehicle. Figure 52 below shows the head acceleration of the available full-scale crash test in black, the results from the simulation with the original Yaris model in blue, and the results from the simulation with the modified vehicle model in green. It must be noted that all other boundary conditions, such as seating position and restraint systems remained the same in both simulations. It is striking that the timing of the head acceleration peak in the test could be captured within a few milliseconds, at around 110ms of the crash event, using the modified vehicle model. This is especially notable since the various occupant and vehicle kinematics make it more difficult to capture such injury mechanism events the later they occur in time. Again, the peak was caused by the interaction of the head with the upper arm during vehicle rotation.

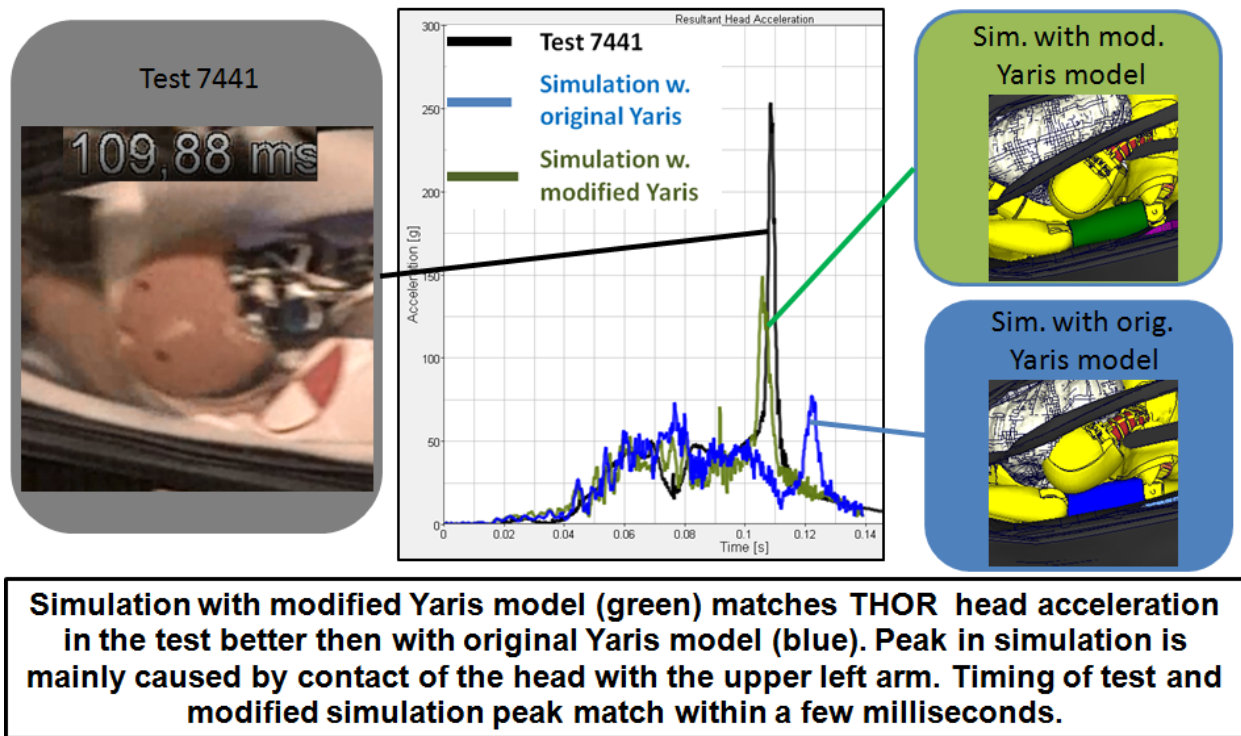


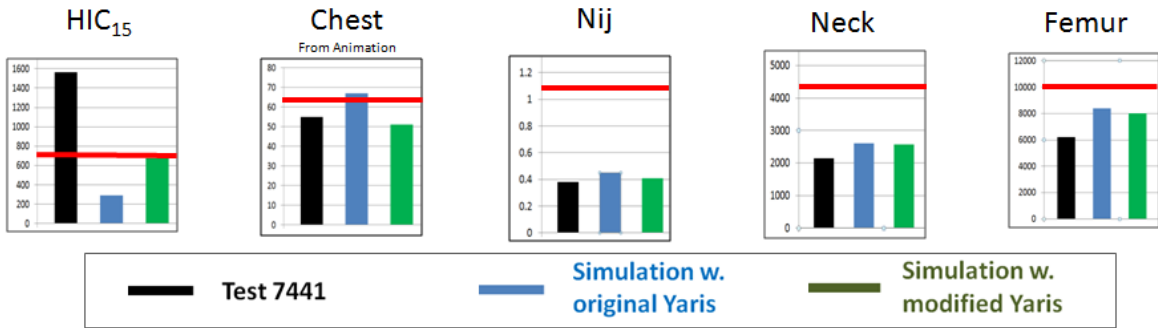
Figure 52: Oblique vehicle model sensitivity

2.4.4 Quantitative evaluation

Figure 53 shows the sensitivity of the absolute values of the THOR dummy measures towards the use of the different vehicle structural models. It can be noticed that especially head and chest values were influenced by the structural changes due to different occupant kinematics and interactions with the restraint systems. It can also be noticed that all body regions show better correlation with the available full-scale crash test results. While the chest, neck, and femur loads

were below the defined thresholds for test and simulation with the modified vehicle structure, the head acceleration was critical. Although the high absolute value of head acceleration peak in the test was not seen to the same extent as in the simulation, a clear peak, timing and cause of the relevant impact interaction of the head with the upper arm could be clearly identified in the performed simulation.

Measurement Description	Driver A1		Test	Simulation w. original Yaris	Simulation w. modified Yaris
	Units	Threshold			
Head Injury Criteria (HIC ₁₅)	N/A	700	1563.50	289	679
Maximum Chest Compression	mm	63	54.94	67	51
Nij	N/A	1.113	0.38	0.45	0.41
Neck Tension	N	4,170	2149.15	2602	2572
Neck Compression	N	4,000	-393.95	-959	-897
Left Femur Force	N	10,008	-4351.16	-1969	-2023
Right Femur Force	N	10,008	-6221.03	-8391	-8027



Quantitative Comparison of Simulation with modified (green) Yaris model shows better correlation than simulation with original Yaris model (blue) when compared to Test 7441

Figure 53: Oblique impact quantitative evaluation.

2.5 Conclusion Subtask II sensitivity analysis

The developed integrated vehicle-occupant model for occupant safety analysis with relevant interior components, generic restraint system components, and respective occupant models, which was extensively evaluated in three different load cases — IIHS 40-percent offset; NCAP full overlap; and 15-degree, oblique 35-percent offset impact — using full-scale test data, was used to perform various sensitivity analyses for various parameters using the three crash configurations.

Variation of relevant parameters (i.e., sensitivity analysis), including the speed, overlap percentage, seating position, belt, air bag, and steering column characteristics, shows results for different load cases and occupants. It can be seen that with the developed model and methodology one is capable of simulating and analyzing situations and effects that go beyond the validated configurations. The accomplishments include:

- ✓ Developed integrated model for occupant safety analysis has been successfully used to study the effects of several parameter variations (sensitivity analysis);
- ✓ NCAP load case was used to study the variation of impact speed, seating position, air bag, seat belt, and steering column characteristics;
- ✓ IIHS load case was used to study the variation of overlap percentage, impact speed, seating position, air bag, and seat belt characteristics;
- ✓ Oblique load case was used to study the effect of different vehicle structural behavior;
- ✓ THUMS occupant model was used to study the effect of different seating positions;
- ✓ Results were achieved and discussed for all performed parameter studies; and
- ✓ Regular meetings and documentation of progress.

VI Subtask III

3. Use and evaluation of different occupant models

The 50th percentile male Hybrid III occupant models were used in the 40-percent offset IIHS and in the full overlap NCAP crash configurations, according to the respective test protocols. The 50th percentile male THOR dummy model was used in the 35-percent overlap, 15 degree oblique impact according to the available full-scale crash of the oblique load case. In Subtask III, the THOR and the Total HUMAN Model for Safety (THUMS) are used and evaluated.

3.1 THOR

The THOR occupant model was included in the 40-percent offset IIHS load case and evaluated against the results from the Hybrid III dummy.

3.1.1 Overall Evaluation

Figure 54 shows the overall comparison of the THOR, shown in blue on the top, and the Hybrid III, shown in black at the bottom. Both occupant models drift to some extent towards the door during the forward displacement and interact with the air bag and the steering wheel "off center" due to the offset impact characteristics. Besides other differences, the longer legs of the THOR, when compared to the Hybrid III, also caused different interaction with the interior and consequently slightly different occupant kinematics.

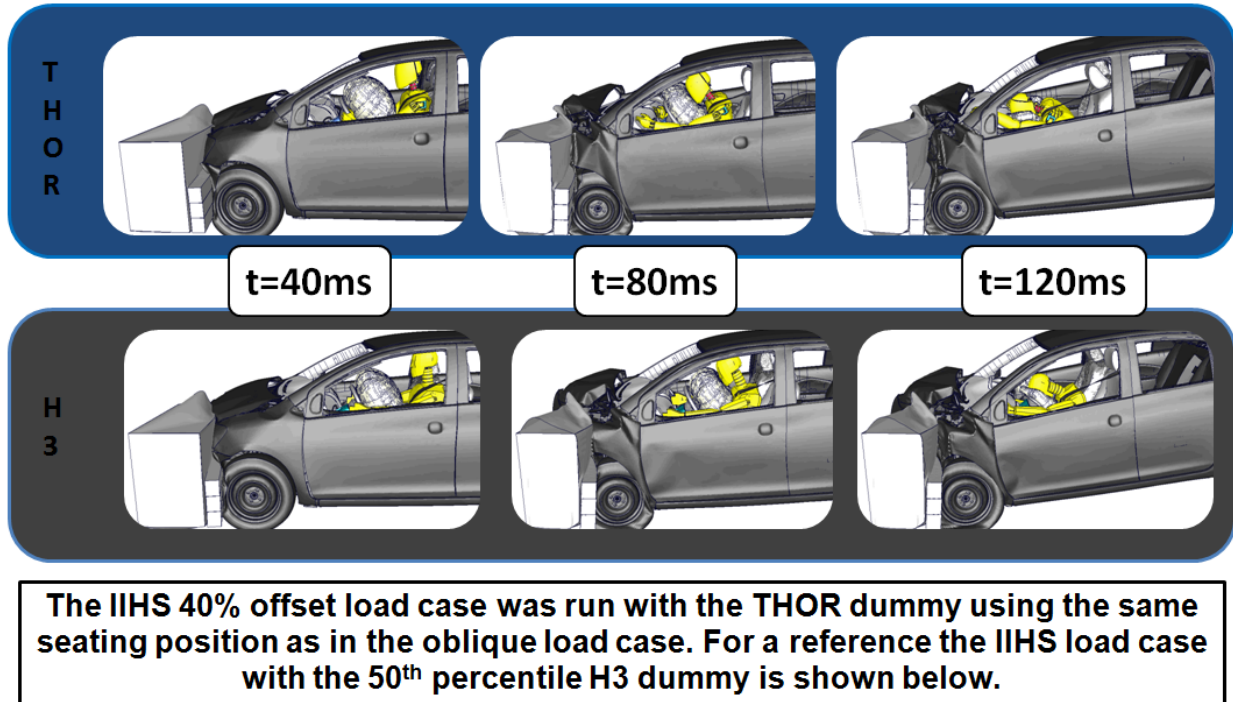
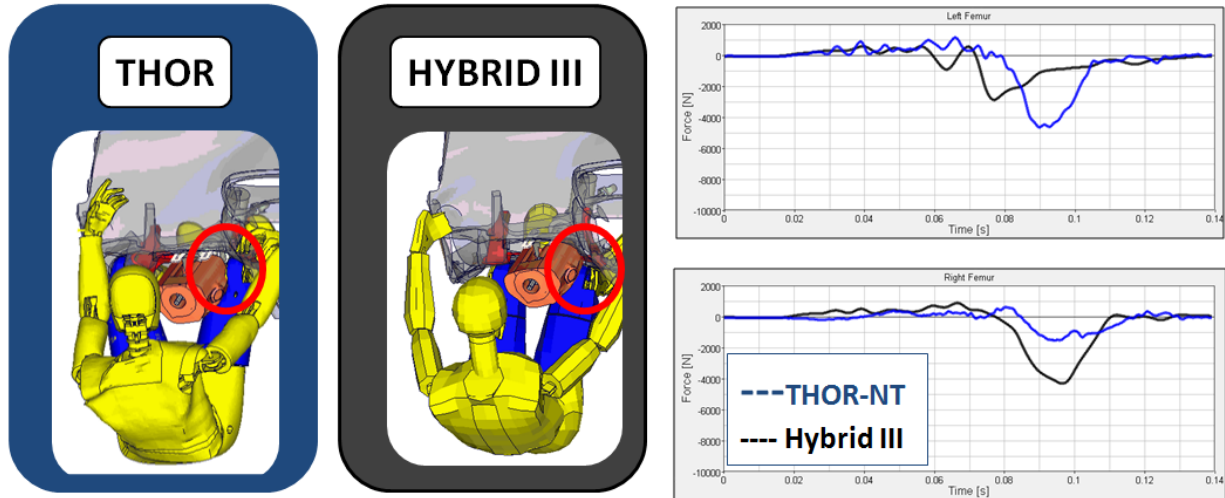


Figure 54: THOR - H3 overall comparison

3.1.2 Femur loads

Figure 55 shows the time history curves of the left and right femur. Test results can be found in section 2. In the left picture the steering wheel, air bag, and seat belt have been removed in order to show the different impact configurations of the THOR in blue and the Hybrid III in black. While the longer legs of the THOR were positioned in a more spread out manner (thereby having a larger distance between the knees), the Hybrid III legs were positioned closer together resulting in a more longitudinal position. For this reason, the Hybrid III knees impacted the interior earlier. In the case of the right leg, a contact between the knee and the steering wheel trim and lock area could be observed, which resulted in a higher femur force peak when compared to the THOR which impacted the instrument panel at areas with less-stiff components and structures. Despite the differences in the time history curve characteristics, both dummies experienced femur loads that were clearly below a threshold of 10kN.



Characteristics and maxima of femur loads are different for the THOR (blue) and H3 (black) dummy in the above simulations due to different impact points. The longer legs and different leg position cause an interaction with different areas of the instrument panel and “steering wheel trim”.

Figure 55: THOR - H3 femur loads

3.1.3 Chest loads

A major difference between the THOR and the Hybrid III dummies is the way chest deflection can be evaluated. The HYBRID III measures the thorax intrusion at a single point in the middle of the sternum. The THOR is equipped with a so-called CRUX device which allows the evaluation at four different locations of the chest: upper right (UR), upper left (UL), lower right (LR), and lower left (LL). The advantage of the advanced instrumentation becomes obvious when analyzing the load to the chest of the two different dummies. As discussed in Subtask II, high sensitivity towards the variation of different parameters could be observed for the Hybrid III. Most of the time, the different location and movement of the belt relative to the one-point measuring device could be deemed accountable for this sensitivity. Looking at the THOR, analysis of the thorax deflection cause/effect relations provides deeper insight into the occurring load and injury mechanisms. It can be noticed in Figure 56 below that deflections at the upper right chest of the THOR, shown in blue on the left, were the highest with a 57mm maximum, followed by the lower right chest location with a 52mm maximum value. This is in accordance with the belt path depicted in the picture below: the belt is located directly on top of the upper right position and only slightly offset from the lower right location. Similar to the observations made using the Hybrid III occupant, the belt could also be identified as a major influence to the chest loads beside the interaction with the air bag. This observation is confirmed by the maximum values on the left side of the THOR dummy, where no direct belt interaction occurs. The maximum value for the upper left side was 37mm, and the belt location was even more

offset. The most striking value is the lower left location with an 11mm maximum and no interaction with the belt at all. In summary, it could be noticed that the values were higher the closer the belt was located to the respective measuring location of the THOR dummy. While this observation is in agreement with the analysis of the chest loads to the Hybrid III in the various studies, the THOR offers a much more distinct analysis of the loads to the different chest locations.

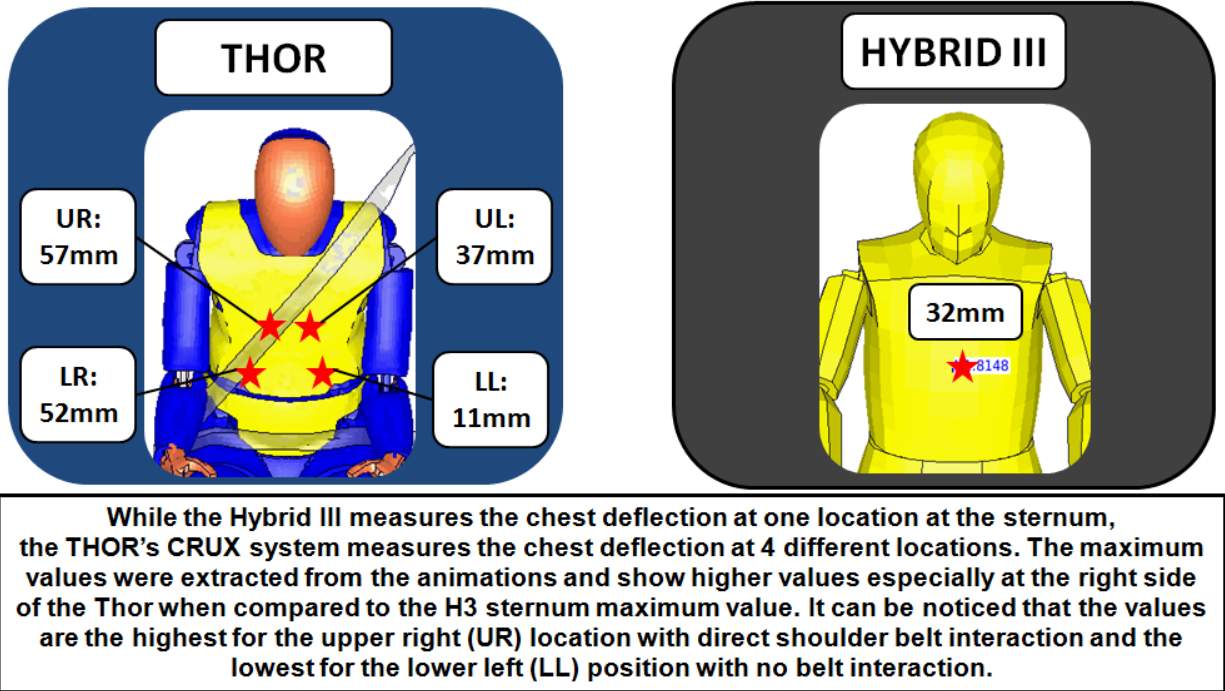
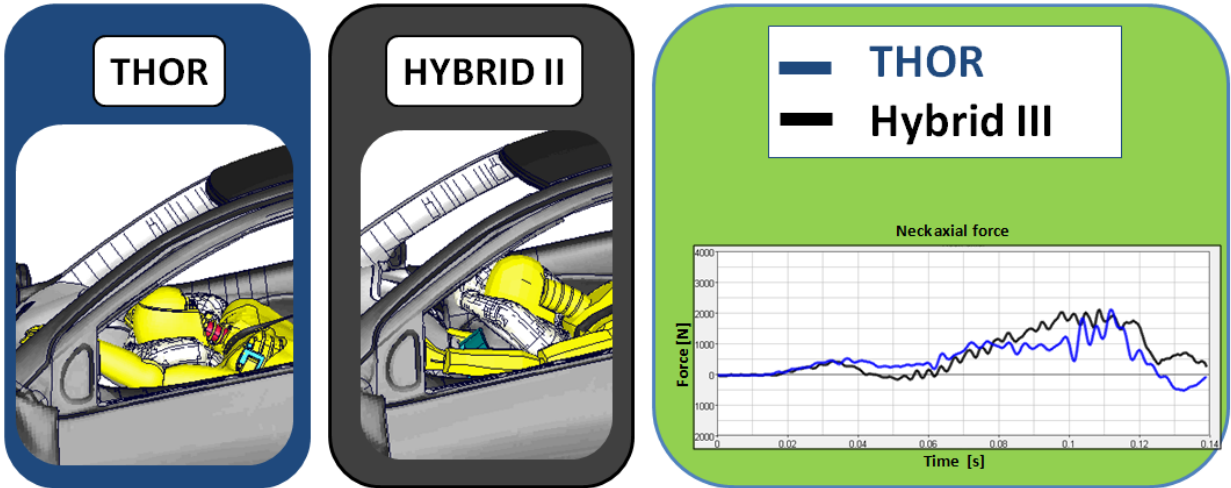


Figure 56: THOR - H3 chest loads

3.1.4 Neck loads

Figure 57 shows the comparison of the neck axial force of the THOR dummy in blue and the Hybrid III dummy in black. Although similar maximum values could be observed for the two different dummies, differences were obvious using overall and qualitative evaluations. Due to the different occupant kinematics (initiated by the different leg biomechanical characteristics and position, and further caused by the different seat belt-air bag-occupant interactions), differences in the time history curve characteristics and in the head impact locations could be observed.

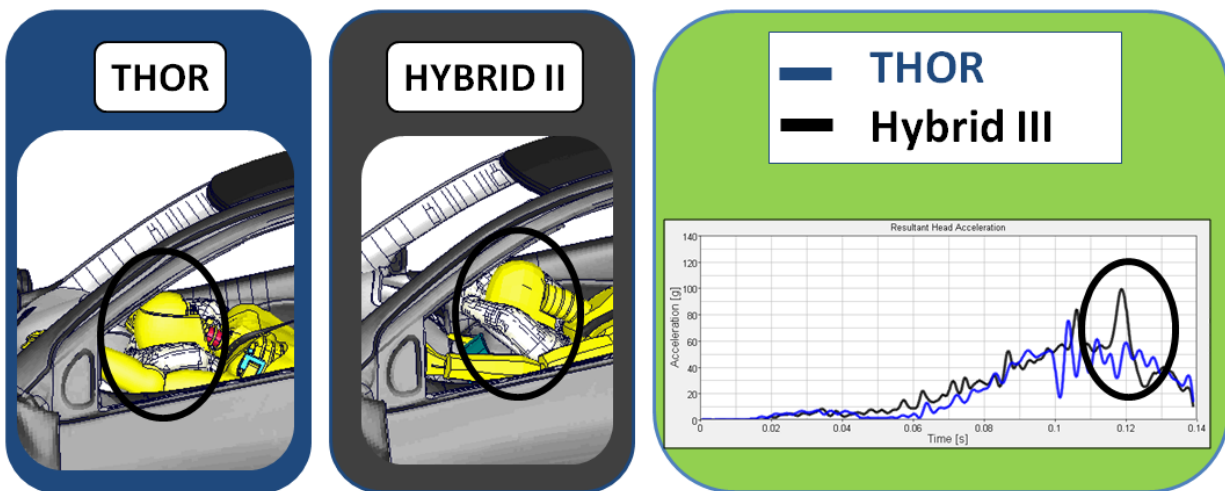


Neck forces of THOR (blue) and Hybrid III (black) dummy show similar maximum values in the above simulations. Characteristics differ due to different occupant kinematics and different interaction with airbag and steering wheel.

Figure 57: THOR - H3 neck loads

3.1.5 Head acceleration

When comparing the head acceleration of the two dummy types in the IIHS 40-percent offset configuration, it can be noticed in Figure 58 that a high acceleration peak occurs for the Hybrid III, shown in black, but not for the THOR, shown in blue. While the bottoming-out effect and consequently the direct contact of the HYBRID III with the steering wheel hub was well analyzed in the simulations and in the validation with the full-scale crash test described previously in this report, such an effect could have been also expected for the THOR dummy when looking at the two states with the maximum forward displacement of the head in Figure 58 below. The reason for the "missing" acceleration peak was the changed impact location of the head. Due to different occupant kinematics the head of the THOR moved more forward in between the steering wheel hub and steering wheel rim, and consequently a lower load was induced.



Due to differences in seating position and occupant kinematics, the H3 hits the steering wheel hub after airbag bottoming out, and the THOR hits the steering wheel rim, which doesn't cause an acceleration peak as seen in the simulation with the H3 dummy. Other than that, head acceleration curves have similar characteristics due to same airbag performance.

Figure 58: THOR - H3 head acceleration

3.1.6 THOR - Hybrid III comparison conclusion

Using the IIHS 40-percent offset crash configuration once with the Hybrid III and once with the THOR occupant model, it was found that the absolute values, when put into relation to common thresholds, were comparable for both dummies despite differences in curve characteristics and

occupant kinematics. Major differences are obvious for the chest deflections, which were measured at only one location for the Hybrid III, and at four distinct locations for the THOR. Besides the advanced injury analysis capabilities using the THOR, higher maximum values could be observed for this advanced dummy at the locations with direct seat belt interaction, as compared to the maximum Hybrid III sternum deflection. These simulations suggest that the maximum chest deformation takes place under the path of the belt, and the THOR is better able to detect this greatest extent of torso compression.

3.2 THUMS human model

In addition to the anthropomorphic test device models, the Total HUMan Model for Safety (THUMS) was evaluated using the developed integrated vehicle-occupant model.

3.2.1 THUMS description

The human model was developed by Toyota and distributed by Livermore Software Technology Corporation. It represents a 50th-percent adult male occupant. The academic version 4.0 (containing all skeletal bones, structures, and internal organs) consists of about 1.7 million elements and about 1,300 different parts. It was completed in 2010 and is shown in Figure 59 below.

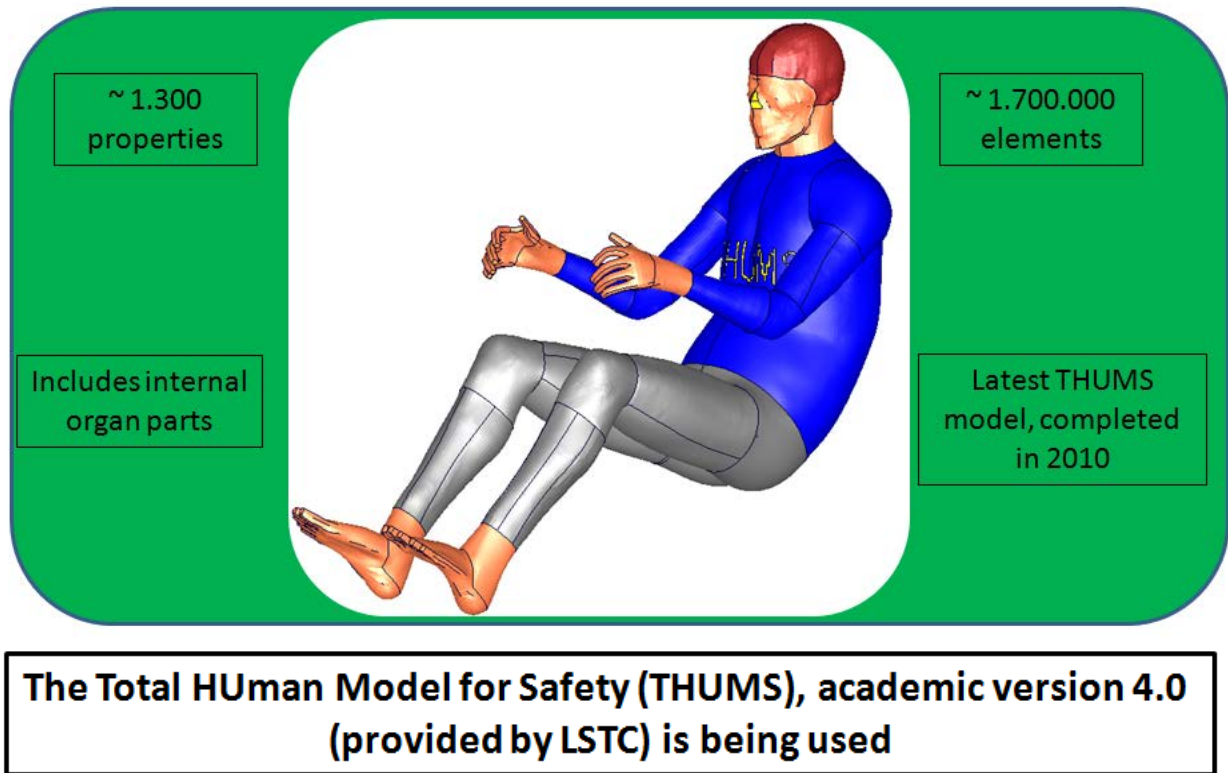
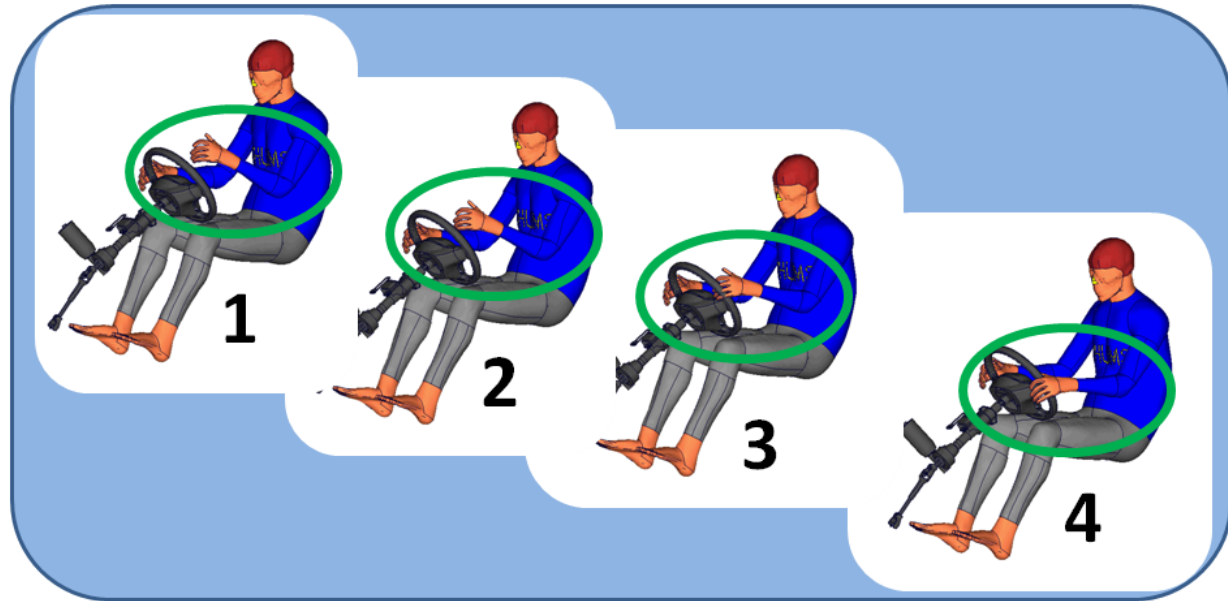


Figure 59: THUMS description

3.2.2 THUMS preparations

Before the THUMS occupant model could be used in an integrated vehicle-occupant simulation using the developed models and methodologies, some numerical modifications had to be made. Then the same procedures regarding seat squash (integration into the seat) and seat belt fitting

were used, as described previously for the Hybrid III and THOR occupant models. Pre-simulations were used to position the legs and the arms into the appropriate position. Figure 60 shows sequences of the left arm positioning. Forces were applied in such a way that the hands fit well around the steering wheel for example.

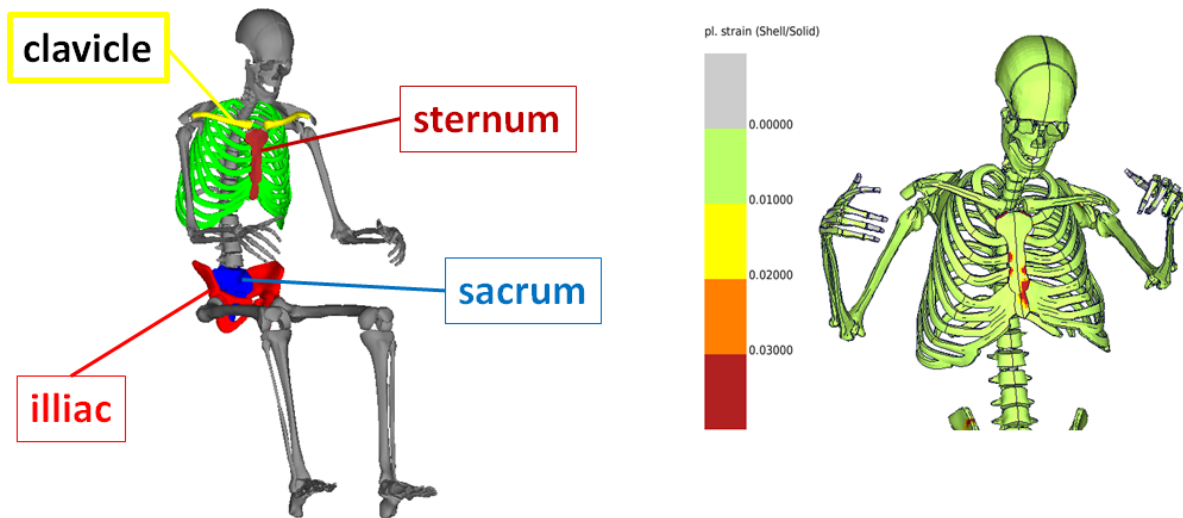


Arms, legs, and hands (around steering wheel) were positioned using pre simulations. Sequence above shows positioning of left arm.

Figure 60: THUMS pre-simulation

3.2.3 THUMS evaluation of loads

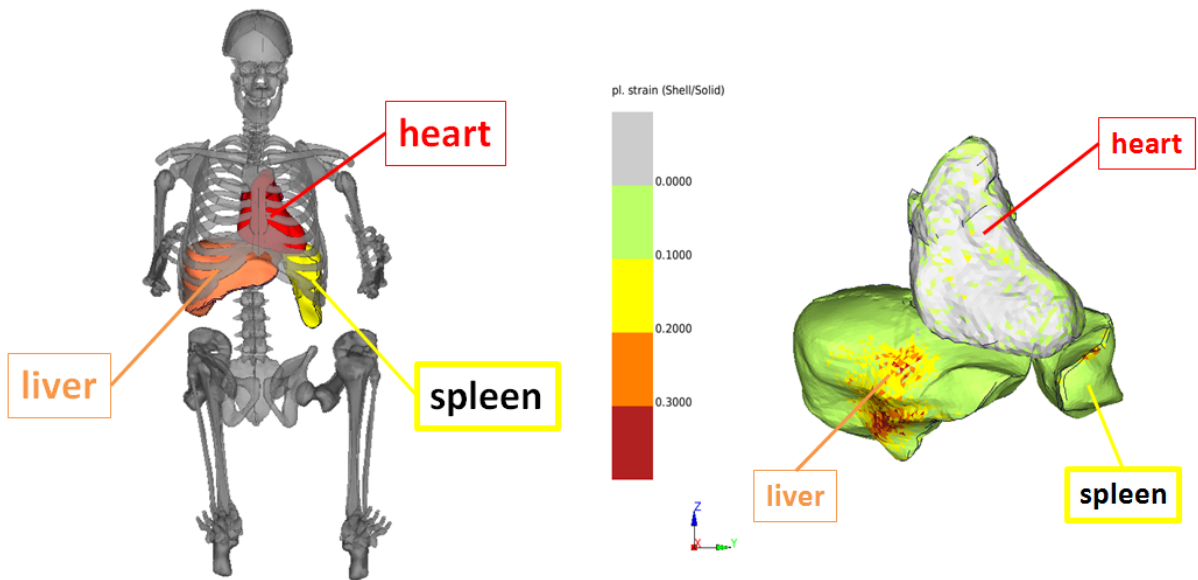
In addition to allowing biomechanical criteria, such as chest deflection, the human model allows the analyst to directly evaluate loads to skeleton bones and internal organs. Figure 61 show the human skeleton with ribs in green, sternum and iliac in red, sacrum in blue, and clavicle in yellow. In order to evaluate potential injury risks to bones effective plastic strain values have been analyzed. According to studies by Burstein et al. (1976) and McCalden et al. (1993) a threshold of 3-percent strain was used to predict potential risks of bony fractures.



Potential risk of bony fractures in the THUMS model will be evaluated using an effective plastic strain threshold of 3% according to studies by Burstein et al. (1976) and McCalden et al. (1993)

Figure 61: THUMS skeleton criteria

Similarly effective plastic strain evaluations have been used to analyze loads to internal organs, such as the liver, spleen, and heart. A threshold of 30-percent effective strain was used to predict potential injuries to these organs, as suggested by Yamada (1970) and Melvin et al. (1973). An example is shown in Figure 62 below. The plastic strain fringe plot scale indicates values above 30 percent in red, values between 20 percent and 30 percent in orange, values between 10 percent and 20 percent in yellow, and values between 0 percent and 10 percent in green. The main focus was applied to organs that have been found to have a high risk of injury in real world accidents, such as the liver (shown in orange), the spleen (shown in yellow), and the heart (depicted in red). The right picture in Figure 62 below shows an example of such evaluation, using a fringe plot of the effective plastic strain values at a deformed stage. Values above 30 percent are colored in red and indicate a high risk of injury at that area.



An effective plastic strain threshold of 30% will be used to evaluate injury risks to the heart, liver, and spleen, as suggested by Yamada (1970) and Melvin et al. (1973).

Figure 62: THUMS internal organ criteria

3.2.4 IIHS results using THUMS

The IIHS 40-percent offset crash configuration was used to evaluate the loads to the THUMS. Figure 63 shows the overall evaluation using a side view and a section cut view of the occupant kinematics at the beginning of the crash event, at 40ms, 80ms, and 120ms. It can be seen how the human model is being restrained by the seat belt before it couples with the air bag and finally reaches its most forward position and rebounds. The section cut view allows insight into the model showing internal organs in yellow, bones in red, skin and flesh in orange, and the brain in gray.

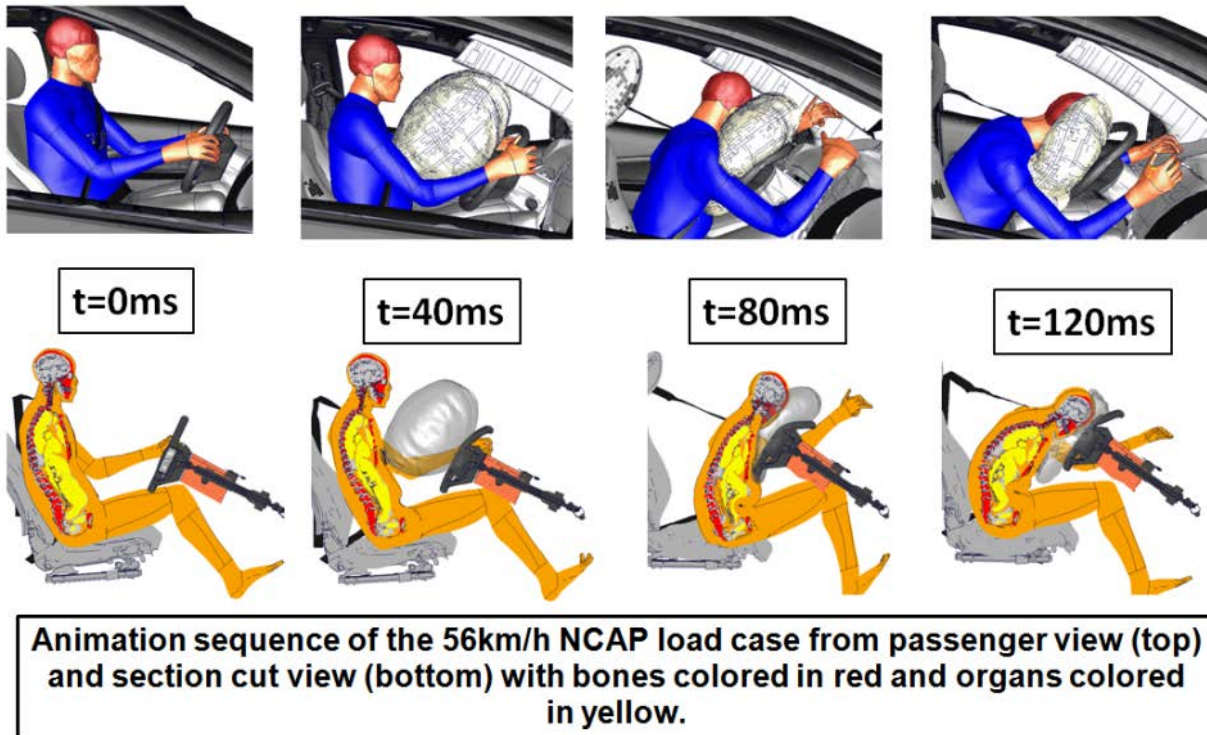
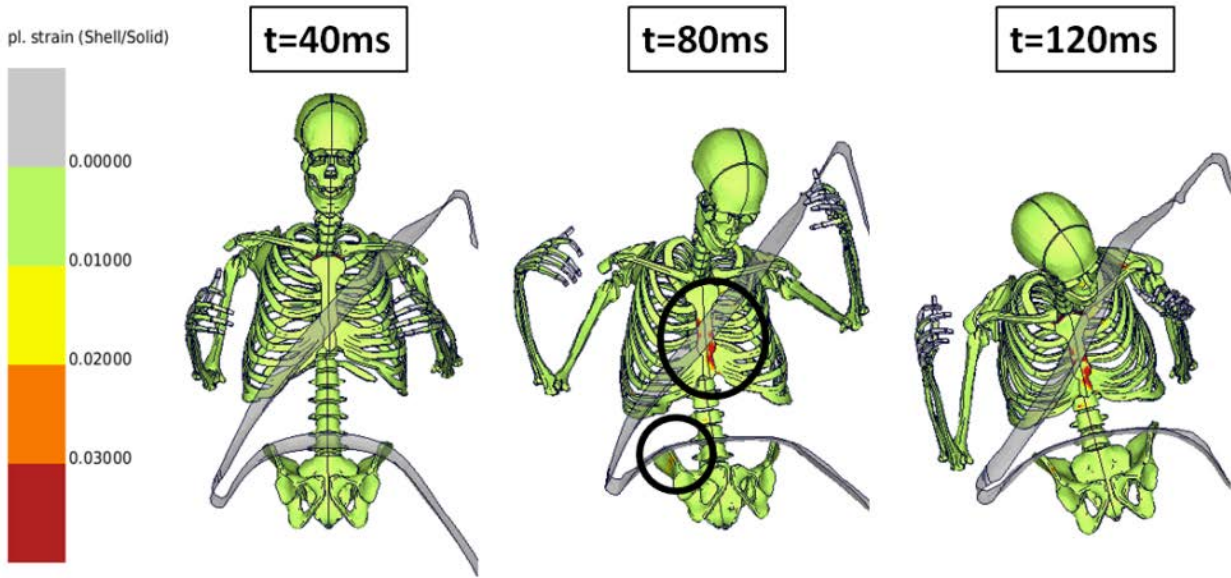


Figure 63: IIHS overall evaluation

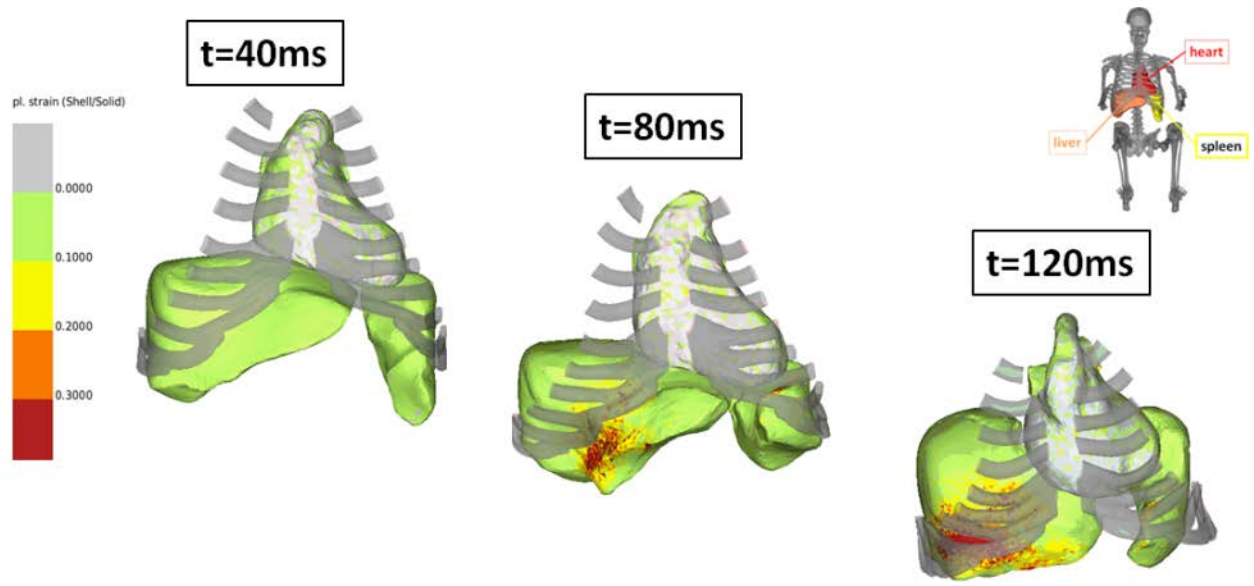
Evaluation of loads to the skeleton in the IIHS load case is shown in Figure 64 below. Ranges with different effective plastic strain values were used in order to identify areas of potential injury risk. Values above 3 percent are shown in red, indicating a risk of bony fractures. Such areas could be identified at the sternum, representing potential AIS = 2 injuries, and to some extent at the right iliac where the belt interacts with the pelvis bone. It can be noticed that the pelvis belt is located just below the upper edge of the iliac during the entire crash event, preventing submarining and a more severe intrusion of the belt into the abdominal area.



Plastic strain values above 3% can be observed in the middle of the Rib cage at the sternum and to some extent at the right illiac (pelvis hip bone)

Figure 64: IIHS skeleton loads

In analyzing the effective plastic strain distribution regarding internal organ injuries in Figure 65, it is observed that values above 30 percent (colored in red) occurred in the liver. The location of maximum loads is close to the lower right CRUX deflection instrumentation point of the THOR dummy in the IIHS load case, which was discussed in chapter 3.1.3. Again, the seat belt interaction with the chest and abdominal area was determined to be the main cause for the potential injury risk at this location. Lower effective plastic strain values could be observed where no direct chest belt interaction occurred, such as the heart and the spleen at the left side of the THUMS, from the driver's perspective.



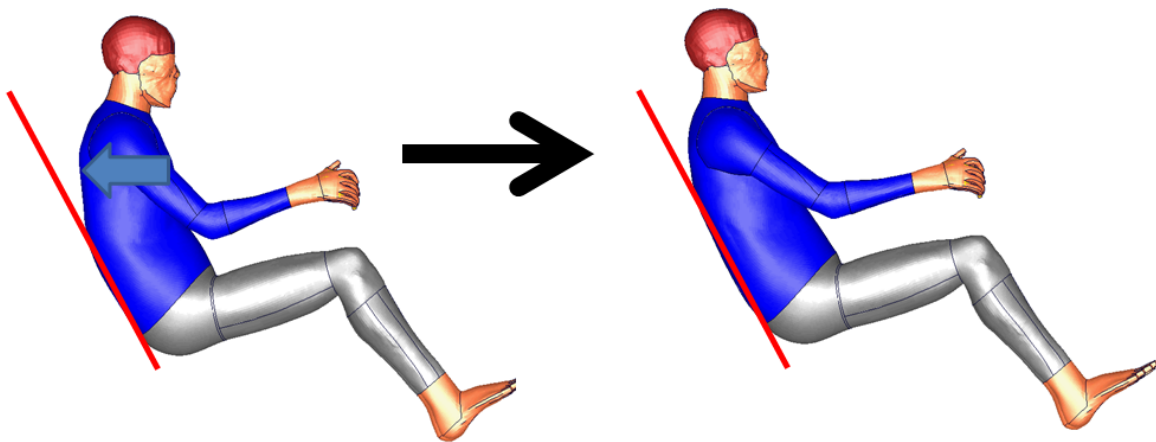
Plastic strain values above 30% can be observed in the liver and to some extent in the spleen.

Figure 65: IIHS loads to organs

3.2.5 THUMS torso posture evaluation

In order to evaluate occupant results of different seating positions of the THUMS, a sensitivity study using different upper body postures was conducted.

Figure 66 shows the upper body posture of the THUMS model as provided by LSTC on the left. The spine is curved causing a bent-forward sitting posture. Although this can be a realistic sitting position of a human occupant, the upper body torso posture was modified in order to achieve a more upright sitting position, similar to the ones used for the different dummy models. Again a pre-simulation was used to create the new position, shown in Figure 66, where hands, legs, and pelvis location were not modified. Only the position of the arms, upper body and head position were changed. The head center of gravity in the new position was located 92mm further back in x-direction when compared to the original position.

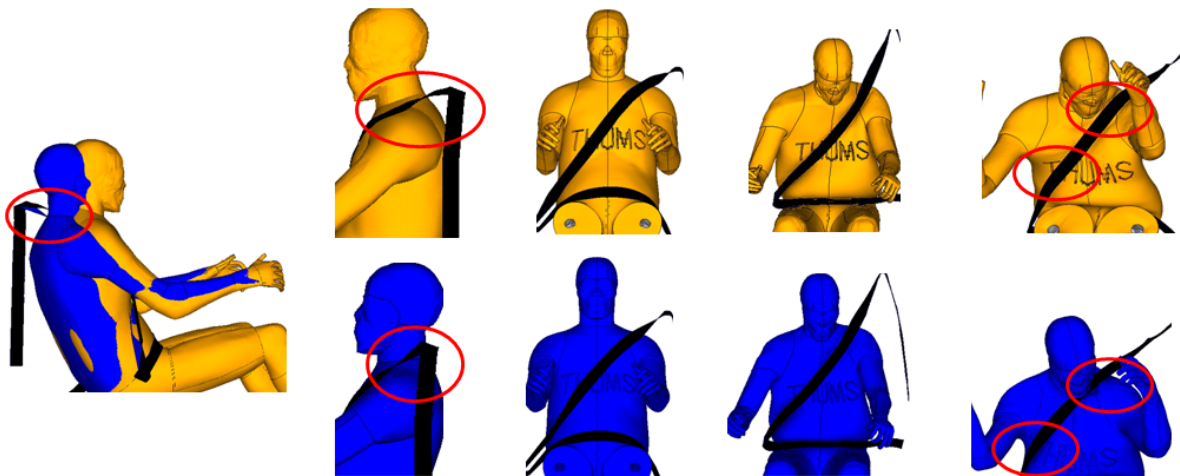


A pre-simulation was conducted in order to achieve a more upright seating position, similar to the dummy models used. The different torso angles will be used in the following sensitivity study.

Figure 66: Torso pre-simulation

When comparing the seat belt path and the overall kinematics of the two different upper body postures in Figure 67 below, it is informative and illuminating that the shoulder belt path is less horizontal close to the d-ring when the occupant is seated in the less upright seating position (shown in blue). Since the pelvis angle was kept unchanged, the upper shoulder area and the head were located further back, when compared to the more bent-forward position (shown in yellow), allowing the seat belt to have a steeper path from the d-ring towards the chest. This difference had consequences for the chest belt interaction in the later phase of the crash. The more bent-forward position (shown in yellow), having a more horizontal belt path coming from

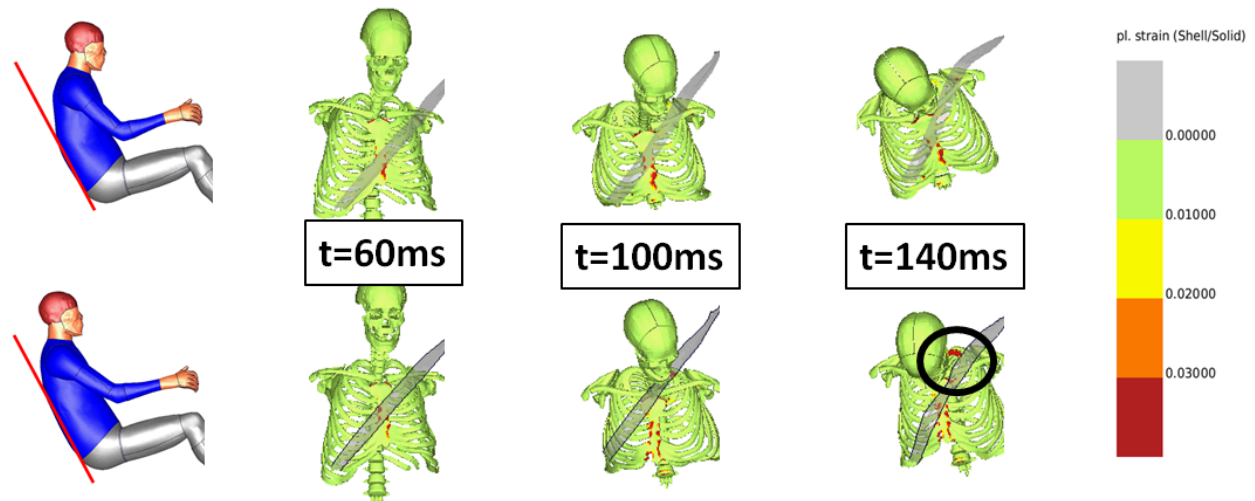
the d-ring, created higher normal forces during the forward displacement between the belt and the chest and therefore allowed the belt to remain at its original position due to higher frictional forces. It can be noticed from the last picture in Figure 67 that this was not the case for the more upright seating position (shown in blue), where the belt moved towards the neck and upper chest during the crash event.



The different torso angles affect the path of the shoulder belt. In the simulation with the more forward bent torso, the belt “couples” better with the occupant due to a higher “normal force”. The simulation with the more upright seating position causes a more steep shoulder belt path which allows more relative movement towards the neck and off the chest

Figure 67: THUMS torso angle overall evaluation

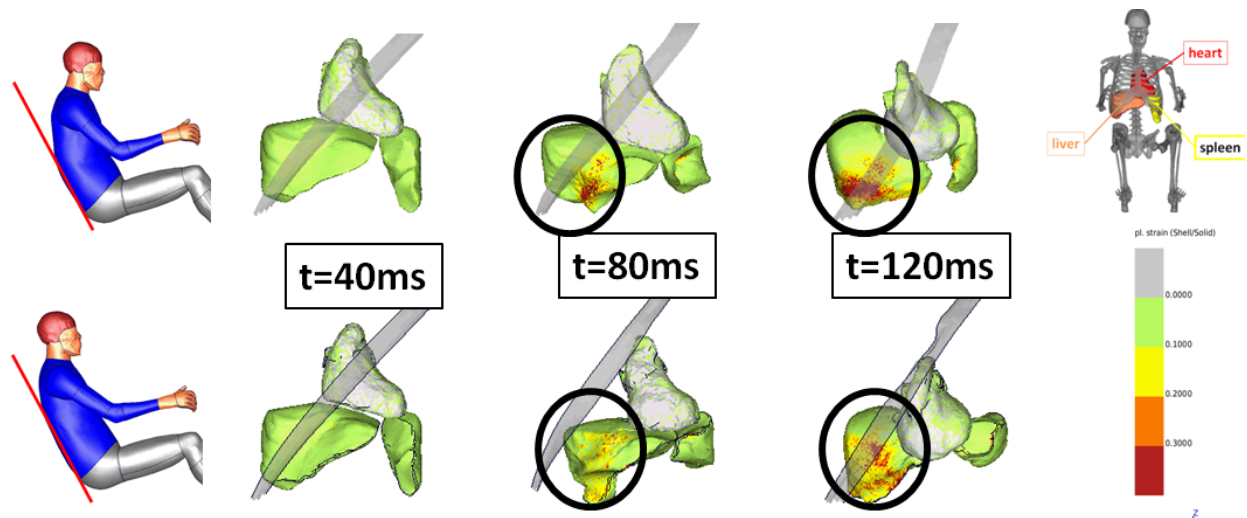
The different sitting positions and chest belt interaction influenced the load to the skeletal bones and the internal organs of the THUMS model. Figure 68 shows the comparison of the two cases using fringe plots of the skeleton with areas which exceed critical effective plastic strain values of 3 percent colored in red. Again it can be noticed that the shoulder belt moved towards the neck and upper torso area during the impact for the more upright seating position at the bottom of Figure 68, causing different loads to the sternum area and to the first rib, due to the changed seat belt torso interaction.



It can be noticed that the different torso angles affect the plastic strain values in the rib cage slightly. The biggest difference can be seen in the top left rib: The THUMS with the straighter seating position shows higher values which are mainly caused by the different occupant belt interaction.

Figure 68: THUMS torso angle skeleton evaluation

Figure 69 below shows the effect on the loads seen at the internal organs, heart, liver, and spleen. Again a threshold of 30-percent maximum plastic strain was used to indicate potential injury risk to these abdominal organs. Higher loads could be observed for the original sitting posture, which allowed the belt to remain at its original position relative to the liver, for example.



It can be noticed that the different torso angles affect the plastic strain values especially in the liver. The sitting posture and consequently slightly different shoulder belt path causes a difference in loading of the liver by the belt. The more bend forward position shows higher loads to the liver than the straighter seating position.

Figure 69: THUMS torso angle internal organs

Comparing the effects, it can be noticed that on one hand the different torso angle and shoulder belt path resulted in higher loads to the skeleton in the sternum and upper left torso area, and on the other hand resulted in lower loads to the liver.

3.3 Conclusion Subtask III

The developed integrated vehicle model for occupant safety analysis with relevant interior components, generic restraint system components, and respective occupant models (which was extensively evaluated in three different load cases — IIHS 40-percent offset, NCAP full overlap, and 15 degree oblique 35-percent offset impact — using full-scale test data) was used to evaluate different, more detailed occupant models.

First, the occupant model of the advanced THOR dummy was simulated and analyzed in the IIHS 40-percent offset crash configuration. When comparing the results with the Hybrid III 50th percentile occupant model, it was found that absolute values, when normalized to the appropriate common injury assessment thresholds, were comparable for both dummies despite differences in curve characteristics and occupant kinematics. Major differences were obvious for the chest deflections, which are measured at only one location for the Hybrid III and at four distinct locations for the THOR. Besides the advanced injury analysis capabilities using the THOR, higher maximum values could be observed for this advanced dummy at locations where direct seat belt interaction occurred as compared to the maximum Hybrid III sternum deflection.

Second, the Total HUMAN Model for Safety (THUMS) was included in the 40-percent overlap IIHS load case. In addition to allowing instrumentation dependent criteria, such as chest deflection, the human model allows the analyst to directly evaluate loads to skeleton bones and internal organs, for example. Effective plastic strain values were analyzed and areas with potential injury risks according to reported thresholds were evaluated. In addition to the original THUMS sitting torso posture, the results of a more upright seating position were determined.

VII Summary and Acknowledgment

4. Summary and acknowledgment

An integrated vehicle model for occupant safety analysis was developed and used under FHWA contract no. DTFH61-09-D-00001.

In Subtask I, an integrated vehicle-occupant model was developed using an available Toyota Yaris structural model together with generated relevant interior components, generic restraint system components, and respective occupant models.

The developed model was extensively validated using three different load cases — IIHS 40-percent offset, NCAP full overlap, and 15-degree oblique 35-percent offset impact — using full-scale test data.

In Subtask II, the developed integrated vehicle model for occupant safety analysis with relevant interior components, generic restraint system components, and respective occupant models was used to perform various sensitivity analyses for various parameters, using all three crash configurations.

Variation of relevant parameters (sensitivity analysis), including speed, overlap percentage, seating position, belt, air bag, and steering column characteristics showed interesting and realistic results for different load cases and occupants. It can be seen that with the developed model and methodology, the safety analyst is capable of simulating and analyzing situations and effects that go beyond the validated configurations.

In Subtask III, the developed integrated vehicle-occupant model for occupant safety analysis was used to evaluate different, more detailed occupant models.

First, the occupant model of the advanced THOR dummy was simulated and analyzed in the IIHS 40-percent offset crash configuration. When comparing the results with the Hybrid III 50th percentile occupant model, it was found that absolute values, when normalized to the appropriate common thresholds, were comparable for both dummies despite differences in curve characteristics and occupant kinematics. Major differences were obvious for the chest deflections, which are measured at only one location on the Hybrid III, and at four distinct locations on the THOR. Besides the advanced injury analysis capabilities using the THOR, higher maximum values could be observed for this advanced dummy at locations where direct seat belt interaction occurred, as compared to the maximum Hybrid III sternum deflection.

Second, the Total HUMAN Model for Safety was included in the 40-percent overlap load case. In addition to using instrumentation dependent criteria, such as chest deflection, the human model allows the analyst to directly evaluate loads to skeletal bones and internal organs, for example. Effective plastic strain values were analyzed and areas with potential injury risks determined according to cited thresholds have been evaluated. In addition to the original THUMS sitting torso posture, the results of a more upright seating position were determined.

Throughout 2013, methodologies, results, and analyses were regularly presented, discussed and documented using PowerPoint presentations, videos, and this report.

The authors would like to express their great appreciation for being able to conduct this project and for the productive cooperation and fruitful discussions with NHTSA during the regular meetings. The authors thank the Toyota Motor Corporation for making the THUMS model available for independent, academic research and thank the Livermore Software Technology Corporation for its occupant models and its LS-DYNA support.

VIII Appendix

5. Appendix

The purpose of this appendix is to document the details of the technical validation of the 2010 Toyota Yaris in the NHTSA Oblique frontal test.

5.1. FE model of 2010 Toyota Yaris

The FE model of 2012 Toyota Yaris was generated by the NCAC. The FE vehicle model consists of 1.0 million elements, 1.0 million nodes, and 771 parts. The structure of the FE vehicle model was validated by conducting frontal NCAP and IIHS 40-percent offset test simulations as shown in Figure 70 and Figure 71. For the NCAP frontal test and the IIHS 40-percent offset test, the simulation results show good correlation with the actual test results.

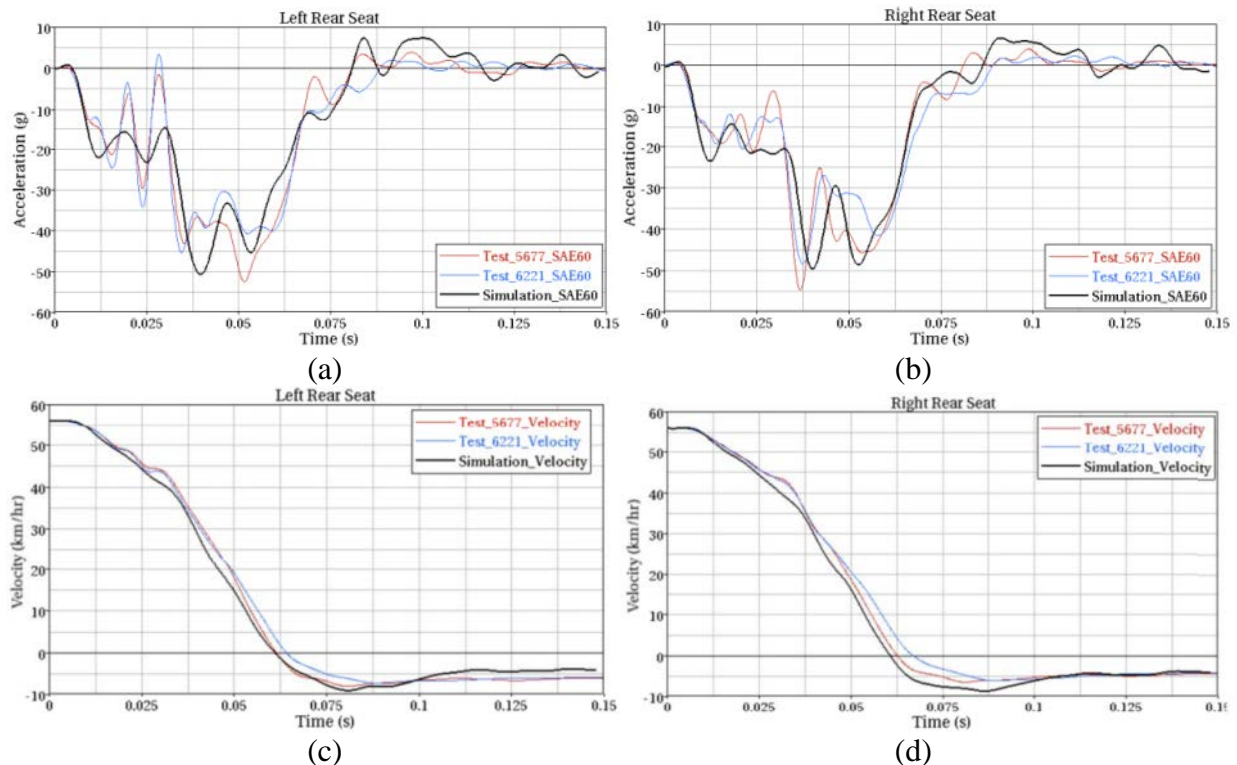


Figure 70: Vehicle acceleration and velocity in frontal NCAP test

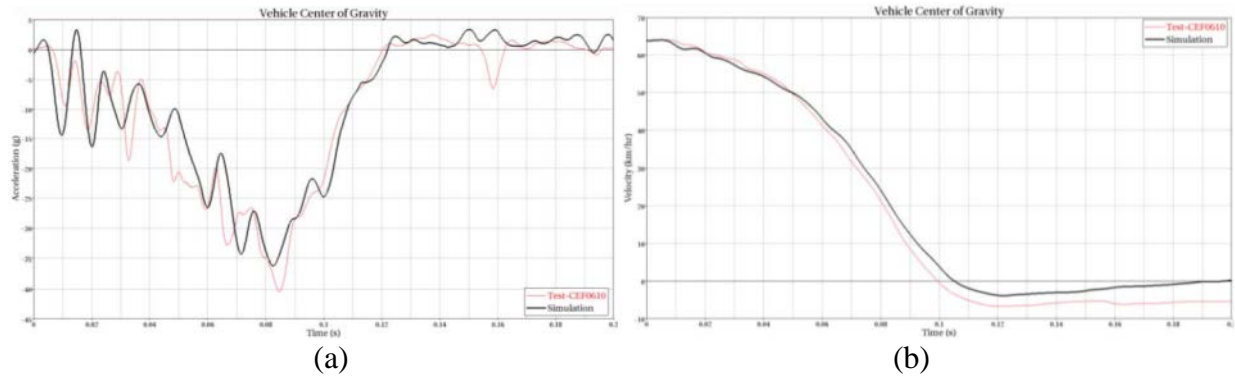


Figure 71: Vehicle acceleration and velocity in frontal IIHS offset test

5.2. NHTSA frontal oblique test

The NHTSA oblique frontal test was investigated and validated. In the NHTSA oblique frontal test, the research moving deformable barrier (RMDB) impacts a vehicle as shown in Figure 72. The initial FE model of the RMDB was obtained from NHTSA.

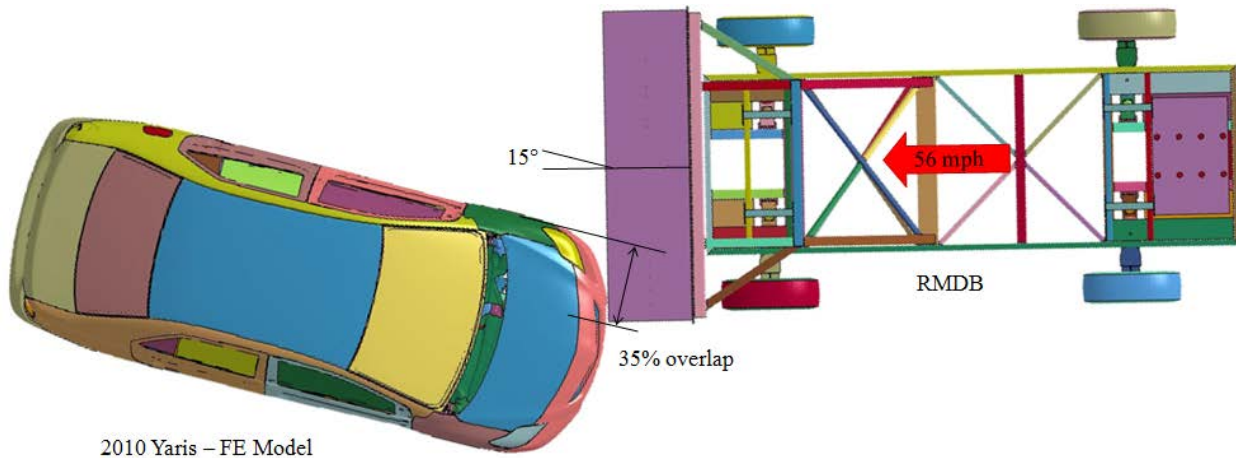


Figure 72: The setup of the NHTSA Oblique frontal test

The initial simulation of frontal oblique test showed some discrepancy compared to the actual laboratory test. Figure 73 shows the vehicle accelerations, which are different from the actual test responses in terms of peak timing and peak value. To improve the simulation results, both FE models of vehicle and RMDB were investigated.

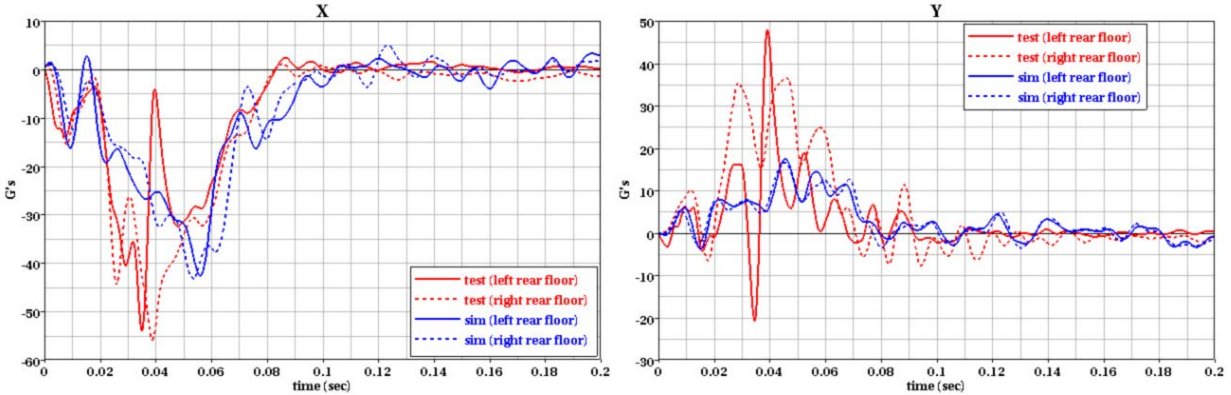


Figure 73: Vehicle acceleration in frontal oblique test (initial run)

Basically, technical differences were found between the vehicles in the simulation and laboratory test. The vehicle in the test had an automatic transmission, and the FEM 2010 Toyota Yaris (the one in the simulation) had a manual transmission. As shown in Figure 74, the shapes of the automatic and manual transmissions are quite different. Consequently, the transmission in the FE vehicle model was remodeled to have the same shape of automatic transmission, as shown in Figure 74(d).

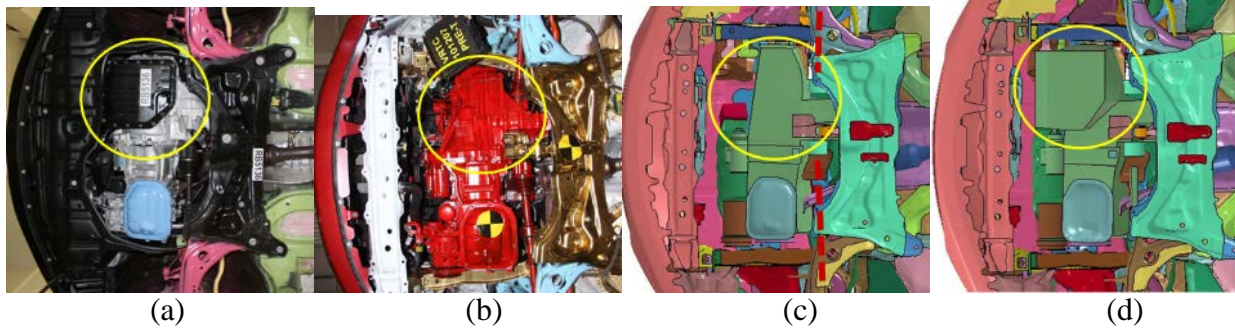


Figure 74: Transmission of Yaris: (a) automatic, (b) manual, (c) manual in the original FE model, and (d) automatic in the modified FE model.

In the Oblique frontal test, the front structure of a vehicle experiences not only longitudinal loading, but also transverse loading conditions. This loading pattern is unlike the mostly longitudinal loading condition in frontal NCAP and IIHS offset tests. In the original FE model, the front axle, which is the connecting rod between the transmission and front wheels, was not modeled. Thus, it can be seen that the lateral motion of the engine of the original FE vehicle model was exaggerated as shown in Figure 74(b). In the modified (remodeled to have automatic transmission) FE model, the front axles were added, which reduced the lateral movement of front vehicle structure and improves the engine movement. It can be seen that the modified FE model shows comparable result as shown in 75(c).

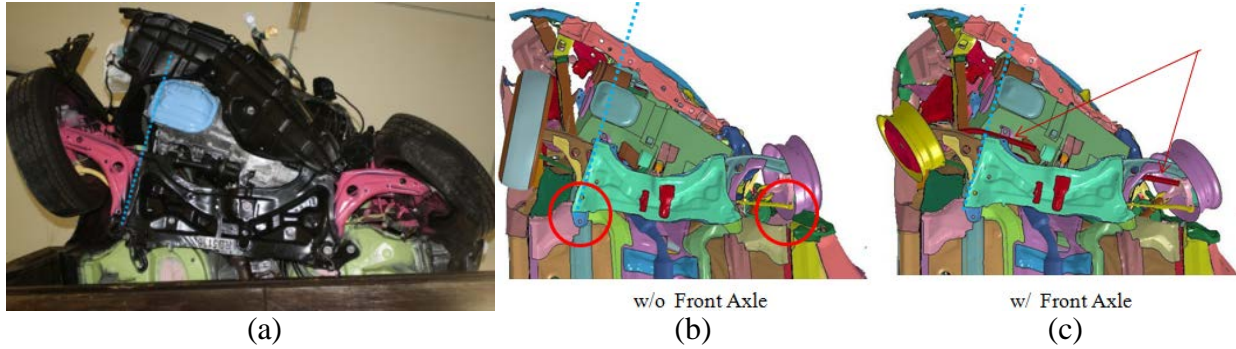


Figure 75: Deformation of frontal vehicle structure in Oblique frontal test: (a) actual vehicle, (b) original FE model, and (c) modified FE model.

In the modified FE vehicle model, the steering system shown in Figure 76 was also improved. The steering system consists of two universal joints and an energy-absorbing collapsible steering column. These components were added in the modified FE model.

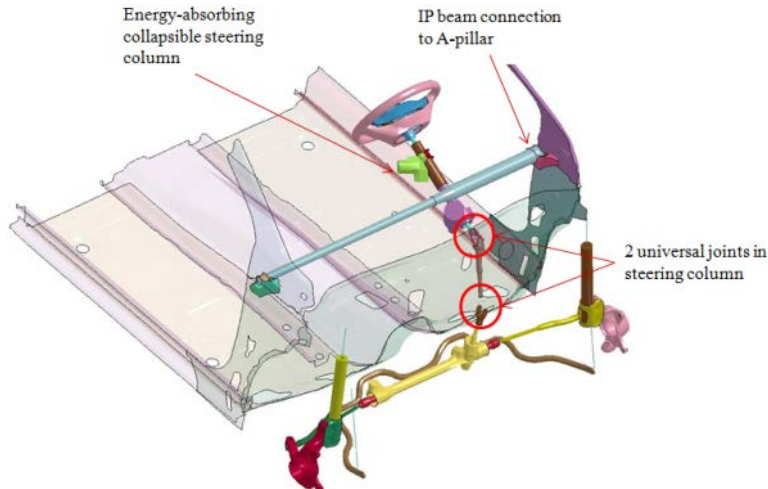


Figure 76: Steering system of Yaris

In the Oblique frontal test, it can be observed that connections and components failed because the laboratory vehicle experienced harsh deformation. Figure 77 shows failures in the Yaris. In the original FE model, failure never occurred since failure was not considered. In many cases, failure is critical to vehicle response and the deformation mode. In order to investigate the failure effect, failure was modeled in the FE model, as shown in Figure 78. In the FE model, failure was initiated at a certain time. Based on the study with various failure times, it was found that failure did not meaningfully improve the vehicle responses in the Oblique frontal simulations.

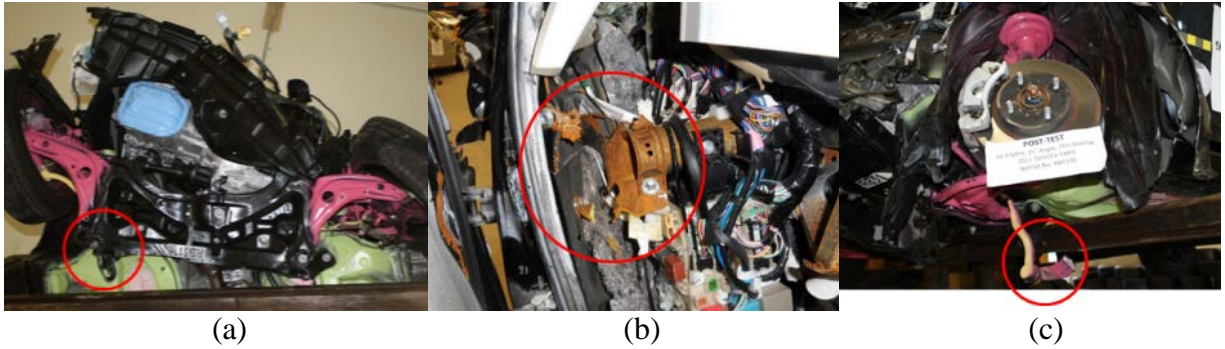


Figure 77: Failures in frontal oblique test: (a) connect between floor and sub-frame, (b) connection between IP beam and A-pillar, and (c) steering arm.

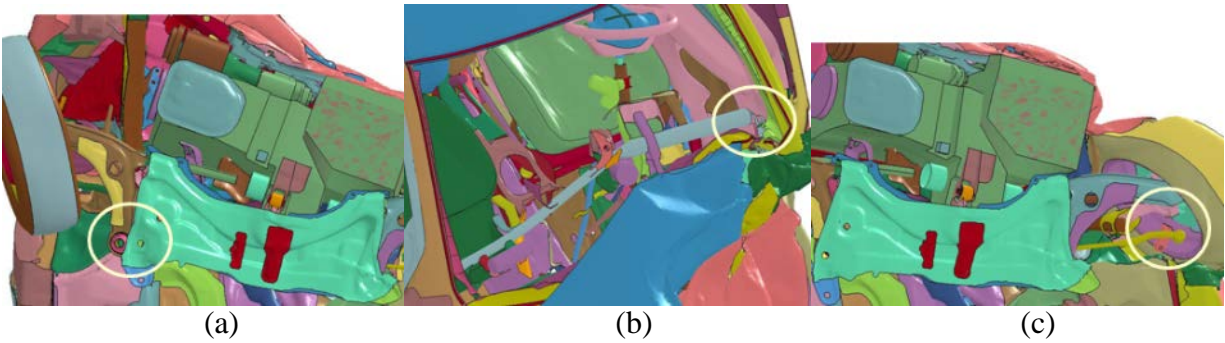


Figure 78: Failures in the FE model: (a) connect between floor and sub-frame, (b) connection between IP beam and A-pillar, and (c) steering arm.

As noted, the RMDB FE model shown in Figure 78(a) was obtained from NHTSA. Its specifications are shown in Figure 78(b). The FE model consists of 0.54 million nodes and 1.1 million elements. The honeycomb is modeled by shell elements.

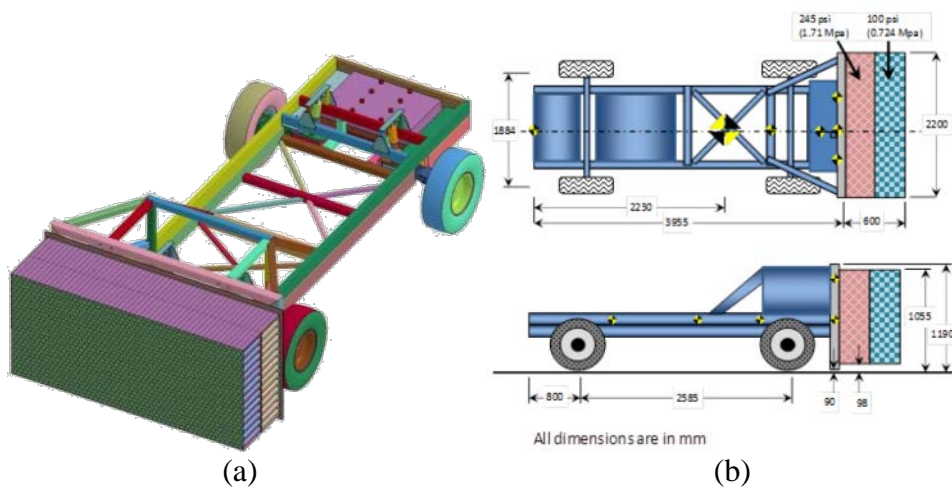


Figure 79: RMDB: (a) FE model and (b) specification

The RMDB performance was tested by a simple impact test as shown in Figure 79. The impactor weight was 1.7 ton and its impact speed was 33.15 km/h. The impact test was simulated using the original FE model of RMDB. The results in Figure 80 show that the original RMDB

provided a softer response than in the laboratory test. To improve the performance of the RMDB FE model, a modified RMDB FE model was developed by conducting iterative simulations. Modifications were made in both models of honeycomb and cover plate. In the honeycomb model, the foil thickness of overlapped sides was set twice and the stress-strain plastic hardening curve was scaled up to considered air pressure effect inside honeycomb cells. In the cover plate model, the thickness of the certain areas (edges, mid-front line, and half-diagonal lines) of the plate was set twice because double plates were used at those areas. The modified RMDB FE model provided much improved impact performance in the laboratory impact test simulation as shown in Figure 81.



Figure 80: impact test of RMDB

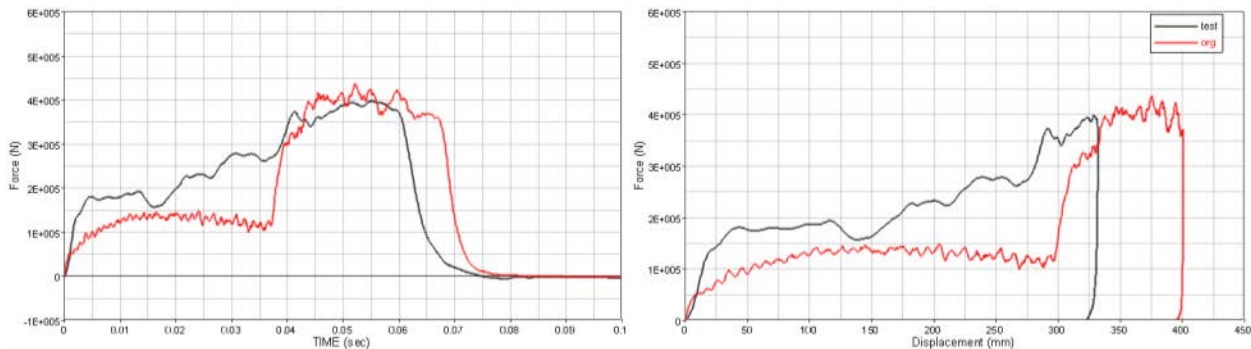


Figure 81: Result of impact test using the original FE model of RMDB

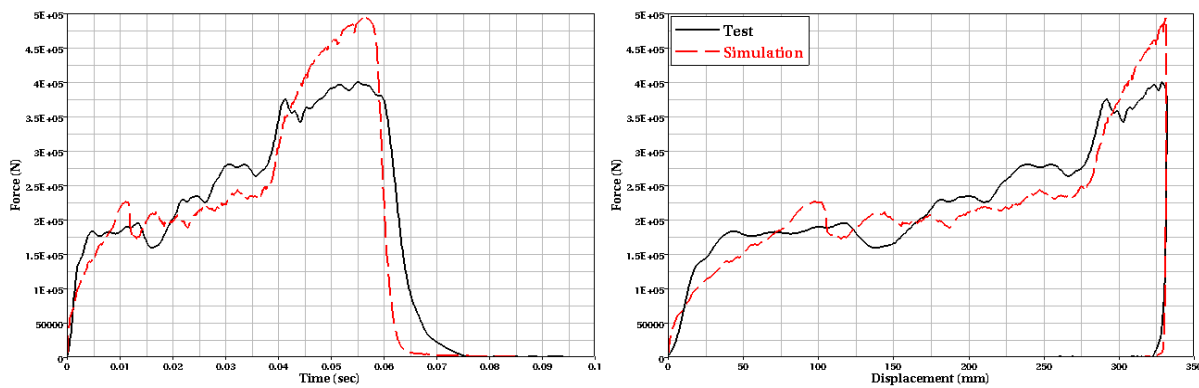


Figure 82: Result of impact test using the modified FE model of RMDB

Figure 81 and Figure 82 show the result of the frontal oblique simulation with modified vehicle and RMDB FE models. The acceleration results show improved responses in terms of peak timing compared with Figure 83. The RMDB responses in simulation are comparable to the test results, as depicted in Figure 84.

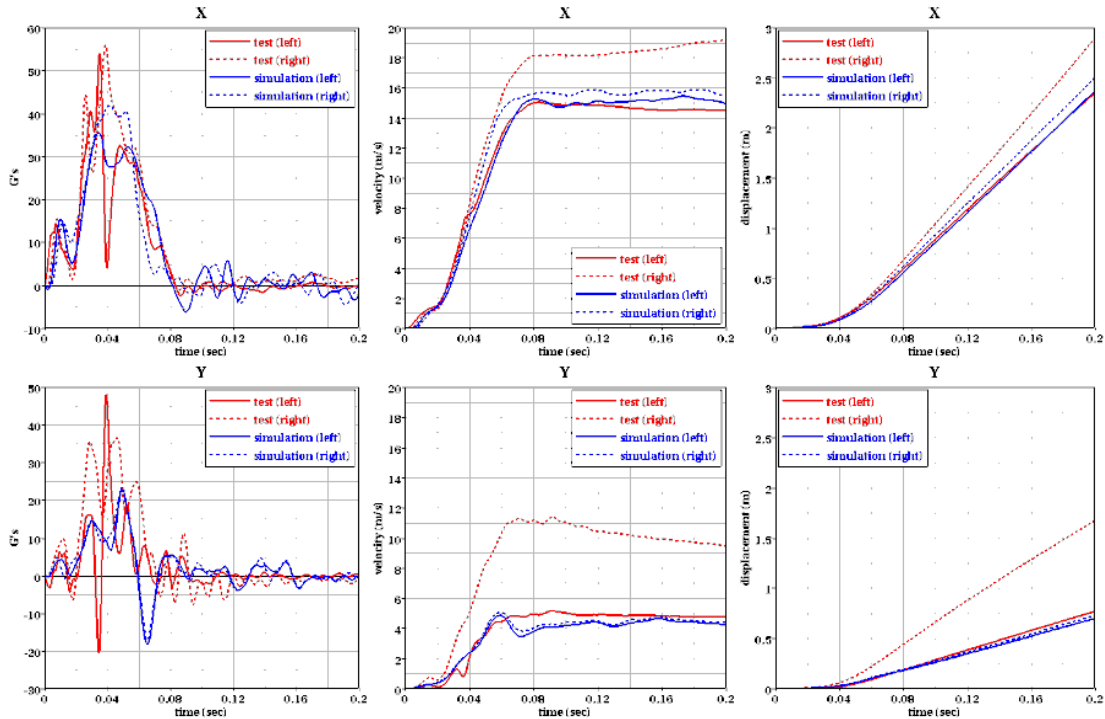


Figure 83: Vehicle responses in frontal oblique simulation using modified vehicle and RMDB FE models

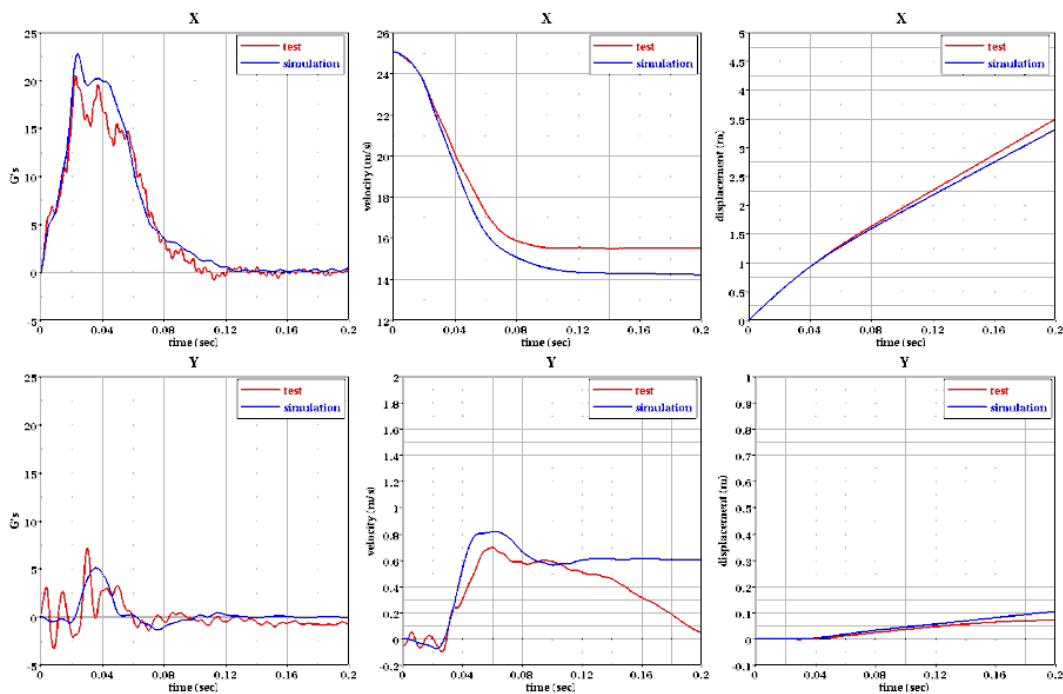


Figure 84: RMDB responses in frontal oblique simulation using modified vehicle and RMDB FE models

DOT HS 812 087
December 2014



U.S. Department
of Transportation
**National Highway
Traffic Safety
Administration**



10886-112614-v2a